Promoter Selection and Smith-Magenis Syndrome Protein Retinoic Acid Induced-1 in Neuronal Activity-Dependent Transcription

by

Patricia M. Garay

A dissertation submitted in partial fulfillment
of the requirements for the degree of
Doctor of Philosophy
(Neuroscience)
in the University of Michigan
2021

Doctoral Committee:

Professor Shigeki Iwase, Chair
Professor Gabriel Corfas
Assistant Professor Monica Dus
Professor Roman Giger
Professor Stephen Parker

Patricia M. Garay

pmgaray@umich.edu

ORCiD ID: 0000-0003-1659-8126

DEDICATION

This dissertation is dedicated to the people with Smith-Magenis Syndrome, Potocki-Lupski Syndrome, and their families. It is also dedicated to the mentors who made this path possible for me, including Professor Blaine Moore, who introduced me to the marvels of molecular biology and activated my ambition, Dr. Vince Groppi who took a chance on me and hired me for my first scientific position, and Dr. Lauren McGillicuddy, who made me dream I could make it in graduate school.

ACKNOWLEDGEMENTS

This dissertation was possible through the training and mentorship of Professor Shigeki Iwase. Further mentorship came from Professor Mike Sutton, Professor Monica Dus, and Professor Steve Parker. Support for the RAI1 and alternative promoter projects came from Professor Ken Kwan, Professor Young Ah Seo, Professor Kevin Jones, and Professor Roman Giger. Dr. Takao Tsukahara contributed his scientific effort and skills to every project and taught me the value of diplomatic communication. Further critical experiments were performed by Dr. Yumie Nakamura, Owen Funk, Alex Chen, Jean Carlos Rodríguez Díaz, Dr. Rafi Kohen, Margarete Wallner, Jonathan Richards, and Yu (Celine) Chuo, all of whom taught me valuable lessons in collaboration. Authors of the published RAI1 paper and review article contributed to dissertation writing. Support for the Bru-seq protocol and analysis was provided by Dr. Saurabh Agarwal and Professor Mats Ljungman. Innumerable faculty and students across the University of Michigan offered advice and inspiration for my many projects. Constructive scientific discussions and moral support came from my labmates Dr. Yumie Nakamura, Dr. Takao Tsukahara, Dr. Christina Vallianatos, Dr. Robert S. Porter, and Katie Bonefas. The members of my committee, Professors Gabriel Corfas, Monica Dus, Roman Giger, and Steve Parker motivated me with expansive discussions. The work of PRISMS organization aided in my understanding of Smith-Magenis syndrome and funded work related to this dissertation. Further financial support was provided from the Neuroscience Graduate Program, Rackham Graduate School, and the National Science Foundation. My time in graduate school was enriched by the team at the Office of Graduate and Postdoctoral Scientists, by Dr. Debbie Willis and the Rackham Graduate School DEI Certificate Program, by the Neuroscience Graduate Program staff, and by my fellow graduate students. My friends and family have inspired me, supported me, and taught me skills to grow and change throughout this time. A special acknowledgement to my sister Carolyn who edited my grants, listened to my practice talks, and when needed, reminded me of the joy in pursuing visions of the patterns in life.

TABLE OF CONTENTS

DEDICATION ..... **ii**

ACKNOWLEDGMENTS ..... **iii**

LIST OF FIGURES ..... **vii**

LIST OF APPENDICES ..... **ix**

LIST OF ABBREVIATIONS ..... **x**

ABSTRACT ..... **xi**

CHAPTER 1. Introduction **1**

CHAPTER 2. Development of the Approach to Analyze Activity-Dependent Transcription **5**

Introduction 5

Altered neuronal network activity triggers genome-wide transcriptional changes 7

Discussion 10

CHAPTER 3. RAI1 Regulates Activity-Dependent Nascent Transcription and Synaptic Scaling **12**

Loss of RAI1 function is associated with Smith-Magenis Syndrome 12

RAI1 suppresses the TTX-induced transcriptional program in resting networks 13

RAI1 deficiency promotes synaptic upscaling 17

RAI1 promotes transcriptional responses triggered by reductions in network activity 22

RAI1 dissociates from chromatin in response to activity changes 26

RAI1 directly controls activity-responsive gene transcription in stable networks 28

RAI1 directly contributes to transcriptional response to TTX.....29

Loss of RAI1 prevents synaptic upscaling but not downscaling 31

Discussion.....34

Speculation on the RAI1 complex.....36

Potential Lessons 38

CHAPTER 4. Potential Roles of RAI1 in Circadian Rhythms.....40

Introduction.....40

Loss of RAI1 alters genes associated with CLOCK and PER2 Regulation 41

Discussion.....43

CHAPTER 5. Neuronal Activity-Dependent Promoter Selection.....46

Introduction.....46

A minority of expressed genes contain multiple active promoters in mixed neuronal cultures....47

Activity-dependent differential usage of promoters (ADDUP) in multi-promoter genes 49

ADDUP in *in vivo* stimulation of mouse visual cortex.....51

Cell-type specificity of alternative promoter usage.....53

Protein sequence is altered by promoter usage.....55

Promoter-dependent subcellular localization drives synaptic changes in PDE2A 58

Overexpression of differential promoter isoforms of PDE2A alters electrophysiology.....58

Discussion.....60

Broader Perspectives.....61

CONCLUSION 65

APPENDICES **67**

REFERENCES **86**

LIST OF FIGURES

Figure 1-1 Pathway from experience to change in behavior 1

Figure 2-1 Genome-wide transcriptional response to bi-directional activity alterations 6

Figure 2-2 Bru-seq Validation and Characterization.....9

Figure 3-1 *Rai1*-KD alters transcription of TTX-response genes at the baseline.....14

Figure 3-2 RAI1 protein is expressed primarily in neuronal nuclei, related to Fig. 3-1 16

Figure 3-3 *Rai1*-KD increases the synaptic efficacy at baseline activity condition.....19

Figure 3-4 Electrophysiology of *Rai1*-KD cultures at baseline, related to Fig. 3-3.....21

Figure 3-5 RAI1 positively regulates the transcriptional response to TTX. 24

Figure 3-6 Impact of RAI1 loss on transcription after TTX or BIC, related to Fig. 3-5.....25

Figure 3-7 Activity-dependent chromatin engagement of RAI1 27

Figure 3-8 Further RAI1 ChIP-seq analysis 30

Figure 3-9 *Rai1*-KD impairs synaptic upscaling but not synaptic downscaling 32

Figure 3-10 RAI1 is a state-dependent transcriptional regulator of TTX-response genes 33

Figure 3-11 Putative RAI1 complex.....36

Figure 4-1 RAI1-dependent Per2 transcription in baseline and inactivity state.....42

Figure 4-2 RAI1-target genes are regulated by PER2 and CLOCK.....43

Figure 5-1 Multiple promoters found in mixed *in vitro* neuronal cultures.....48

Figure 5-2 Activity-dependent differential usage of promoters (ADDUP 50

Figure 5-3 *In vivo* brain tissue reveals differential promoter usage in response to physiological neural stimulation.....52

Figure 5-4 Excitatory-cell specific, ribosome-associated mRNA transcripts reveal alternative promoter usage *in vivo* 54

Figure 5-5 Activity-dependent differential usage of promoters yields predicted protein N-terminal changes 57

Figure 5-6 Expression of promoter-dependent isoforms of ADDUP gene *Pde2a* alters mEPSC amplitude and frequency 59

Figure A-1 Effect of Post-Trizol Purification Method on RNA yield and integrity 67

Figure A-2 Effect of Time and Concentration on Fragmentation 70

Figure A-3 Effect of Temperature on RNA fragmentation 71

Figure A-4 Effect of Magnesium Concentration on RNA fragmentation 71

Figure A-5 Ampure purification protocol is robust to small changes in protocol 73

Figure A-6 Effect of Dry Time on RNA Yield in Ampure purification 73

Figure A-7 Comparison of Nanodrop and Qubit measurements of RNA concentration in water 74

Figure A-8 RNA Input's effect on filtered and unfiltered read counts 76

Figure A-9 RNA Input's effect on normalized read counts 77

Figure A-10 Mapping reads to genes and TSS regions from low-input samples 77

LIST OF APPENDICES

Appendix A. Development of Low-Input DLAF RNA-seq Library Preparation Protocol 67

Appendix B. Materials and Methods.....78

LIST OF ABBREVIATIONS

ADDUP: activity-dependent differential usage of promoters

BIC: bicuculline

BrU: bromouridine

BrU-seq: bromouridine-sequencing

ChIP-seq: chromatin immunoprecipitation-sequencing

Cyto-PDE2A: cytoplasm-localized PDE2A, PDE2A3 in literature

KD: knock-down

LV: lentivirus/lentiviral

mEPSC: miniature excitatory post synaptic current

Mito-PDE2A: mitochondria-localized PDE2A, PDE2A2 in literature

mRNA: messenger ribonucleic acid

PTLS: Potocki-Lupski Syndrome

qPCR: quantitative polymerase chain reaction

RAI1: Retinoic acid induced 1

shRNA: short hairpin RNA

SMS: Smith-Magenis Syndrome

TTX: tetrodotoxin

Veh: vehicle

ABSTRACT

The brain adapts to the environment by converting signals of neural activity into altered synaptic connections. Long-term reshaping of synapses depends upon neural activity-dependent transcription. Activity-dependent transcription, in turn, requires proper packaging of the DNA through chromatin regulation. Genes encoding chromatin regulators, transcription factors, and synaptic proteins are all associated with autism spectrum conditions and rare intellectual disabilities. Such neurodevelopmental conditions may result, then, from a convergence on similar molecular pathways, such as activity-dependent synaptic plasticity. Indeed, forms of synaptic plasticity such as long-term potentiation/depression and synaptic scaling are known to require specific synaptic proteins and transcription factors. However, the roles of chromatin regulating proteins in these processes remain poorly understood.

In part, this is due to the difficulty of examining how chromatin regulators directly guide activity-dependent transcription. Chromatin regulators' direct effects are obscured by the commonly used technique of seeking differentially expressed genes from steady-state mRNA profiles. Furthermore, compared to transcription factors, chromatin regulators can have fewer dramatic gene-specific effects on transcription. Therefore, I used the nascent RNA sequencing method BrU-seq and adapted RNA-seq analyses to examine chromatin regulator function in the context of activity-dependent transcription associated with synaptic scaling. I then revealed a role for the Smith-Magenis Syndrome protein Retinoic Acid Induced-1 (RAI1) as a regulator of activity-dependent transcription and synaptic strength in the baseline and low-activity states of neurons.

In a distinct project, I found that neural activity shifts alter not only gene expression, but also gene promoter selection. I determined that multi-promoter genes make up nearly 10% of expressed genes in neuronal cultures, and that neuronal activity guides differential promoter usage in ~10% of them. I also observed differential promoter/transcription start site usage *in vivo* in physiological models of neuronal activity induction and found evidence of excitatory-neuron-

specific promoter switching. Differential promoter usage predominately predicts altered N-terminal protein sequences of synaptic and phosphodiesterase family genes. Promoter-specific isoforms of the phosphodiesterase PDE2A revealed differential organelle-targeting and altered electrophysiological properties, suggesting promoter usage can regulate subcellular protein localization and synaptic function.

In sum, these two projects detail new concepts of activity-dependent transcription and synaptic homeostasis that may be critical to human neurodevelopment and mature brain function.

CHAPTER 1

Introduction

Neuronal activity-dependent transcription is critical for synaptic restructuring

Changes in behavior during neurodevelopment and in adulthood are mediated by synaptic plasticity—the physical modifications of synaptic structures in response to experience. When an environmental stimulus activates a set of neurons, cascades of intracellular events lead to long-term alterations in synaptic connections. This process requires new RNAs to be transcribed and

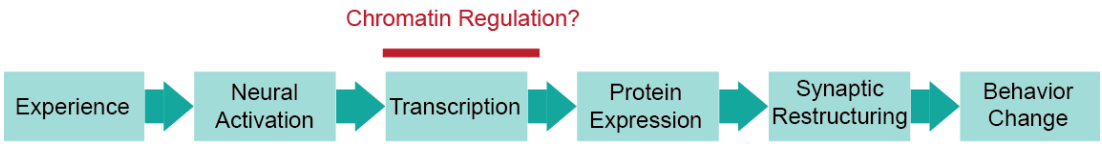

Figure 1-1. Model of the mechanistic pathway from experience to change in behavior.

translated into the proteins that restructure the synapse (Figure 1-1.)

The general framework of activity-dependent transcription is as follows. First, neuronal firing leads to an influx of calcium and a series of calcium-response signaling, which reaches the nucleus within a neuron. Constitutively-expressed transcription factors such as cyclic AMP-responsive element (CRE)-binding protein (CREB) and serum response factor (SRF) are then activated via post-translational mechanisms, primarily phosphorylation, which subsequently initiate the "first wave" of transcription of a set of genes [7] [8]. The first wave genes encode effector proteins such as ARC and BDNF and a number of transcription factors: e.g. FOS, NPAS4, EGR1, and C/EBPβ [8]. These transcription factors, in turn, activate a "second wave" of activity-dependent gene expression [8]. The second wave genes encode many synaptic and dendritic proteins that can modulate neuronal connectivity [9,10], making downstream set of genes an intriguing set to analyze what processes are implemented to modulate synaptic plasticity and cell-wide adaptations to a changing environment.

Activity-dependent transcription mediates several forms of synaptic plasticity

Proper activity-dependent transcription is essential for learning and memory [11], and multiple forms of synaptic plasticity, such as synaptic scaling, long-term potentiation (LTP), and long-term depression (LTD) [12]. While LTP and LTD selectively modulate the strength of specific synapses in order to tune specific neural circuits, synaptic scaling is a model of a homeostatic process to buffer destabilizing shifts in network activity [13-15]. That is, in response to a sustained increase in neuronal firing rate, neurons decrease, or "scale-down", the receptivity of the neuron to excitatory neurotransmitters. Conversely, global decreases in firing rate cause neurons to "scale-up" and increase synaptic efficacy. Synaptic scaling therefore provides a mechanism of negative feedback to long-lasting increases of individual synaptic efficacy, which left uncompensated, would result in positive feedback loops to produce over- or under-active circuits [16]. Like LTP and LTD, synaptic scaling plays important roles in neurodevelopment, learning, memory, and sleep [17-19]. Better understanding of learning, memory and sleep will arise from unearthing the underlying transcriptional regulation.

Chromatin regulation mediates neuronal activity-dependent transcription and synaptic scaling

Transcriptional regulation is mediated by site-specific transcription factors (TFs) that can recruit RNA polymerase II machinery to promoter and enhancer regions. However, there are far more TF-specific target sequences across the genome than TFs actually bind, revealing that additional layers of regulation are at work. For transcription factors to make contact with the proper genomic loci, the DNA must first be organized and the proper loci made accessible by a group of proteins called chromatin regulators. In this way, chromatin regulators may prime the DNA for activity-dependent transcription and thereby modulate the downstream effects on the synapse (Figure 1-1). Supporting this idea, genes encoding chromatin regulators have been found to feature disrupted in synaptic plasticity, including the PRC2 histone modification complex subunit EED and DNA methyltransferase (DNMT) proteins [20] for LTP/LTD, and for synaptic

scaling, TET3 DNA demethylase [21], EHMT1/2 histone H3K9 methyltransferases [22], and L3MBTL1 methyl-histone binding factor [23].

Transcription factors, chromatin regulators, and synaptic proteins are associated with neurodevelopmental disorders

Considering that transcription factors and chromatin regulators are integral to processes of synaptic plasticity, including those involved in learning and memory, one would assume that disruption of genes encoding these factors may result in aberrant neurodevelopment and brain function. Indeed, exome-sequencing studies in the past decade have identified that genes that encode transcription factors, chromatin regulators, and synaptic proteins are enriched in cases of autism spectrum conditions and neurodevelopmental disorders (NDD) [24,25]. Experience-dependent synaptic restructuring may then be a pathway onto which such neurodevelopmental disorders converge (Figure 1-1.)

This is reflected in recent functional studies that examine the cellular function of NDD-associated chromatin regulator genes. For example, histone methyltransferase MLL1 and the histone demethylase LSD1, both of which are implicated in NDDs, appear to be required for optimal activity-dependent transcription [26-28]. In addition to these H3K4me regulators, an H3K9 methyltransferase G9a/GLP [29], an H3K27 demethylase KDM6B [30], L3mbtl, an H3K4me1/2 reader [23] and engage in activity-dependent transcription and alter synaptic phenotypes.

Improved methods to delineate the roles of chromatin regulators in activity-dependent transcription

Although the link between chromatin regulators and activity-dependent transcription associated with synaptic plasticity has been established, there remain several ways in which the field is relatively unexplored. Firstly, as activity induction is known to elicit changes at the post-transcriptional level the analysis of chromatin regulators roles in transcription must be dissected from post-transcriptional effects including mRNA decay [31 32 33] and mRNA transport and local translation [34]. To exclusively examine transcriptional effects, one can use nascent RNA profiling, which has been rarely used in previous studies. To develop an approach to examine chromatin regulation in the context of bona fide transcription, I applied a nascent RNA sequencing

approach, BrU-seq, in an *in vitro* model of synaptic scaling (Chapter 2). I next characterized the nucleosome binding protein Retinoic Acid-Induced 1 (RAI1) in this process (Chapter 3). I then discuss the resulting hypothesis that RAI1 interacts with circadian transcription (Chapter 4).

In the second branch of my dissertation, I explore the phenomenon of multiple promoter usage in the context of activity-dependent transcription (Chapter 5). Neuronal activity has been found to initiate differential usage of promoters in a few genes such as the neurexins and BDNF [35-37]. Activity-dependent transcription encompasses mechanisms such as enhancer activation, alternative splicing, A-to-I editing, alternative 3' end usage, and microRNA expression [31,32,38,39]. In contrast, profiling the use of alternative promoters has been limited to steady-state mouse brains [40], disease states [41], or across developmental timescales [42]. In this dissertation I reveal the discovery, through BrU-seq, that alternative promoter usage is a more widespread phenomenon in activity-dependent transcription. I validate this process *in vivo*, using a custom low-RNA input sequencing protocol (Appendix A) to profile whole-tissue and excitatory neuron-specific usage of promoters using physiological stimuli to model activity-dependent transcription. I demonstrate that alternative promoter usage alters the predicted N-terminal amino acids and may alter protein subcellular localization and electrophysiological properties of neurons.

CHAPTER 2.

Development of the Approach to Analyze Activity-Dependent Transcription

Introduction

Several technical obstacles limit our understanding of chromatin regulators' role in activity-dependent transcription. RNA-sequencing (RNA-seq) is an unbiased approach that has been used to quantify the RNAs isolated from neurons stimulated by neuronal activity [21,43]. However, the methods by which RNA is conventionally collected and quantitated are not well-suited to identify short-term changes in transcription because of the presence of long-lived RNA transcripts. Additionally, many protocols for RNA-seq, including single-cell sequencing, do not provide information across the entire length of RNA, particularly in the proximal (5') end of the RNA molecule. The 5' end of the RNA contains biologically relevant information that guides RNA stability and encodes protein sequence. These two technological obstacles limit the analysis of activity-dependent transcription and its regulation.

To dissect the precise mechanisms by which these chromatin regulators contribute to transcription, accurate monitoring of transcriptional responses is critical. Most prior studies have monitored steady-state mRNA levels, using RT-qPCR, cDNA microarray, and mRNA-seq. The brain exhibits notorious complexity of post-transcriptional regulation, Therefore, reliance on steady-state mRNA measurements may obscure the roles of chromatin regulators in transcription, and certainly in the dynamic transcription in response to stimuli.

To overcome the major limitation of steady-state RNA-seq, we adopted Bromouridine-sequencing (Bru-seq), a genome-wide profiling technique of nascent transcripts [44,45]. We prepared primary forebrain-neuron cultures from E18 mouse embryos and allowed them to mature for 17 days *in vitro* (DIV). To monitor bidirectional transcriptional responses to activity

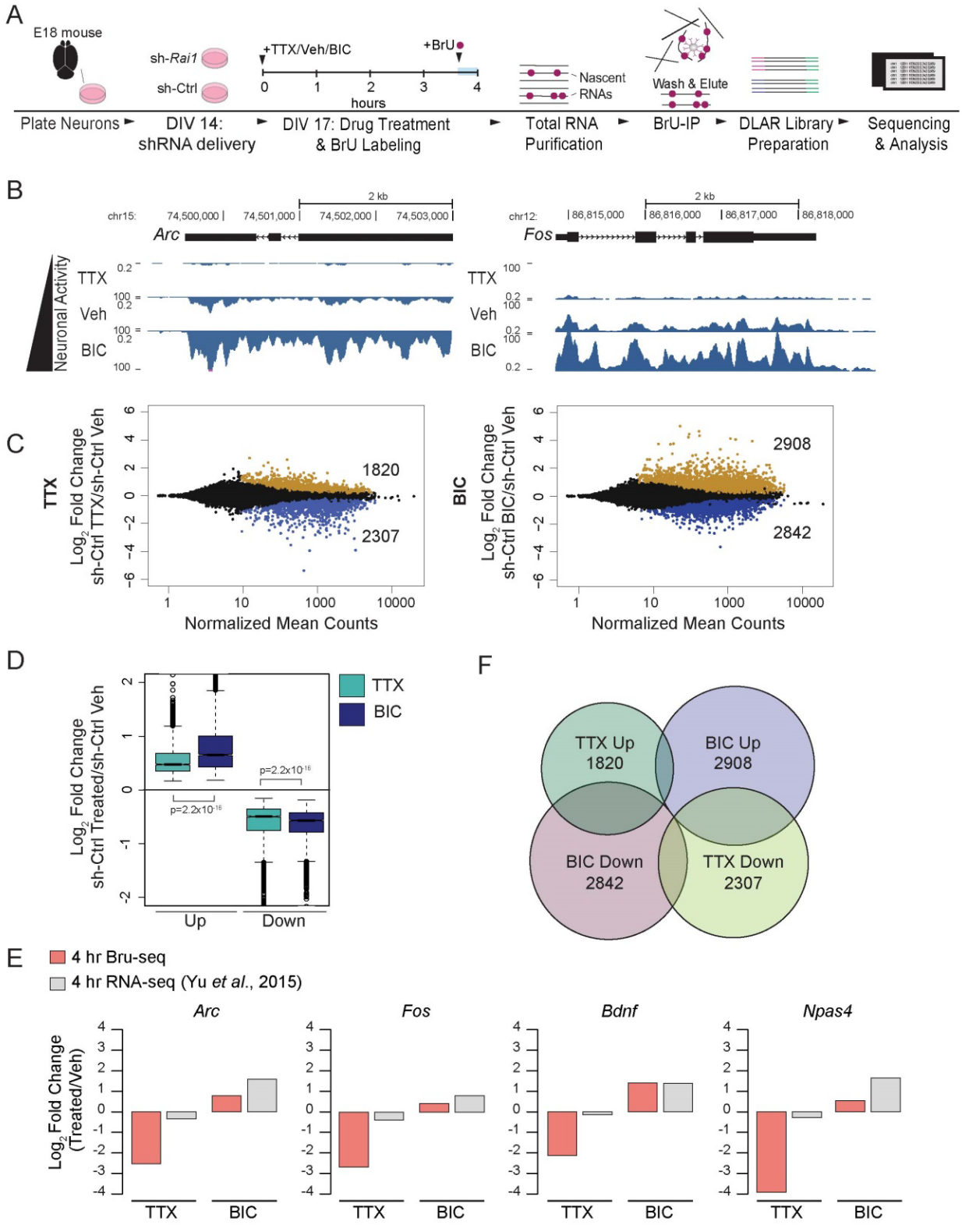
A
E18 mouse
sh-Rai1
sh-Ctrl
+TTX/Veh/BIC
+BrU
0 1 2 3 4
hours
Nascent RNAs
Wash & Elute
Plate Neurons
DIV 14: shRNA delivery
DIV 17: Drug Treatment & BrU Labeling
Total RNA Purification
BrU-IP
DLAR Library Preparation
Sequencing & Analysis
B
chr15: 74,500,000 74,501,000 74,502,000 74,503,000
2 kb
Arc
chr12: 86,815,000 86,816,000 86,817,000 86,818,000
2 kb
Fos
Neuronal Activity
TTX
Veh
BIC
C
TTX
Log2 Fold Change sh-Ctrl TTX/sh-Ctrl Veh
1820
2307
Normalized Mean Counts
BIC
Log2 Fold Change sh-Ctrl BIC/sh-Ctrl Veh
2908
2842
Normalized Mean Counts
D
Log2 Fold Change sh-Ctrl Treated/sh-Ctrl Veh
TTX
BIC
p=2.2x10-16
p=2.2x10-16
Up
Down
F
TTX Up 1820
BIC Up 2908
BIC Down 2842
TTX Down 2307
E
4 hr Bru-seq
4 hr RNA-seq (Yu et al., 2015)
Log2 Fold Change (Treated/Veh)
Arc
Fos
Bdnf
Npas4
TTX
BIC

Figure 2-1. Genome-wide transcriptional response to bi-directional activity alterations.

(A) Experimental procedure.

(B) UCSC Browser views of Bru-seq signals at *Arc* and *Fos*. Intronic reads are characteristic of nascent RNA.

(C) Differential gene expression analysis (DESeq2) reveals widespread transcriptional changes in response to TTX and BIC ($_{padj<}$0.05).

(D) BIC-response genes show a greater median fold change (Wilcoxon rank-sum test, upregulated genes: $p=2.2 \times 10^{-16,}$ downregulated genes: $p=6.9 \times 10^{-16}$). Whiskers represent 1.5 times the inter-quartile range (IQR) and the notch represents the 95% confidence interval of the median.

(E) The majority of TTX and BIC response genes are uniquely regulated (70%). 24% of genes are reciprocally regulated and 6% are commonly regulated.

(F) Downregulation of immediate early gene in the TTX condition is captured more sensitively in Bru-seq data compared to mRNA-seq data (Yu et al., 2015b).

shifts, network activity was elevated by 20 µM bicuculline (BIC, a $GABA_A$-receptor antagonist) or suppressed by 1 µM tetrodotoxin (TTX, a sodium channel blocker) for 4 hours. During the last 20 minutes of BIC or TTX treatment, we added bromouridine (BrU) to the culture medium to label newly synthesized transcripts. We isolated the labeled RNAs using an anti-BrU antibody and subjected them to next-generation sequencing (Fig. 2-1A).

Altered neuronal network activity triggers genome-wide transcriptional changes

Our Bru-seq data set demonstrated the expected induction of *Arc* and *Fos* by BIC (Fig. 2-1B). Abundant intronic reads indicate that detected transcripts were recently generated and yet to be spliced. Other well-characterized activity-dependent genes such as *Npas4*, *Egr1*, *Homer1*, *Tet3*, and *Txnip* also showed expected transcriptional induction. Differential gene expression analysis of the Bru-seq data using DESeq2 [46] revealed widespread transcriptional changes, in which 45% of expressed genes (7,592/16,682) were up- or down-regulated by network activity shifts ($p_{adj} <$ 0.05, Fig.1C). BIC increased transcription of 2,908 genes, while TTX did so for 1,820 genes. The magnitude of transcriptional induction is higher in BIC treatment compared to TTX (Fig. 2-1D). To examine the relationship between nascent and steady-state transcriptomes, we compared our Bru-seq data to published mRNA-seq datasets of mouse cortical neurons treated with TTX or BIC for 4 or 6 hours [21,43] with identical data processing. Our 4-hr Bru-seq results showed a much stronger similarity with 4-hr mRNA-seq compared to 6-hr mRNA-seq data (Fig. 2-2B). Thus, Bru-seq reliably captures known transcriptional responses to bidirectional shifts in network activity.

Bru-seq might be a better approach than mRNA-seq to detect downregulation of transcription, because persistence of RNAs after transcription does not contribute to Bru-seq signals. Indeed, we found significantly larger suppression of *Fos*, *Arc*, *Bdnf*, and *Npas4* (4 to 16-fold) by TTX treatment in Bru-seq compared to mRNA-seq performed with 4-hr BIC/TTX treatments, in which downregulation was less than 2-fold (Fig. 2-1E) [21,43]. The magnitude of upregulation in response to BIC was smaller in Bru-seq, likely because the early transcriptional induction is largely complete four hours after BIC treatment. In a genome-wide scale, Bru-seq allowed us to detect transcriptional suppression of numerous genes (BIC; 2,842, TTX: 2,307). These data highlight an advantage of the Bru-seq approach to probe mechanisms underlying highly-dynamic activity-dependent transcription.

Based on the behavior of well-defined activity-response genes (Fig. 2-1E), one could assume that BIC and TTX trigger reciprocal transcriptional responses. Unexpectedly, only a small fraction of activity-response genes (24%, 1,798/7,592) displayed such mirror images between BIC and TTX treatments (Fig. 2-1F). 6% (487/7,592) of activity-response genes altered their transcription levels in the same direction after BIC and TTX treatments. The remaining majority of genes (70%, 5,307/7,592) responded to BIC or TTX uniquely. These data suggest that synaptic up-scaling and down-scaling involves distinct transcriptional programs.

Recent studies have reported that different cell types such as astrocytes and neuronal subtypes induce distinct sets of genes in an activity-dependent manner [47,48]. We sought to assess the contribution of various cell types in our datasets. Using immunocytochemistry of a set of cell-type markers, NeuN, GAD67, GFAP, CD11b, and Olig2, we estimated that our cultures comprise 41% excitatory neurons, 11% inhibitory neurons, 33% astrocytes, 15% of cells within the oligodendrocyte lineage, and no microglia (Fig. 2-2D-E). We found several non-neuronal genes in our dataset, including *Thbs1*, a synaptic regulator expressed specifically in astrocytes [49]. We detected enrichment of biological processes specific for both neurons and non-neuronal cell types. Intersection of the Bru-seq data with published cell type-enriched genes [50] revealed that the majority (> 80%) of activity-response genes do not exhibit cell-type-specific expression (Fig. 2-2F). Thus, the current dataset represents an aggregate view of transcriptional response occurring in multiple cell types.

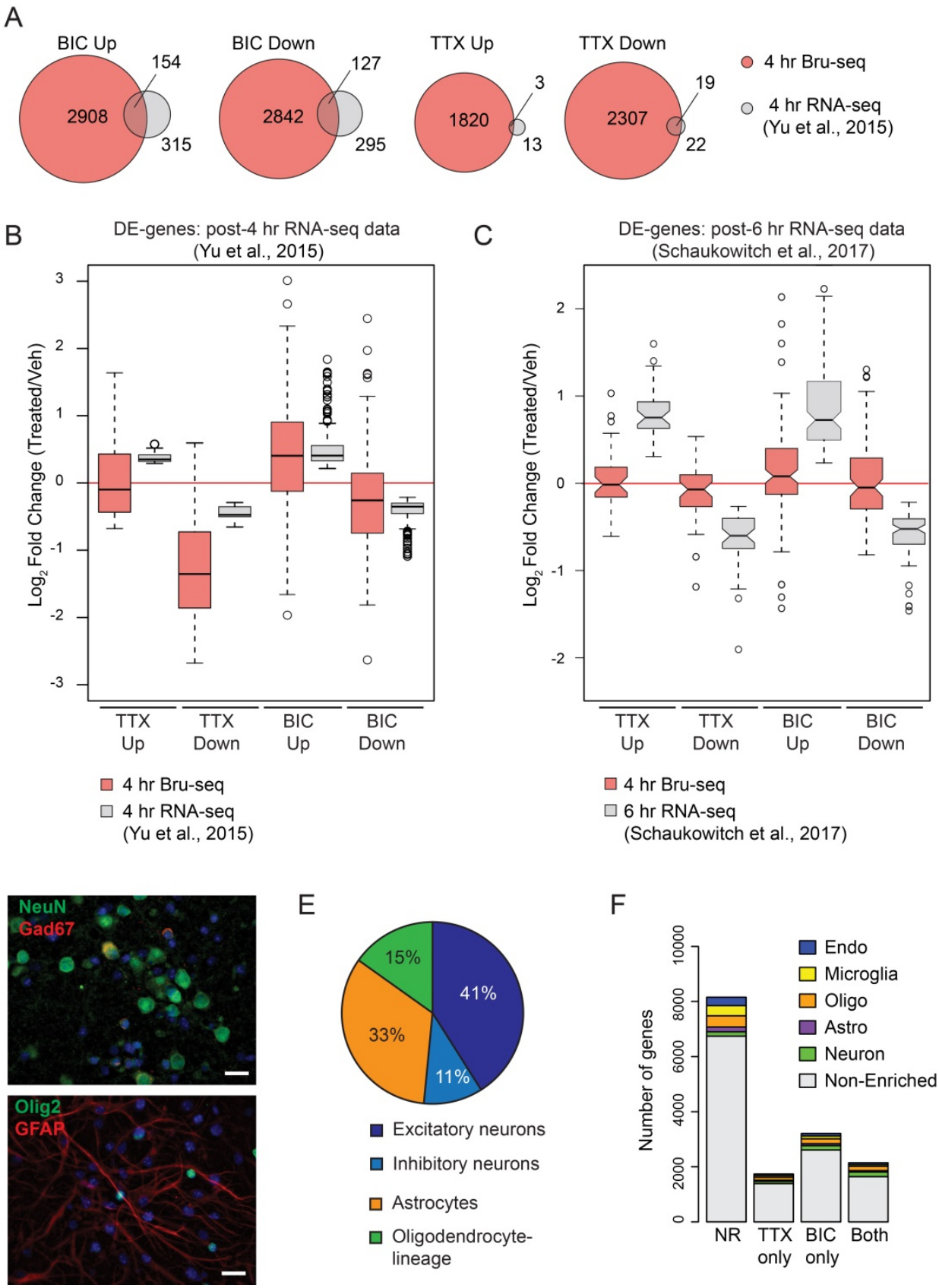
A
BIC Up
154
2908
315
BIC Down
127
2842
295
TTX Up
3
1820
13
TTX Down
19
2307
22
4 hr Bru-seq
4 hr RNA-seq
(Yu et al., 2015)
B
DE-genes: post-4 hr RNA-seq data
(Yu et al., 2015)
Log2 Fold Change (Treated/Veh)
TTX Up
TTX Down
BIC Up
BIC Down
4 hr Bru-seq
4 hr RNA-seq
(Yu et al., 2015)
C
DE-genes: post-6 hr RNA-seq data
(Schaukowitch et al., 2017)
Log2 Fold Change (Treated/Veh)
TTX Up
TTX Down
BIC Up
BIC Down
4 hr Bru-seq
6 hr RNA-seq
(Schaukowitch et al., 2017)
D
NeuN
Gad67
Olig2
GFAP
E
15%
41%
33%
11%
Excitatory neurons
Inhibitory neurons
Astrocytes
Oligodendrocyte-lineage
F
Number of genes
Endo
Microglia
Oligo
Astro
Neuron
Non-Enriched
NR
TTX only
BIC only
Both

Figure 2-2. Bru-seq Validation and Characterization, related to Fig. 2-1.

(A) Overlap of DE genes in Bru-seq and mRNA-seq. DE genes were called using identical DESeq2 parameters. mRNA-seq datasets were obtained from from (Yu et al., 2015b).

(B) Expression changes of DE-genes upon BIC and TTX treatments in Bru-seq and mRNA-seq (4 hr post-treatment) (Yu et al., 2015b).

(C) Comparison of Bru-seq data and mRNA-seq data of 6 hr post-treatment (Schaukowitch et al., 2017).

(D) Representative immunofluorescence images of the primary forebrain neuron culture (DIV17) with antibodies against NeuN, Gad67, GFAP, or Olig2. Nuclei were visualized by DAPI. Scale bar: 20 μm.

(E) Quantification of cell types. Cell types were determined as follow. Excitatory neurons; NeuN(+), Gad67(−), Inhibitory neurons; NeuN(+), Gad67(+), Astrocytes; NeuN(−),GFAP(+), Olig2(−). 33.5%, and Oligodendrocyte lineage cells; NeuN(−), Olig2(+). We did not observe cells with CD11b, a microglia marker. Each cell type was calculated as the % of all DAPI+ cells and shown as an average of two biological replicates.

(F) The number of cell type-specific genes and their response to TTX or BIC in the Bru-seq data. Cell type-specific genes were obtained from mRNA-seq data of separated cells by immunopanning of P7-P17 mouse cortices (Zhang et al., 2014). Oligo: cells within the oligodendrocyte lineage. NR: Non-responsive genes. Both: Genes that respond to both TTX and BIC.

Discussion

In sum, we found widespread transcriptional responses to network activity shifts owing to Bru-seq's high sensitivity in detecting transcriptional downregulation. Most dynamically regulated genes altered by hyperactivity or suppression are unique rather than reciprocal (Fig. 2-1). This is interesting given that gene expression studies have focused on reciprocal regulation of genes (e.g. *Arc*, *Fos*, *Homer1*, *Bdnf*) [51]. Our results agree with a nascent proteome study on rat hippocampal neurons, in which the authors observed unique, common, and reciprocal changes in protein synthesis upon TTX and BIC treatments [52]. These observations suggest that besides the reciprocal transcriptional changes of key factors, distinct transcriptional mechanisms may underlie upscaling and downscaling. Interestingly, a small proportion of genes are coordinately regulated (e.g. upregulated and downregulated during both upscaling and downscaling), suggesting that transitioning from the baseline state may require a common transcriptional response.

The dataset of nascent RNA-sequencing is a resource to discover bona fide transcriptional changes at a specific timepoint during synaptic scaling or after neuronal activation. It lends itself particularly to the examination of motif analysis enrichment in gene regions of interest, e.g.

promoter regions. Indeed, analysis of TTX and BIC response genes in control cultures demonstrated enrichment of specific motifs unique to each gene set. For example, KLF14 is enriched exclusively in BIC-downregulated genes. KLF14 is a transcription factor exclusively expressed in excitatory neurons (Greenberg single cell) and an imprinted, rapidly evolving gene in humans. BIC-downregulated genes have been less well-studied in the role of activity-dependent gene response, and KLF14 may be a key component in this process. Interestingly, BIC-upregulated genes have less strong p-values for enrichment compared to TTX-downregulated genes, suggesting that downregulation in response to TTX is more carefully tuned by site-specific trans factors, while BIC-upregulation may be more dependent on general changes in chromatin state.

What mechanisms could cause transcription to differ between TTX and BIC state? Transcriptional machinery itself is a possible avenue by which TTX and BIC states are controlled. TFIID is composed of TBP and TBP associated factors (TAFs) of which there are 13 types[53]. In our dataset, transcription of TAF1, TAF4, TAF13, and TAF15 are regulated by BIC or TTX. In a nascent proteomic study, TAF9 was found to be upregulated by BIC [52]. This suggests these subunits may be preferentially found in Pol-II complexes in TTX and BIC states. Co-immunoprecipitation of Pol II and its TFIID subunits from cultured excitatory neurons stimulated with TTX or BIC could be analyzed through Western blotting or mass spectrometry to see if there is a significant change in TFIID complex composition. TAF proteins have differential effects on transcription, including transcription of inducible genes at baseline and the return of inducible genes to baseline levels in *Drosophila* models [53,54]. This suggests TAF proteins may have interesting roles in the inducible gene expression in neurons. Another approach may be to overexpress or knockdown expression of these factors and screen for changes in synaptic properties or transcription of key genes. Indeed, mutations in TAF proteins TAF1 and TAF8 have been shown to be associated with neurodevelopmental disorders while having limited impact on non-neuronal transcription, suggesting brain-specific roles for these genes that may converge upon neuronal activity-dependent transcription[55,56].

CHAPTER 3.

RAI1 Regulates Activity-Dependent Nascent Transcription and Synaptic Scaling

Loss of RAI1 function is associated with Smith-Magenis Syndrome

RAI1 is the primary gene implicated in Smith-Magenis syndrome (SMS, MIM: 182290) and Potocki-Lupski Syndrome (PTLS, MIM: 610883, Table 1). SMS is characterized by low intellectual quotient (IQ), delayed motor and speech abilities, altered sleep cycles, obesity, hypotonia, specific craniofacial characteristics, and self-injurious behaviors such as face-slapping and polyembolokoilamania [57,58]. SMS is most commonly associated with heterozygous microdeletions of chromosome 17p11, which span the minimal 1.5 Mb region that contains 13 genes including *RAI1* [59]. Truncation and missense mutations in *RAI1* have been reported in individuals with prototypical SMS, implicating *RAI1* as the major gene contributing to the neurodevelopmental and behavioral symptoms (reviewed in [60,61]).

Interestingly, duplication of the same 17p11.2 interval containing *RAI1* is associated with PTLS [62]. PTLS and SMS share similar symptoms of low IQ and hypotonia. However, in contrast to the obesity and self-injurious behavior in SMS, individuals with PTLS are characterized with reduced body weight, hyperactivity and autistic behaviors. While individuals with SMS experience daytime sleepiness and nighttime awakenings, individuals with PTLS display sleep apnea [61,63]. The 125 kb duplication region common to all PTLS cases overlaps only with *RAI1*, strongly supporting a causative role of *RAI1* duplication in PTLS [64].

RAI1 has also been genetically associated with other autism-related conditions [65] and schizophrenia [66]. RAI1 protein levels were altered in post-mortem prefrontal cortex from patients with schizophrenia, bipolar disorder and major depression [67]. In addition, *RAI1* expression levels

were shown to be commonly decreased in multiple intellectual disability syndromes that are not directly associated with *RAI1* mutations. These include brachydactly with mental retardation (BDMR, MIM: 600430), caused by deletion of *HDAC4*-containing chromosome 2q37 region [68], and 2q23.1 deletion syndrome (MIM: 156200) [69]. This suggests *RAI1* might be a downstream effector in other neuropsychiatric conditions.

Mouse models with syntenic microdeletions or microduplications, *Rai1* knockout, or *Rai1* overexpression, recapitulate learning disabilities, metabolic disorders, craniofacial features, and/or sleep abnormalities observed in SMS or PTLS individuals [70-75 2,76]. These observations strongly suggest that RAI1 exerts an evolutionarily-conserved, dosage-sensitive role in neurodevelopment. RAI1 is expressed in the brain throughout embryonic and adult brain [2,76]. Studies in mouse models and human patient cells have uncovered roles of RAI1 in gene expression, neuronal structure, and behavior [2,70,74,77,78].

However, little is known about RAI1's roles in activity-dependent transcription and synaptic plasticity. Because of the described relevance to neurodevelopment, we then used the Bru-seq approach to uncover a role for RAI1 in this transcriptional program.

RAI1 suppresses the TTX-induced transcriptional program in resting networks

We developed an anti-RAI1 antibody and confirmed that RAI1 protein was present in virtually all MAP2-positive neurons and primarily localized to the nucleus with subtle signals in the soma (Fig. S2A). We found lower RAI1 levels in non-neuronal (MAP2-negative) cell nuclei (Fig. S2A), highlighting its important role in neurons. Widespread presence of RAI1 in neurons is consistent with previous studies [2,79](Fig. S2B-C).

Having established nascent transcription profiling in neural ensembles and presence of RAI1 in the culture, we sought to test if RAI1 has any roles in synaptic scaling and transcriptional responses to altered neuronal activity. We knocked down (KD) *Rai1* in primary cortical cultures using lentiviral vectors (LV) carrying *Rai1*- or scrambled shRNAs (sh-Ctrl). To minimize impact of RAI1 loss on network connectivity, we delivered LV shRNA at DIV14, a time by which functional synapses have formed. The KD achieved near complete loss of RAI1 protein by 3

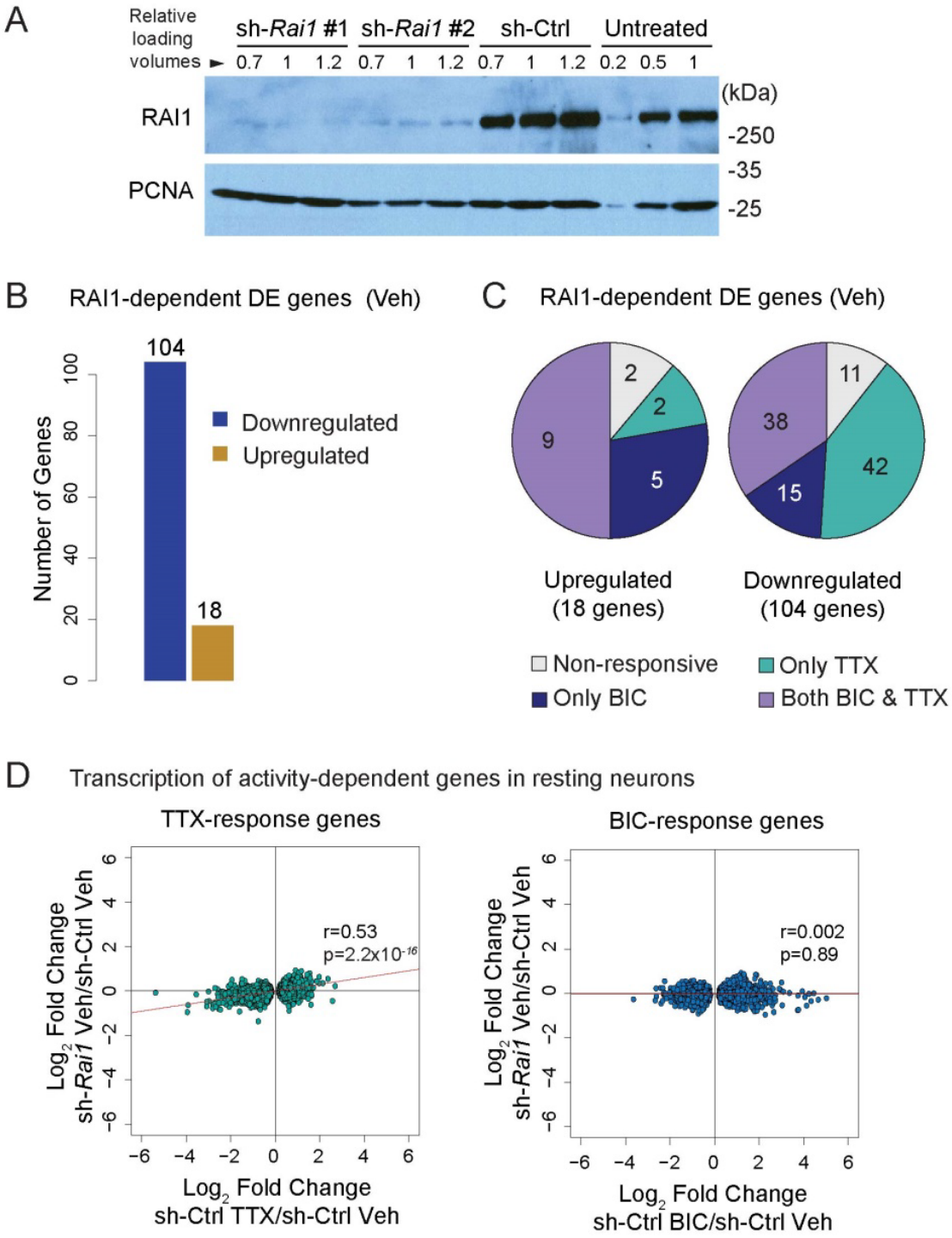

Figure 3-1. *Rai1*-KD alters transcription of TTX-response genes at the baseline.

(A) Validation of *Rai1*-KD with Western blot. Mouse forebrain neuron cultures were transduced with lentivirus expressing sh-*Rai1* or sh-Ctrl for three days.

(B) Number of DESeq2-called differentially expressed genes (sh-Ctrl v sh-*Rai1*, padj<0.05) after Vehicle treatment.

(C) Many *Rai1*-KD DE-genes are TTX and BIC-response genes.

(D) The fold changes of TTX- and BIC-response genes by *Rai1*-KD at baseline. Note that *Rai1*-KD cultures displays transcriptional profile similar to TTX-treated normal cultures. r= Spearman's rank correlation coefficient.

days post-LV infection (Fig. 2A). We then modulated network activity of LV-treated cultures by applying TTX or BIC for four hours and carried out Bru-seq as described above.

We initially tested if *Rai1*-KD alters nascent transcription in control "resting" neuronal cultures with stable basal levels of activity. DESeq2 analysis revealed 122 differentially expressed (DE) genes: 104 downregulated and 18 upregulated following *Rai1*-KD (p_{adj} <0.05, Fig. 3-1B, Table S3). The greater number of downregulated genes is consistent with previous studies [2,58]. A majority of genes altered by *Rai1*-KD at baseline were BIC- or TTX-response genes (Fig. 3-1C). To further characterize the relationship between RAI1 deficiency and BIC- or TTX-response genes, we examined how individual genes behave upon *Rai1*-KD. We found a clear positive correlation between the normal transcriptional response to TTX and the transcriptional impairment by *Rai1*-KD at baseline (Spearman rank correlation coefficient r=0.53, t-test $p=2.2x10^{-16}$, Fig. 3-1D, left panel). BIC-response genes showed no correlation with *Rai1*-KD (Fig. 3-1D, right panel). The group of genes that respond reciprocally to TTX and BIC (Fig. 1F) showed a similar correlation as there was with all TTX-responsive genes (Fig. 3-2D). When we removed all DE genes upon *Rai1*-KD from the plot, the correlation remained significant (r=0.52, $p=2.2x10^{-16}$, Fig. 3-2E), suggesting that the DE genes are not the sole driver for the observed correlation. We also analyzed the published mRNA-seq of the *Rai1*-KO cortices [2] and found a similar trend in expression pattern of the TTX- and BIC-response genes *in vivo* (Fig. 3-2F). These data show that RAI1 deficiency shifts the transcriptional profile towards the TTX-treated state without drug application and that *Rai1*-KD does not affect transcription of non-reciprocal BIC-responsive genes.

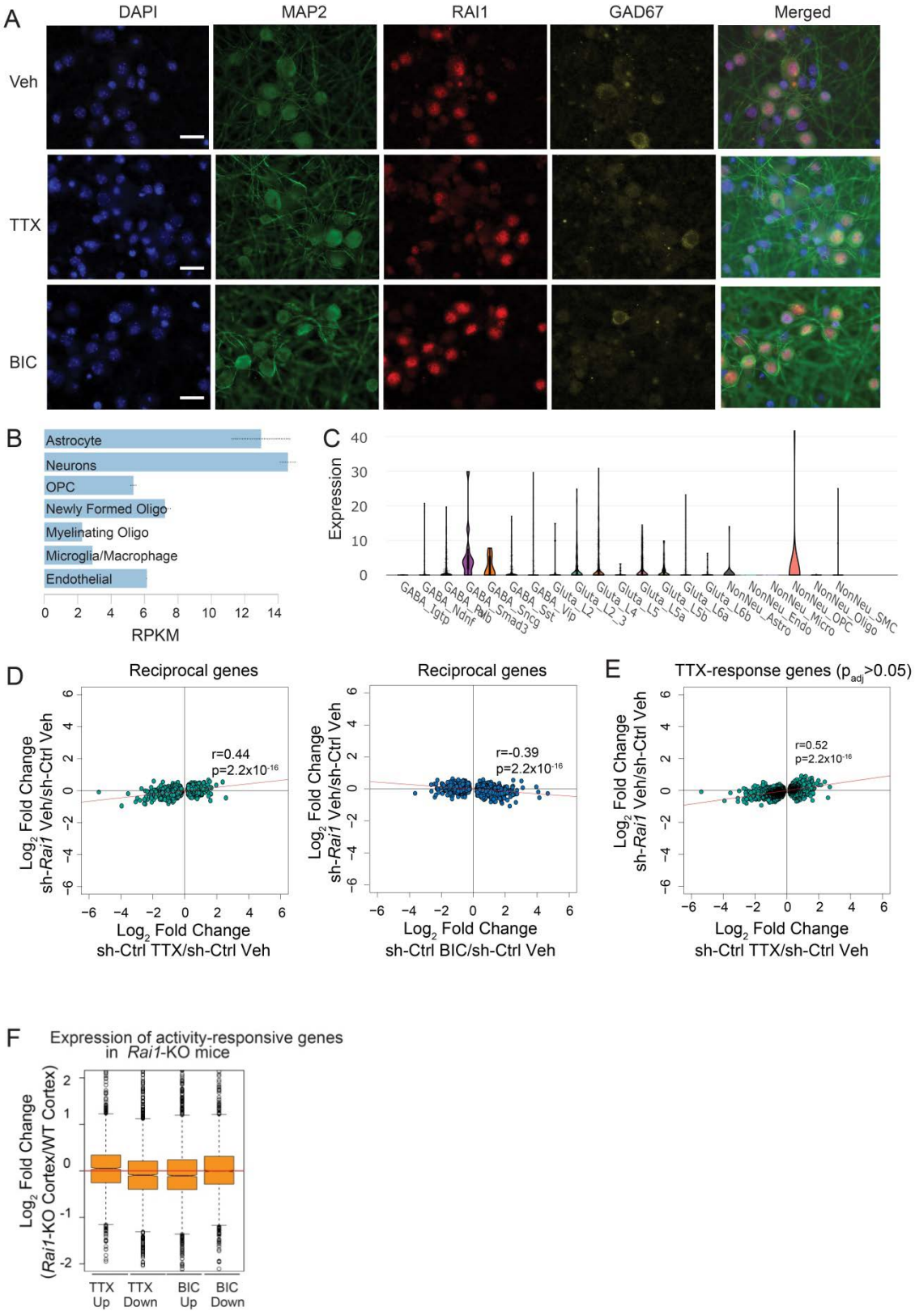
A
DAPI
MAP2
RAI1
GAD67
Merged
Veh
TTX
BIC
B
Astrocyte
Neurons
OPC
Newly Formed Oligo
Myelinating Oligo
Microglia/Macrophage
Endothelial
RPKM
C
Expression
GABA_Igtp
GABA_Ndnf
GABA_Pvlb
GABA_Smad3
GABA_Sncg
GABA_Sst
GABA_Vip
Gluta_L2
Gluta_L2_3
Gluta_L4
Gluta_L5
Gluta_L5a
Gluta_L5b
Gluta_L6a
Gluta_L6b
NonNeu_Astro
NonNeu_Endo
NonNeu_Micro
NonNeu_OPC
NonNeu_Oligo
NonNeu_SMC
D
Reciprocal genes
r=0.44
p=2.2x10-16
Log2 Fold Change sh-Rai1 Veh/sh-Ctrl Veh
Log2 Fold Change sh-Ctrl TTX/sh-Ctrl Veh
Reciprocal genes
r=-0.39
p=2.2x10-16
Log2 Fold Change sh-Rai1 Veh/sh-Ctrl Veh
Log2 Fold Change sh-Ctrl BIC/sh-Ctrl Veh
E
TTX-response genes (padj>0.05)
r=0.52
p=2.2x10-16
Log2 Fold Change sh-Rai1 Veh/sh-Ctrl Veh
Log2 Fold Change sh-Ctrl TTX/sh-Ctrl Veh
F
Expression of activity-responsive genes in Rai1-KO mice
Log2 Fold Change (Rai1-KO Cortex/WT Cortex)
TTX Up
TTX Down
BIC Up
BIC Down

Figure 3-2. RAI1 protein is expressed primarily in neuronal nuclei and supporting figures to Figure 3-1.

(A) Sub-cellular RAI1 localization was assessed by immunofluorescence in the mouse forebrain neuron culture (DIV17) using an anti-RAI1 antibody. RAI1 displayed nuclear localization in excitatory and inhibitory neurons. RAI1 did not show any sub-cellular or sub-nuclear localization by TTX and BIC treatments for 4 hr. We obtained similar results at other time points (15 minutes, 1 hr, 2 hr, 8 hr, and 24 hr, data not shown).

(B) Rai1 mRNA levels in neurons and non-neuronal cells of the adult mouse cortices (Zhang et al., 2014).

(C) Rai1 mRNA levels in single cell mRNA-seq data of mouse visual cortex (Basic et al., 2016).

(D) Transcription of reciprocal genes in the Rai1-KD culture at baseline show a positive correlation with TTX-treated transcriptome and a negative correlation with BIC-treated transcriptome of the normal culture.

(E) Premature TTX-response of Rai1-KD culture is still observed after excluding the RAI1-dependent genes at baseline.

(F) Expression of TTX- and BIC-response genes in the pan-neuronal *Rai1*-knockout (KO) cortex. mRNA-seq data were obtained from 3 week-old *Rai1*flox/flox: *Nestin*-Cre and control mice (Huang et al., 2016). Fold changes in KO vs Control mice were calculated using the RPKM values. The *Rai1*-KO mRNA expression shows a trend of TTX-treated transcription states.

RAI1 deficiency promotes synaptic upscaling

Chronic perturbation of neuronal activity by BIC or TTX induces decreases and increases in synaptic strength, which respectively, underlie homeostatic synaptic downscaling and upscaling [13-15]. Given that *Rai1*-KD shifted the nascent transcriptome towards the TTX-like state, we asked whether *Rai1*-KD would similarly shift excitatory synapse function towards a state similar to synaptic upscaling. We used sparse transfection of DIV12-14 hippocampal cultures with either *Rai1*- or scrambled shRNA, and recorded miniature excitatory postsynaptic currents (mEPSCs) from transfected pyramidal-like neurons 48 hours later. If *Rai1*-KD induces synaptic strengthening in a cell-autonomous manner, we would expect to see a rightward shift in the distribution of mEPSC amplitudes as is observed during synaptic upscaling following chronic activity suppression with TTX. Consistent with this idea, we found that the expression of two distinct shRNAs targeting *Rai1* mRNA each induced a significant increase in baseline mEPSC amplitude (Fig. 3-3A-B), without significantly altering mEPSC frequency or decay time (Fig. 3-3C-D and Fig. 3-4A-E). Moreover, *Rai1*-KD induced a clear rightward shift in the cumulative probability distribution of mEPSC amplitudes relative to control neurons (Fig. 3-3E and Fig. 3-4E), an effect that was significantly (albeit partially) rescued by expression of RNAi-resistant RAI1 ($F(2, 41) = 4.452$, $p = 0.017$. sh-Ctrl, sh-*Rai1* #1 and Rescue: n = 15, 15 and 14, sh-Ctrl vs. sh-*Rai1* #1; $p=0.068$, sh-*Rai1* #1 vs. Rescue; $p = 0.0359$, sh-Ctrl vs. sh-*Rai1* #2: n = 14-13, $p = 0.0012$, Fig. 3A-E). The shift in distribution of mEPSC amplitudes with *Rai1*-KD bears a

striking similarity to changes in mEPSC distributions following chronic TTX treatment (Fig. 3-3F), although *Rai1*-KD did not shift mEPSC amplitudes to quite the same degree as TTX. An increase in surface expression of AMPA receptors (AMPARs) at synapses is a signature of synaptic upscaling following activity suppression. Consistent with previous observations, surface expression of the GluA1 AMPAR subunit at PSD-95-labeled excitatory synapses is significantly increased following chronic (24 hr) TTX treatment (sh-Ctrl Vehicle vs. TTX: n = 13-12, p = 0.0019, Fig. 3-3G); likewise, we found a similar enhancement of surface GluA1 at synapses following 72 hr *Rai1*-KD (sh-Ctrl vs. sh-*Rai1*: n = 6-6 p = 0.0065, Fig. 3-3G). Together, these

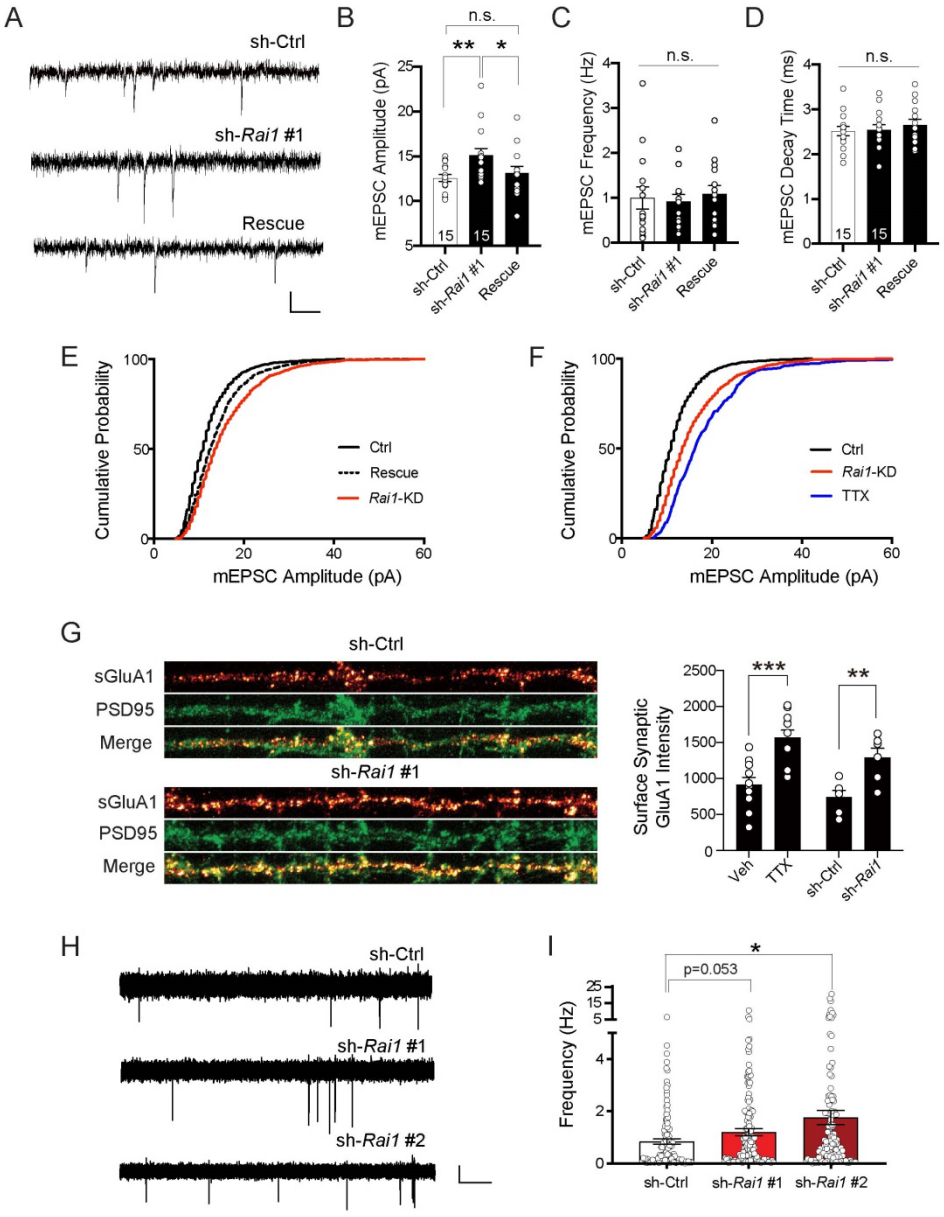

Figure 3-3. *Rai1*-KD increases the synaptic efficacy at baseline activity condition.

(A-D) Example traces and mean ± SEM mEPSC amplitude (B), frequency (C), and decay time (D) for cultured rat hippocampal primary neurons recorded after transient transfection (48 hr) with either non-targeting shRNA (sh-Ctrl), Rai1 targeting shRNA or sh-*Rai1* #1 with RNAi resistant RAi1 expressing construct (Rescue) at DIV12-14. Scale bar, 10 pA, 75 ms (sh-Ctrl, sh-*Rai1* #1 and Rescue, n = 15, 15 and 14, respectively)

(E) Cumulative distribution of mEPSC amplitudes of sh-Ctrl (left), sh-*Rai11* (middle) or Rescue (right) transfected neurons.

(F) Cumulative distribution of mEPSC amplitudes of sh-Ctrl transfected neurons treated by either vehicle or 1 µM TTX (left) and sh-Ctrl or sh-*Rai1* transfected neurons (right).

(G) Representative images of surface GluA1 (sGluA1, fire), PSD-95 (green) and sGluA1 & PSD-95 (merge) of sh-Ctrl and sh-*Rai1* infected dendrites. Scale bar 10 µm. Bar graph of mean sGluA1 signal intensity in PSD-95 positive regions for vehicle or TTX (n = 13-12), and sh-Ctrl or sh-*Rai1* (n = 6-6) treated neurons. All bar graphs represent mean ± SEM. One-way ANOVA, followed by post-hoc Fisher's LSD test were performed for B-D and unpaired Student's t-tests were performed for G. *p < 0.05, **p < 0.01, ***p < 0.001

(H) Prototypical local field potential recordings from individual electrodes exhibiting a single neuronal unit from cultures transfected with: sh-Ctrl, sh-*Rai1* #1 or sh-*Rai1* #2 lentivirus. Scale bars are 25 ms and 10 µV, 25 µV or 40 µV for sh-Ctrl, sh-*Rai1* #1, and sh-*Rai1* #2, respectively.

(I) Firing frequency of individual neuronal units recorded from cultures transfected with sh-Ctrl, sh-*Rai1* #1, or sh-*Rai1* #2 (n = 115, 140, and 131, for sh-Ctrl, sh-*Rai1* #1 or sh-*Rai1* #2, respectively). Statistical comparisons were made using Kruskal-Wallis test followed by post-hoc Dunn's multiple comparisons test. K-W: 9.358, p value 0.0003. Bar graphs represent mean ± SEM. Significance in Dunn's test indicated by **p < 0.01, ***p < 0.001.

results suggest that reduced *Rai1* expression induces functional changes in excitatory synaptic function that mimic synaptic upscaling induced by activity suppression.

Two scenarios could explain the increase in mEPSC amplitude by *Rai1*-KD accompanied by TTX-like transcription in resting neurons. The first possibility is that *Rai1*-KD suppresses network activity, which in turn, indirectly promotes a TTX-like transcriptional program and synaptic upscaling. An alternative possibility is that release of RAI1-mediated suppression of a TTX-responsive transcriptional program directly upscales synapse function. To distinguish these possibilities, we measured ongoing basal network activity of control hippocampal cultures and *Rai1*-KD cultures using 60 channel microelectrode arrays (MEAs, Fig. 3-4F-G). On DIV 11, we transduced the cultures with LV control- or *Rai1*-shRNA and recorded network activity on DIV 14. We used semi-automatic principal component analysis to sort individual neuronal units (Figure 3-4H-K). If the changes in mEPSCs and transcriptional dynamics are an indirect effect secondary to *Rai1*-KD suppressing network activity, then we would predict a marked decrease in neural firing. Contrary to this prediction, *Rai1*-KD did not suppress firing in the network, and instead led to 1.4-2.1-fold increase in spontaneous firing rate compared to scrambled shRNA

(Fig. 3-3H-I, Kruskal-Wallis test: 9.36, $p = 0.009$; Dunn's post-hoc test: sh-Ctrl vs sh-*Rai1* #1 $p = 0.053$; sh-Ctrl vs sh-*Rai1* #2 $p = 0.010$) likely due to enhanced excitatory drive that accompanies *Rai1*-KD-mediated synaptic strengthening. These data thus support the second explanation, where RAI1 suppresses a TTX-responsive transcriptional program and synaptic upscaling in naïve neural networks.

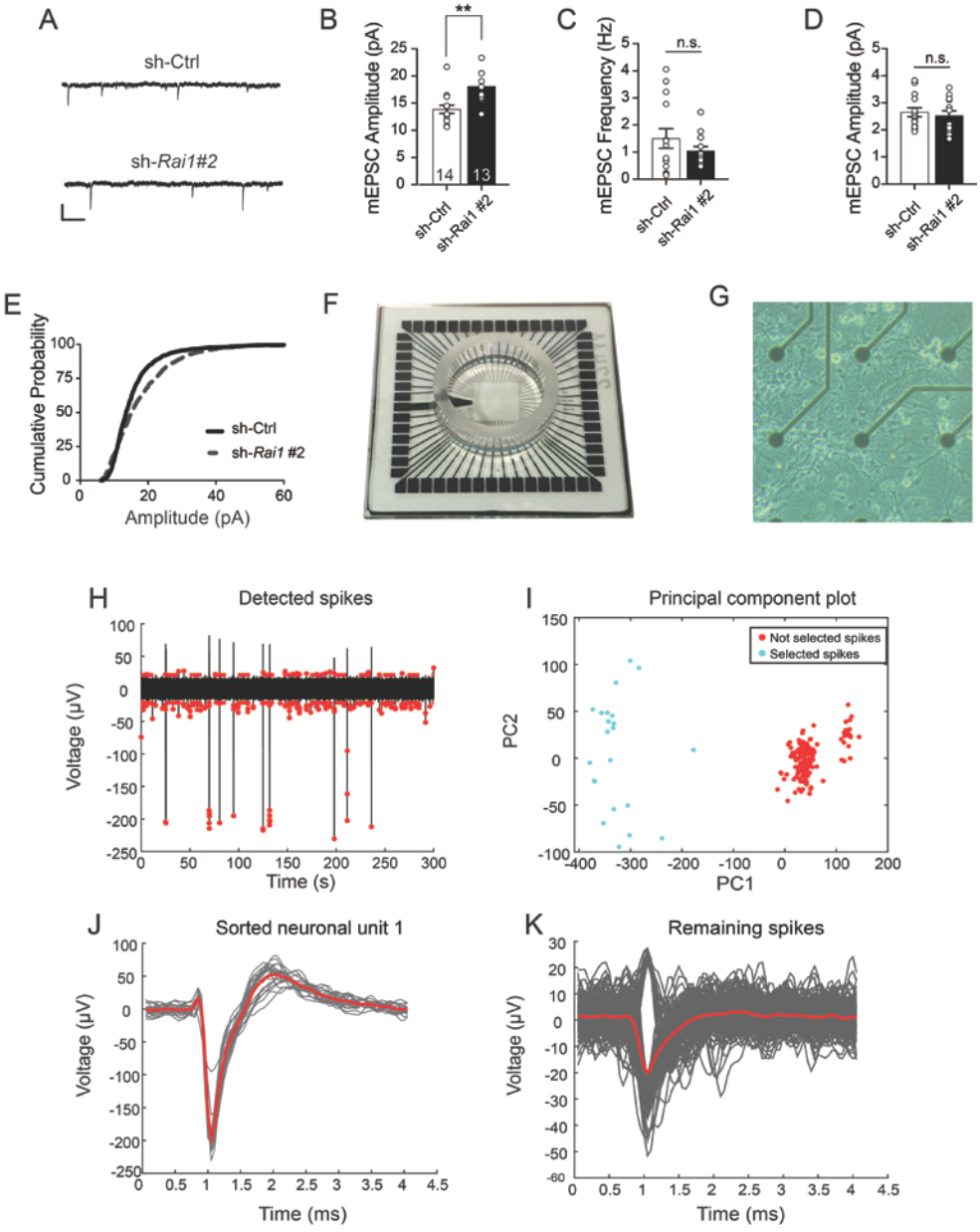

Figure 3-4. Electrophysiology of Rai1-KD cultures at baseline, related to Fig. 3-3.

(A-D) Example traces and mean ± SEM mEPSC amplitude (B), frequency (C), and decay time (D) for cultured rat hippocampal primary neurons recorded after transient transfection (48 hr) with either non-targeting shRNA (sh-Ctrl) or *Rai1*-shRNA (sh-*Rai1* #2) at DIV12-14. Scale bar, 10 pA, 75 ms (sh-Ctrl, sh-*Rai1* #2; n =14-13)

(E) Cumulative distribution of mEPSC amplitudes of sh-Ctrl (solid) and sh-*Rai1* #2 (dot)-transfected neurons. All bar graphs are represented as mean ± SEM, and unpaired Student's t-tests were performed. **$p < 0.01$

(F) Representative macroscopic image of a 60 channel multielectrode array (MEA) chip.

(G) Brightfield micrograph of dissociated hippocampal neurons growing on an MEA showing multiple cells near electrodes.

(H) Representative local field potential trace exhibiting multiple neuronal units. Each red asterisk indicates a single detected spike.

(I) Representative principal component plot of spike sorting algorithm. Cyan dots represent spikes that were included in the current neuronal unit, red dots represent spikes that were excluded and subsequently resorted for identification of other neuronal units.

(J) Resulting neuronal unit identified from spikes sorted in C. Red foreground trace represents mean spike waveform, individual spike waveforms shown in grey.

(K) Spikes that were excluded from Neuronal Unit 1 (red dots from C) were further sorted to identify additional neuronal units. Blue line represents the mean waveform of the excluded spikes, grey lines represent individual spike waveforms.

RAI1 promotes transcriptional responses triggered by reductions in network activity

Having uncovered that RAI1 was essential to suppress the TTX-associated transcriptional program under basal activity conditions (Fig. 3-2), we next tested if *Rai1*-KD has any impact on transcriptional responses to TTX and BIC treatments. By calculating fold-changes of transcription, we found that *Rai1*-KD led to a significant impairment of transcriptional response to TTX, while transcriptional responses to BIC were slightly weaker only for downregulation (Fig. 3-5A). However, in contrast to the 130 genes transcriptionally altered at baseline, DESeq2 comparing *Rai1*-KD and control revealed only 8 DE genes after TTX or BIC treatment, indicating that the impact of *Rai1*-KD is greater in resting neurons compared to drug-treated neurons (Fig. 3-5B).

We then sought to determine if the strongly-impaired transcriptional response to TTX (Fig. 3-5A) was due entirely to the TTX-like transcriptional state of *Rai1*-KD culture at baseline or if RAI1 also contributes to the transcriptional response to TTX. Differential gene expression analysis by DESeq2 relies on an arbitrary statistical significance cutoff to report differentially expressed genes. However, the individual gene plot in the baseline condition revealed a global transcriptional trend resulting from minor changes in many genes including those that failed to achieve statistical significance (Fig. 3-6E). To define the impact of RAI1 loss after TTX- and BIC-treatment, we therefore used this individual-gene plot approach. We found that, after TTX treatment, the transcriptional changes of TTX-response genes in *Rai1*-KD cultures inversely correlate with their changes upon TTX treatment in the control condition (Fig. 3-5C, left panel, Spearman rank correlation coefficient r=0.32, t-test $p=2.2x10^{-16}$). This result indicates both incomplete downregulation and upregulation upon TTX treatment independent of the impact of *Rai1*-KD in the resting state. The same TTX-response genes did not show obvious changes after BIC treatment of *Rai1*-KD culture (Fig. 3-6A, left panel). Transcription of the BIC-response genes did not show changes by *Rai1*-KD under any condition (Fig. 3-5C, right panel and Fig. 3-6A, right panel). Thus, *Rai1*-deficiency leads to a subtle yet widespread impairment of the transcriptional response to TTX but not to BIC. Taken together, these results led us to conclude that RAI1 is selectively required for the transcriptional response driven by network activity suppression.

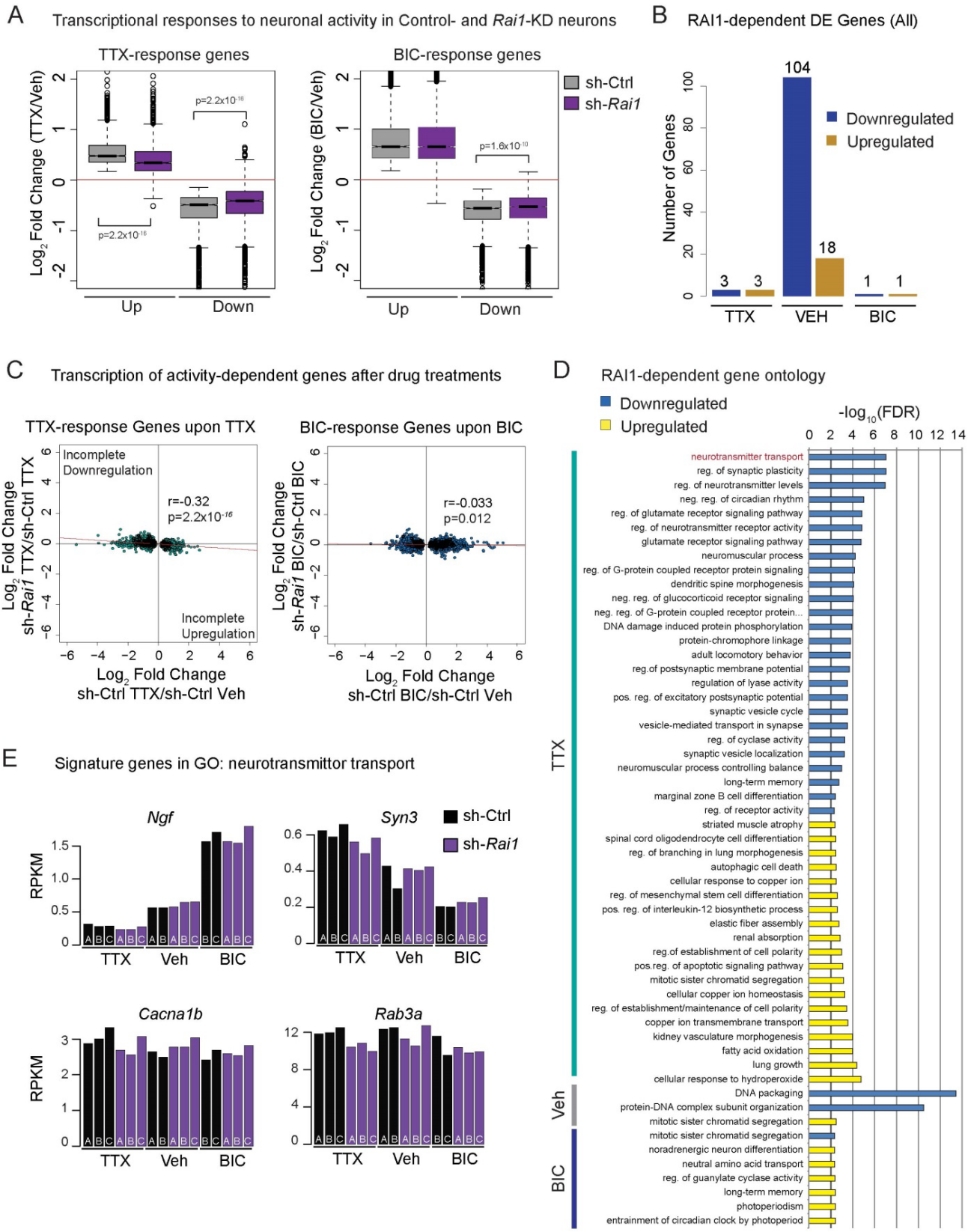
A
Transcriptional responses to neuronal activity in Control- and Rai1-KD neurons
TTX-response genes
BIC-response genes
sh-Ctrl
sh-Rai1
Log2 Fold Change (TTX/Veh)
Log2 Fold Change (BIC/Veh)
p=2.2x10-16
p=2.2x10-16
p=1.6x10-10
Up
Down
B
RAI1-dependent DE Genes (All)
Number of Genes
Downregulated
Upregulated
104
18
3
3
1
1
TTX
VEH
BIC
C
Transcription of activity-dependent genes after drug treatments
TTX-response Genes upon TTX
BIC-response Genes upon BIC
Incomplete Downregulation
Incomplete Upregulation
r=-0.32
p=2.2x10-16
r=-0.033
p=0.012
Log2 Fold Change sh-Rai1 TTX/sh-Ctrl TTX
Log2 Fold Change sh-Rai1 BIC/sh-Ctrl BIC
Log2 Fold Change sh-Ctrl TTX/sh-Ctrl Veh
Log2 Fold Change sh-Ctrl BIC/sh-Ctrl Veh
D
RAI1-dependent gene ontology
Downregulated
Upregulated
-log10(FDR)
neurotransmitter transport
reg. of synaptic plasticity
reg. of neurotransmitter levels
neg. reg. of circadian rhythm
reg. of glutamate receptor signaling pathway
reg. of neurotransmitter receptor activity
glutamate receptor signaling pathway
neuromuscular process
reg. of G-protein coupled receptor protein signaling
dendritic spine morphogenesis
neg. reg. of glucocorticoid receptor signaling
neg. reg. of G-protein coupled receptor protein...
DNA damage induced protein phosphorylation
protein-chromophore linkage
adult locomotory behavior
reg.of postsynaptic membrane potential
regulation of lyase activity
pos. reg. of excitatory postsynaptic potential
synaptic vesicle cycle
vesicle-mediated transport in synapse
reg. of cyclase activity
synaptic vesicle localization
neuromuscular process controlling balance
long-term memory
marginal zone B cell differentiation
reg. of receptor activity
striated muscle atrophy
spinal cord oligodendrocyte cell differentiation
reg. of branching in lung morphogenesis
autophagic cell death
cellular response to copper ion
reg. of mesenchymal stem cell differentiation
pos. reg. of interleukin-12 biosynthetic process
elastic fiber assembly
renal absorption
reg.of establishment of cell polarity
pos.reg. of apoptotic signaling pathway
mitotic sister chromatid segregation
cellular copper ion homeostasis
reg. of establishment/maintenance of cell polarity
copper ion transmembrane transport
kidney vasculature morphogenesis
fatty acid oxidation
lung growth
cellular response to hydroperoxide
DNA packaging
protein-DNA complex subunit organization
mitotic sister chromatid segregation
mitotic sister chromatid segregation
noradrenergic neuron differentiation
neutral amino acid transport
reg. of guanylate cyclase activity
long-term memory
photoperiodism
entrainment of circadian clock by photoperiod
TTX
Veh
BIC
E
Signature genes in GO: neurotransmittor transport
Ngf
Syn3
Cacna1b
Rab3a
sh-Ctrl
sh-Rai1
RPKM
TTX
Veh
BIC

Figure 3-5. RAI1 positively regulates the transcriptional response to TTX.

(A) The fold changes of TTX- and BIC-response genes in cultures treated by sh-Ctrl or sh-*Rai1* (Wilcoxon rank-sum test). Whiskers represent 1.5 times IQR and the notch represents the 95% confidence interval of the median.

(B) Number of DESeq2-called differentially expressed genes (sh-Ctrl v sh-*Rai1*, $p_{adj}<0.05$) after TTX, Vehicle, or BIC treatment.

(C) Incomplete downregulation and upregulation of genes by TTX (left) but not by BIC (right) in *Rai1*-KD cultures. "r" and "p": Spearman's rank correlation coefficient and p values.

(D) RAI1-dependent gene ontologies (Biological Process, padj <0.005) discovered by RNA-Enrich (Lee et al., 2016) and filtered by ReviGO software (Supek et al., 2011).

(E) RPKM values of four Sig-genes downregulated by *Rai1*-KD in the TTX-treated condition. The Sig-genes represent "neurotransmitter transport" (p_{adj} =9.3x10-8), the top-downregulated Biological Processes. The remaining Sig-genes are shown in Figure 3-6. Note slight but consistent inter-replicate changes upon *Rai1*-KD.

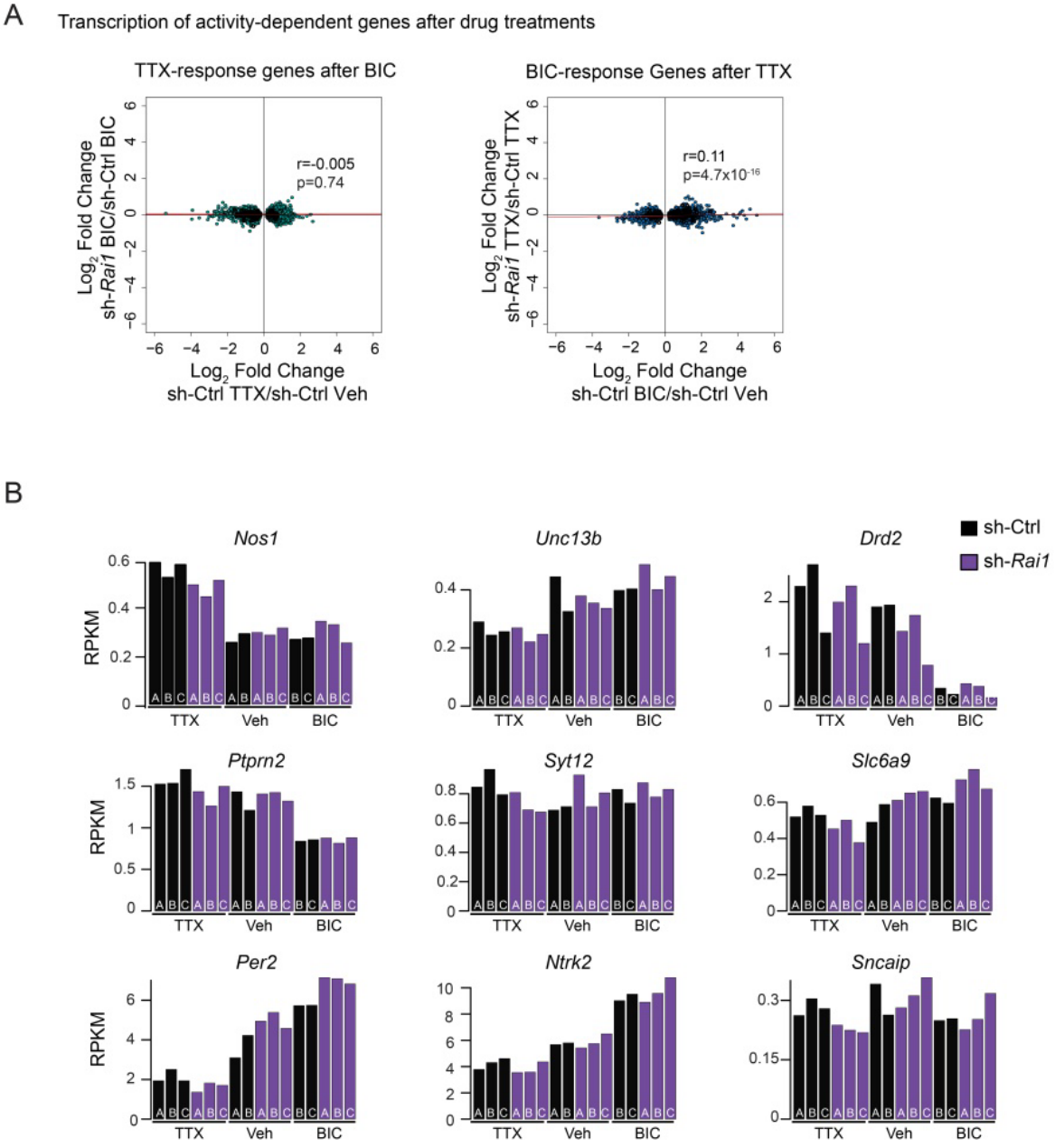

Figure 3-6. Impact of RAI1 loss on transcription after TTX- or BIC-treatments, related to Fig. 3-5.

(A) The fold changes of TTX- and BIC-response genes by *Rai1*-KD after the opposite treatment (BIC or TTX, respectively).

(B) RPKM values of Bru-seq data are represented for Sig-genes of "neurotransmitter transport", which was downregulated by *Rai1*-KD in the post-TTX condition (p_{adj}: 9.3 x 10^{-8}). Note consistent reduction in RPKM across biological replicates in *Rai1*-KD culture in the TTX-treated condition.

We then explored biological implications for the impaired transcriptional response to TTX. We used RNA-Enrich, a gene ontology algorithm, which takes into account weaker changes in gene expression [80,81]. Notably, RNA-Enrich identified many more RAI1-dependent biological processes after TTX treatment than vehicle- or BIC treatments (45 in TTX-, 3 in vehicle-, and 7 in BIC-treated cultures, Fig. 3-5D). The p_{adj} values were evidently lower in the post-TTX transcriptome data compared to BIC conditions. The RAI1-dependent gene ontologies after TTX treatment represent synapse-related processes, whereas those altered in the BIC and vehicle-treated conditions show fewer ontologies directly relevant to neuronal activity (Fig. 3-5D). RNA-Enrich provides the identity of signature genes, called Sig-genes, which significantly contributed to the enrichment of an ontology [80,81]. As expected, Sig-genes for the synapse-related ontologies, including *Ngf*, *Syn3*, *Cacna1b*, *Rab3a,* showed mild yet reproducible transcriptional changes upon *Rai1*-KD (Fig. 3-5E and Fig. 3-6B).

RAI1 dissociates from chromatin in response to activity changes

The activity state-dependent requirement of RAI1 in regulating transcription led us to hypothesize that activity shifts of neuronal network might alter RAI1 distribution on chromatin. To test this, we performed chromatin immunoprecipitation coupled with deep sequencing (ChIP-seq) for RAI1 in DIV17 neuronal cultures treated for 4 hr with TTX, BIC, or Vehicle. We observed clear RAI1-binding at the promoters of RAI1-dependent genes such as *Homer1* and *Per2* (Fig. 3-7A). The control ChIP using *Rai1*-KD cultures showed no such events, demonstrating the specificity of ChIP experiments. RAI1 binding was much weaker in TTX- or BIC-treated cultures (Fig. 3-7A). Consistent with visual observations, peak calling identified only 13 RAI1 peaks across all three *Rai1*-KD ChIP-seq samples (not shown), and they were removed from all subsequent analyses. In control cells, 6,065 RAI1 peaks were found in the Vehicle-treated condition, and a drastic reduction of RAI1 peaks upon TTX- (98 peaks) and the BIC- (1 peak) treatments (Fig. 3-7B). Variable ChIP efficiency or sequencing depth cannot explain the scarce peaks in TTX- and BIC- conditions, because we spiked in *Drosophila* chromatin and fly-specific H2Av antibody and ensured consistent sequencing depth and ChIP efficiency across the samples (Fig. 3-8A). Neither RAI1 protein levels (Fig. 3-8B) nor did nuclear localization (Fig. 3-2A) change after TTX- or BIC treatments. Thus, activity alterations

largely release RAI1 from chromatin, which is remarkably consistent with the greater number of RAI1-dependent genes in resting neurons (Fig. 3-5B).

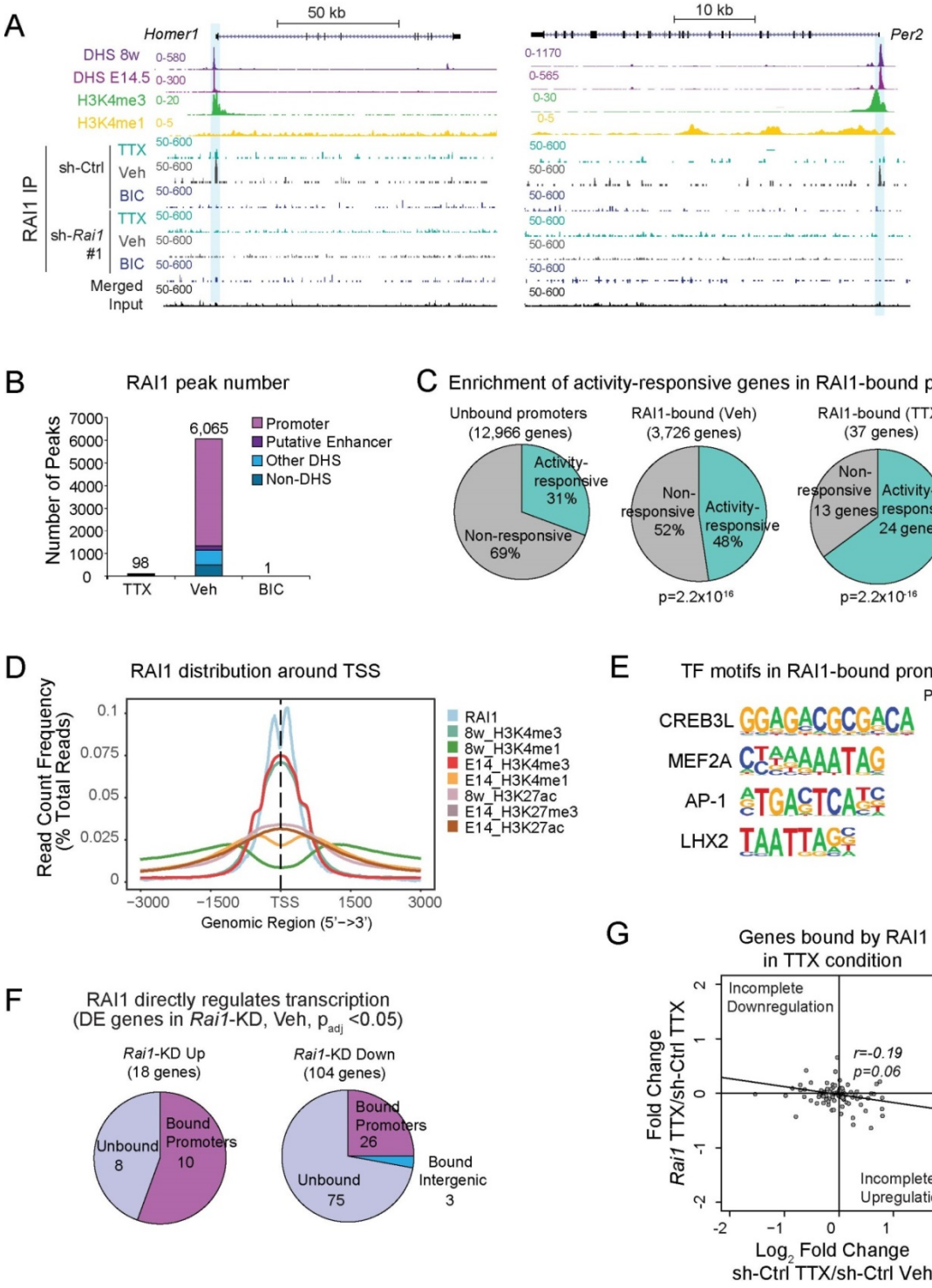

Figure 3-7. Activity-dependent chromatin engagement of RAI1.

(A) UCSC Browser view of RAI1 ChIP-seq signals at *Rai1*-dependent genes *Homer1* and *Per2*.

(B) Number of RAI1 peaks in TTX-, Vehicle-, or BIC- treated cultures.

(C) RAI1-bound promoters are enriched for activity-response genes (Chi-square test, $p = 2.2e^{-16}$).

(D) Bimodal RAI1 distribution around TSS. H3K4me3, H3K4me1, H3K27me3, and H3K27ac levels are plotted as controls (see methods).

(E) Activity-dependent TF motifs enriched in RAI1 peaks.

(F) RAI1 directly up- and down-regulates the transcription in the naïve culture (See Fig. S10E for a statistical enrichment).

(G) RAI1-bound genes in the TTX condition showed incomplete induction and suppression by TTX in *Rai1*-KD cells.

RAI1 directly controls activity-responsive gene transcription in stable networks

Intersection with Bru-seq data revealed that that RAI1-bound genes are much more likely responsive to network activity shifts than RAI1-free genes ($p < 2.2x10^{-16}$, Chi-square test, Fig. 3-7C and Fig. 3-8C). Consistently, RAI1-bound genes associated with plasticity-related ontologies including synapse organization (Fig. S5D). Most of these peaks are present at the promoters in the resting culture (Fig. 5B) and exhibited a bimodal distribution around transcription start sites (TSS) that harbor H3K4me3 (Fig. 5D). Binding motifs of activity-dependent transcription factors (TFs), e.g. MEF2A, AP1, LHX2, CREB3L, are enriched in RAI1-bound promoters (Fig. 3-7D). RAI1 also occupied intra- and intergenic regions. In the resting culture, 54% of such non-promoter regions overlapped with DNAse-I hypersensitivity sites (DHS) identified in 8-week old mouse whole-brain [82], and the rest were DHS-free (Fig. 3-7B). Some RAI1-bound DHS coincided with H3K4me1 or H3K27ac [83], indicating that these elements are likely transcriptional enhancers (Fig. 3-7B, see methods). A substantial fraction (67%) of RAI1 peaks overlapped with previously reported RAI1 peaks in adult mouse brain [2] with common TF motifs (Fig. 3-8E-F). In sum, these analyses show that RAI1 preferentially engages activity-responsive promoters with H3K4me3 in neural networks with stable basal levels of activity.

Are the RAI1-dependent genes found in Bru-seq direct targets of RAI1? Of the genes up- or down-regulated by *Rai1*-KD, RAI1 occupied 40/122 genes (30%) in the baseline culture, which is significantly higher than the genomic average ($p < 0.05$, Chi-square test, Fig. 3-8G). The direct

targets of RAI1 can be up- or down-regulated upon RAI1 loss. Of the 18 genes upregulated by *Rai1*-KD, RAI1 binds to 10 promoters (Fig. 3-7F), while RAI1 occupies 29/104 genes downregulated by *Rai1*-KD. These results support the idea that RAI1 employs both positive and negative regulation to repress the TTX-like transcription state in cultures with stable basal levels of activity (Fig. 3-3B-D). Of note, BIC-response genes, which show no dependence on RAI1, also showed RAI1-peak enrichment (Fig. 3-8C); therefore, RAI1 at these genes is dispensable for suppressing BIC-triggered transcription.

RAI1 directly contributes to transcriptional response to TTX

Finally, we inspected the 98 RAI1 peaks found in TTX-treated cultures, because we detected a compromised transcriptional response of *Rai1*-KD cells to TTX (Fig. 3-5C-E). Most of these peaks were common between the TTX and Veh conditions (promoter-occupied: 89% overlap, non-promoter-occupied: 77% overlap, Fig. 3-8H). We found a much greater proportion of non-promoter peaks (60%) compared to the resting cells (22%) (Fig. 3-8I). Thus, RAI1 at non-promoter regions preferentially persists when network activity decreases. The genes bound or nearest to these RAI1-TTX peaks showed incomplete induction and suppression upon TTX treatment of *Rai1*-KD culture (Fig. 3-7G) but not upon BIC treatment (Fig. 3-8J). These results suggest that RAI1 directly contributes to the transcriptional response (both negative and positive) to TTX and that this role involves primarily non-promoter regulation.

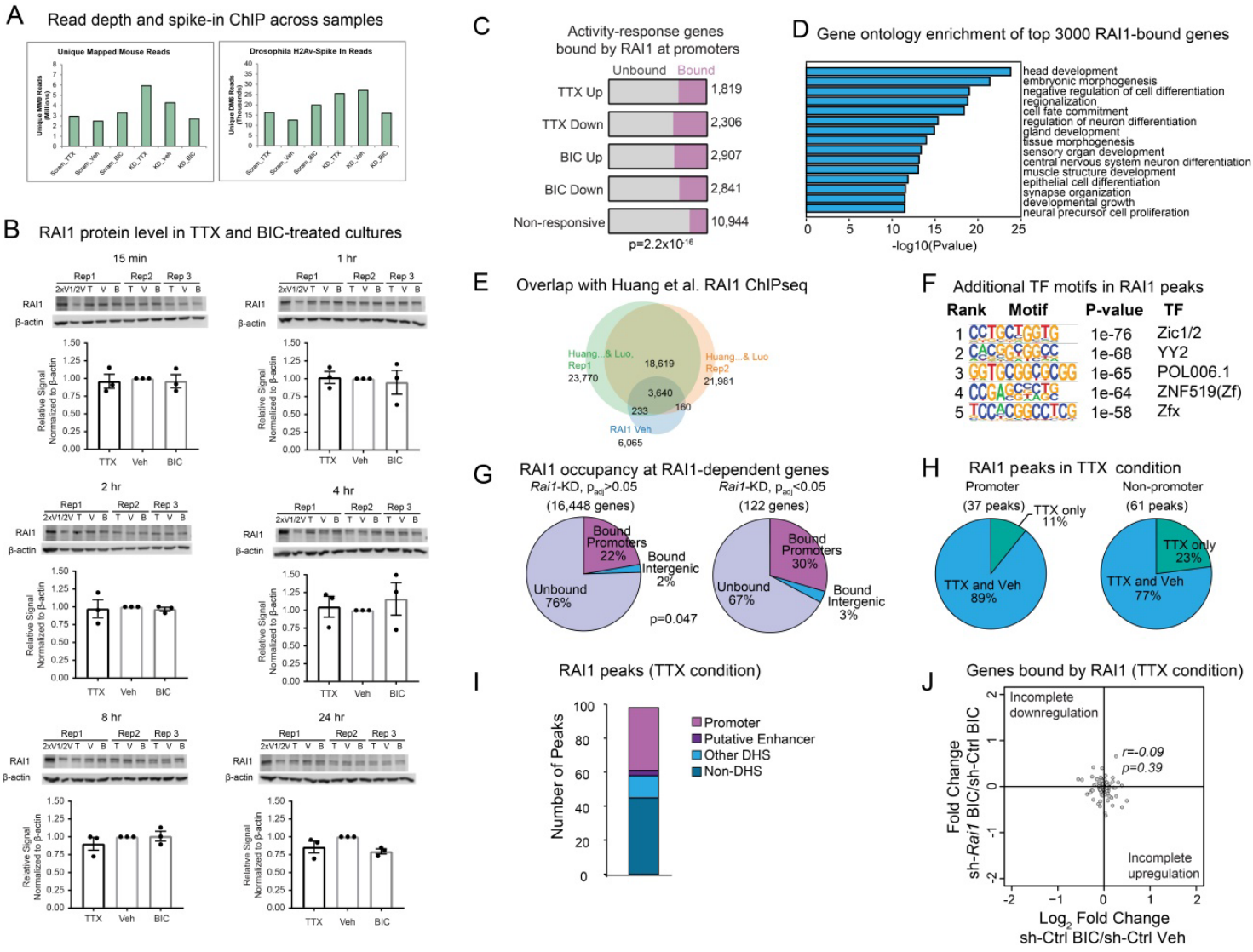

Figure 3-8. Further RAI1 ChIP-seq analysis, related to Fig.3-7.

(A) Number of reads of ChIP-seq samples mapped to mouse (mm9) or fly (dm6) genomes.

(B) Western blot for RAI1 (N=3). Rat cortical neurons (DIV14) were treated with TTX (T), BIC (B) or vehicle (V) for the indicated times. The 270-kDa full-length RAI1 protein band intensity was visualized and quantified in the linear range using LI-COR C-Digit and Image Studio software. No treatment reached $p<0.05$ (one-way ANOVA).

(C) Enrichment of RAI1-peaks at the promoters of TTX up, TTX down, BIC up and BIC down genes. (Chi-square test, p=2.2e-16)

(D) Gene ontology enrichment of RAI1-promoter-bound genes in baseline condition.

(E) The majority of RAI1-promoter-bound genes in our study overlap peaks found in *in vivo* RAI1-ChIP-seq data [2]

(F) Top HOMER Known motifs enriched in RAI1 gene promoters (Veh).

(G) RAI1-binding is enriched in RAI1-dependent genes.

(H) The majority of peaks in the TTX condition are shared in the Veh condition.

(I) The majority of peaks in the TTX condition are non-promoter peaks.

(J) Genes bound by RAI1 in the TTX-treated condition do not show a correlation with incomplete BIC-response.

Loss of RAI1 prevents synaptic upscaling but not downscaling

We next examined RAI1's role in homeostatic synaptic scaling induced by chronic activity suppression (TTX, 24 hr) or chronic network hyperactivation (BIC, 24 hr). Consistent with the dysregulation of TTX-responsive genes by *Rai1*-KD after TTX treatment (Fig. 3-5 and Fig. 3-7), we found that loss of RAI1 significantly impaired the induction of homeostatic upscaling during activity suppression in a cell-autonomous manner. Following transfection of scrambled or *Rai1*-targeted shRNAs (24 hr prior to TTX/BIC), we found that control neurons expressing the scrambled shRNA exhibited the normal increase in mEPSC amplitude 24 hr post-TTX (sh-Ctrl Veh vs TTX: n = 29-21, $p < 0.0001$, Fig. 6A-B) and the distribution of mEPSCs exhibited a clear and multiplicative rightward shift in cumulative frequency plots. By contrast, mEPSCs from neurons expressing either of two distinct *Rai1* shRNAs did not significantly increase following TTX exposure (Fig. 3-9A-C). Importantly, expression of an RNAi-resistant RAI1 fully rescued TTX-induced upscaling (Fig. 3-9A-C). Despite a clear role in homeostatic upscaling, *Rai1*-KD had no effect on the induction of homeostatic downscaling following network hyperactivation with BIC (Fig. 3-9D-F). Both control neurons expressing scrambled shRNA and those neurons expressing *Rai1*-shRNA exhibited significantly decreased mEPSC amplitudes (sh-Ctrl Veh vs BIC: n = 26-17, $p = 0.0026$, sh-*Rai1*-#1 Veh vs. BIC: n = 21-8, $p = 0.0003$ and sh-*Rai1*-#2 Veh vs. BIC: n = 12-8, $p < 0.0001$, Fig. 3-9E), as well as a clear leftward multiplicative shift in mEPSC cumulative probability distributions (Fig. 3-9F). These results demonstrate that RAI is essential for homeostatic upscaling during activity suppression, but is otherwise dispensable for homeostatic downscaling during periods of network hyperactivation.

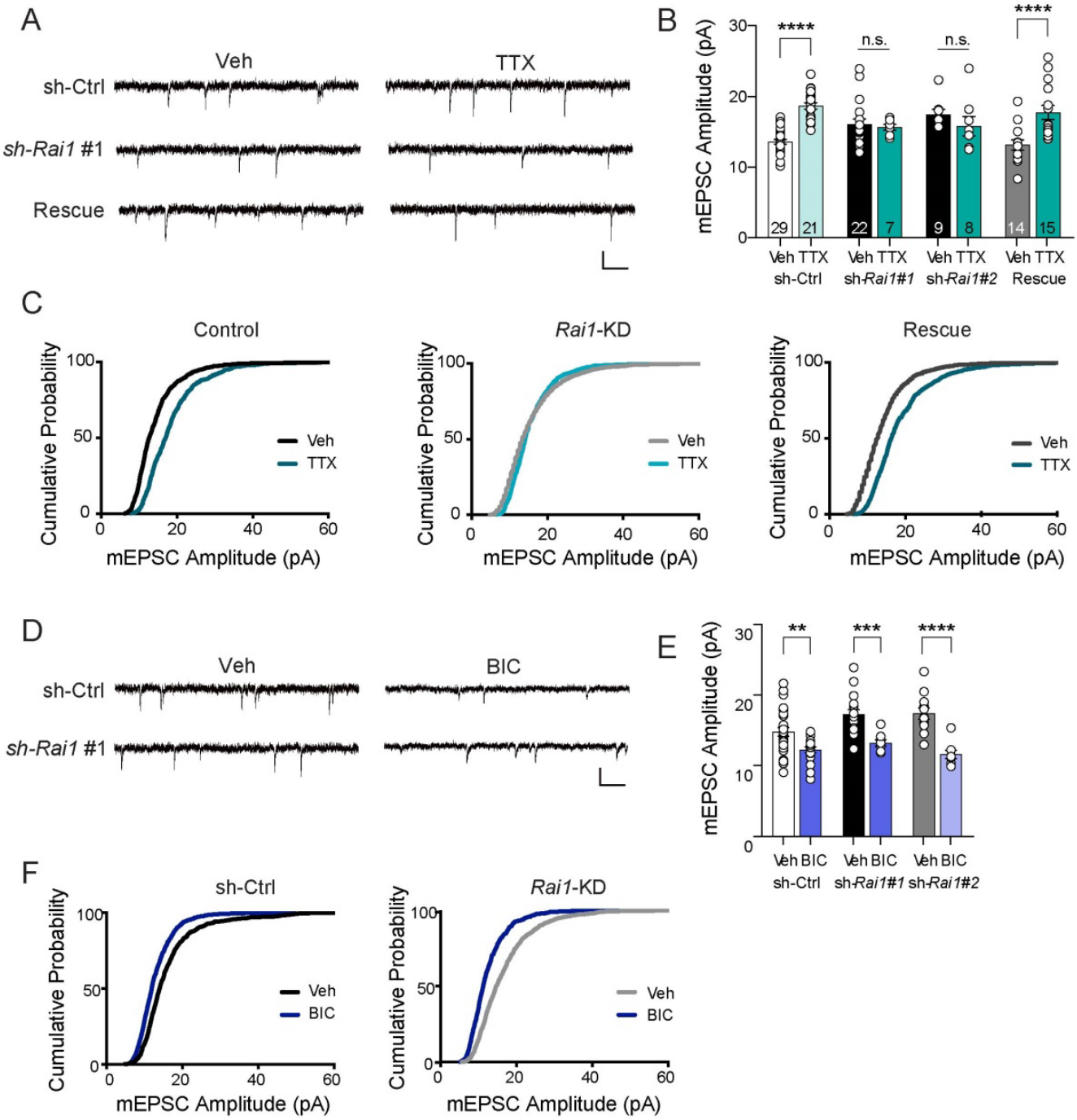
A
Veh
TTX
sh-Ctrl
sh-Rai1 #1
Rescue
B
mEPSC Amplitude (pA)
****
n.s.
n.s.
****
29
21
22
7
9
8
14
15
Veh TTX
sh-Ctrl
sh-Rai1#1
sh-Rai1#2
Rescue
C
Control
Rai1-KD
Rescue
Cumulative Probability
mEPSC Amplitude (pA)
Veh
TTX
D
Veh
BIC
sh-Ctrl
sh-Rai1 #1
E
mEPSC Amplitude (pA)
**
***
****
Veh BIC
sh-Ctrl
sh-Rai1#1
sh-Rai1#2
F
sh-Ctrl
Rai1-KD
Cumulative Probability
mEPSC Amplitude (pA)
Veh
BIC

Figure 3-9. *Rai1*-KD impairs synaptic upscaling but not synaptic downscaling.

(A) Representative mEPSC traces recorded from neurons transfected with either sh-Ctrl, sh-*Rai1* or Rescue and treated with either vehicle or 1 µM TTX. Scale bar, 20 pA, 150 ms

(B) mEPSC amplitude of sh-Ctrl, sh-*Rai1* #1, sh-*Rai1* #2 or Rescue and treated either with vehicle or TTX (sh-Ctrl Veh, TTX n = 29-21, sh-*Rai1* #1 Veh, TTX n = 22-7, sh-*Rai1* #2 Veh, TTX n = 9-8 and Rescue Veh, TTX n = 14-15).

(C) Cumulative distribution of mEPSC amplitude for sh-Ctrl (left), *Rai1*-KD (sh-Rai1 #1 + #2, middle) and Rescue (right) comparing vehicle vs. TTX.

(D) Representative mEPSC traces recorded from neurons transfected with either sh-Ctrl or sh-*Rai1* and treated with either vehicle or 10 µM BIC. Scale bar, 20 pA, 150 ms.

(E) mEPSC amplitude of sh-Ctrl, sh-*Rai1* #1 and sh-*Rai1* #2 treated either with vehicle or BIC (sh-Ctrl Veh, BIC n = 26-17, sh-*Rai1* #1 Veh, BIC n = 21-8, sh-*Rai1* #2 Veh, BIC n = 12-8).

(F) Cumulative distribution of mEPSC amplitude of sh-Ctrl (left) and sh-*Rai1* (sh-*Rai1* #1 + #2) treated with vehicle (black) or BIC (blue). All bar graphs are represented as mean ± SEM, and unpaired Student's t-tests were performed. **p < 0.01, ***p < 0.001 and ****p < 0.0001

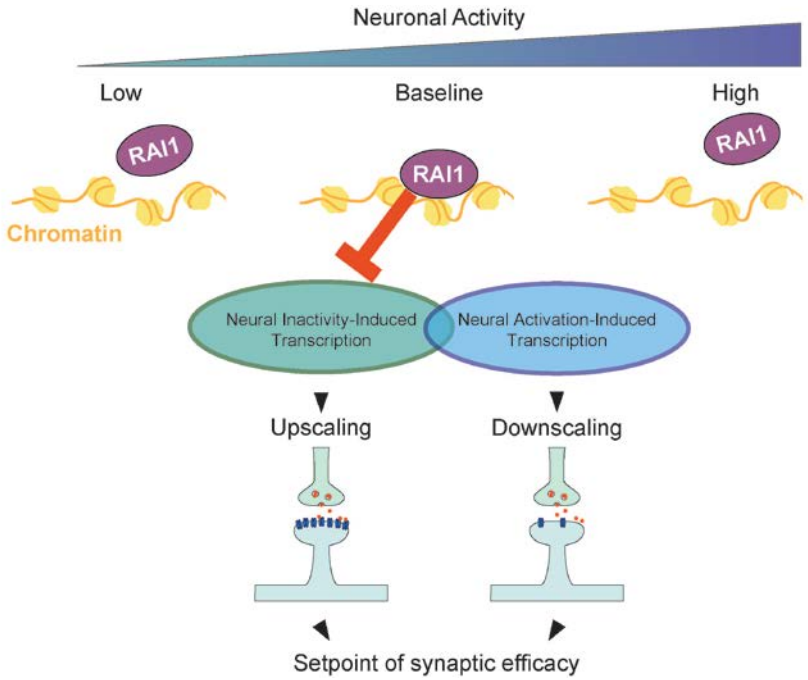

Figure 3-10. RAI1's role as a state-dependent transcriptional regulator of TTX-response genes.

RAI1 alters synaptic efficacy through activity-dependent chromatin binding and plays essential roles in regulating TTX-response genes under baseline and activity-suppressed states.

Discussion

Several lines of evidence support a model where RAI1 acts to constrain synaptic upscaling in networks with baseline levels of activity by preventing premature transcriptional responses normally driven by altered network activity (Fig. 3-10). First, RAI1 deficiency shifts gene expression towards TTX-associated transcriptional states (Fig. 3-3). Second, RAI1 occupies its target promoters strongly in the resting cells, and dissociates when network activity shifts (Fig. 3-5). Third, *Rai1*-KD led to an increase in excitatory synaptic strength, reflected by enhanced mEPSC amplitudes and associated with an increase in network firing rate (Fig. 3-3). Our data further indicate the additional role of RAI1 in promoting synaptic upscaling when the network experiences prolonged activity depression (Fig. 3-9). This latter role of RAI1 again involves direct control of TTX-induced transcriptional responses (Fig. 3-5 and Fig. 3-7). The most remarkable aspect of these observations might be the predictive capability of Bru-seq results for RAI1's roles in chromatin regulation and synaptic plasticity.

It is noteworthy that all the four previously characterized chromatin regulators in synaptic scaling, i.e. TET3, EHMT1/2, L3MBTL1 were chosen for investigations, because network activity alters their expression or target histone modifications [21-23]. We found no indication that neuronal activity influences RAI1 expression (Fig. 3-1A and 3-8B). These observations suggest that chromatin regulators linked to human cognitive disorders could participate in synaptic scaling and other forms of transcription-dependent plasticity, even when their expression remains stable during the process. The predominant chromatin occupancy by RAI1 during stable periods of network activity (Fig. 3-5) is unique among the scaling-associated chromatin factors, which all appear to be activated by network activity alterations. Post-translational modifications on RAI1 itself or chromatin are potential mechanisms for the RAI1 dissociation from chromatin. Thus, RAI1 offers a molecular mechanism that stabilizes network activity and future investigations may uncover a similar mode of action in other chromatin regulators associated with human cognitive deficits.

How do RAI1's roles in synaptic scaling relate to cognitive function? Thorough characterization of cell-type specific *Rai1*-KO mice attributed their learning deficits to GABAergic interneurons

rather than glutamatergic excitatory neurons [2], although human SMS patients exhibit *RAI1* heterozygosity in all cells. Since we measured mEPSCs in the pyramidal cells that incorporated the sparsely transfected *Rai1*-shRNA plasmid, RAI1's role in synaptic scaling is cell-autonomous to excitatory neurons. The lack of learning deficits in forebrain-specific *Rai1*-KO (*Emx1*-Cre: $Rai1^{flox/flox}$) may suggest that impaired cognitive function is independent of RAI1's role in synaptic scaling. Alternatively, unknown genes may compensate for synaptic scaling deficits caused by acute *Rai1* depletion during development thus obscuring the contribution of RAI1 in excitatory neurons. Of note, a recent study reported reduced dendritic spine density in the prefrontal cortex of 4 week old *Rai1*-heterozygous mice [78], suggesting important effects of RAI1 deficiency in excitatory neurons that may relate to RAI1's role in synaptic upscaling identified here. Identifying RAI1-target genes that mediate the synaptic phenotype will illuminate the molecular pathways underlying the cell autonomous roles of RAI1.

A limitation of the Bru-seq approach is the lack of cell-type specificity. Recently, Zajaczkowski *et al*. reported nascent RNA-sequencing specifically in neurons [84]. They used *Synapsin I* promoter-driven expression of uracil phosphoribosyltransferase (UPRT) to label RNAs of neurons. The UPRT system identified over 3,000 depolarization-regulated genes over the 3 hr KCl treatments, which likely detected both nascent transcripts and steady-state mRNAs. Cell-type specificity of the UPRT system comes with the cost of introducing the UPRT transgene and additional experimental steps to label RNAs. Furthermore, single-cell RNA-seq of *Rai1*-KD neurons might illuminate cell-type-specific roles for RAI1. Single-cell RNA-seq, however, mostly characterizes poly(A)-selected steady-state mRNAs. Thus, it will be important to choose the most suitable experimental approach for RNA profiling depending on specific goals of the study.

Our studies further identify a unique role for RAI1 in homeostatic synaptic plasticity, where during stable patterns of activity, it suppresses a transcriptional program engaged during neuronal inactivity. This work underlines the association between neuronal activity dependent transcription and the functional axis of experience dependent synaptic plasticity (Figure 1-1). However, RAI1 demonstrates a role for chromatin regulators in the maintenance of the baseline state of the activity-dependent transcriptome. L3MBTL and EHMT1/2, which perturb synaptic

up- and/or down-scaling, do not perturb baseline synaptic strength, suggesting that baseline state regulation is not a ubiquitous feature of chromatin regulators. It remains to be explored whether RAI1 is one of many nucleosome binding proteins that bind to chromatin and regulate activity-dependent transcription predominately baseline conditions.

Speculation on the RAI1 complex

It is worth considering whether evidence of a RAI1 complex is consistent with our findings. Chromatin regulatory proteins, including H3K4me regulators, generally operate within stable multi-subunit complexes [85]. Such a complex typically contains histone modifying enzymes, reader proteins, and protein scaffolds. Using a unique proteomics approach, Eberl *et al*. discovered that RAI1 is an integral component of a putative chromatin regulatory complex. The authors used a label-free proteomics approach to identify reader proteins that specifically recognize well-characterized histone methylations including histone H3K4me3 [4]. Brain, kidney, and liver tissue lysates taken from adult mice were filtered through columns containing unmethylated H3K4 or H3K4me3 peptides, and eluates were analyzed by tandem mass spectrometry. Consistent with a previous report [86], PHF21A was identified as a protein that binds to unmodified H3K4 and repelled by H3K4 methylation. In the H3K4me-repelled fraction, they identified a novel protein complex, which consists of iBRAF, Retinoic Acid Induced 1 (RAI1), Plant Homeodomain-containing Factor 14 (PHF14), and Transcription Factor 20/Stromelysin-1 Platelet-derived growth factor-responsive element Binding Protein (TCF20/SPBP).

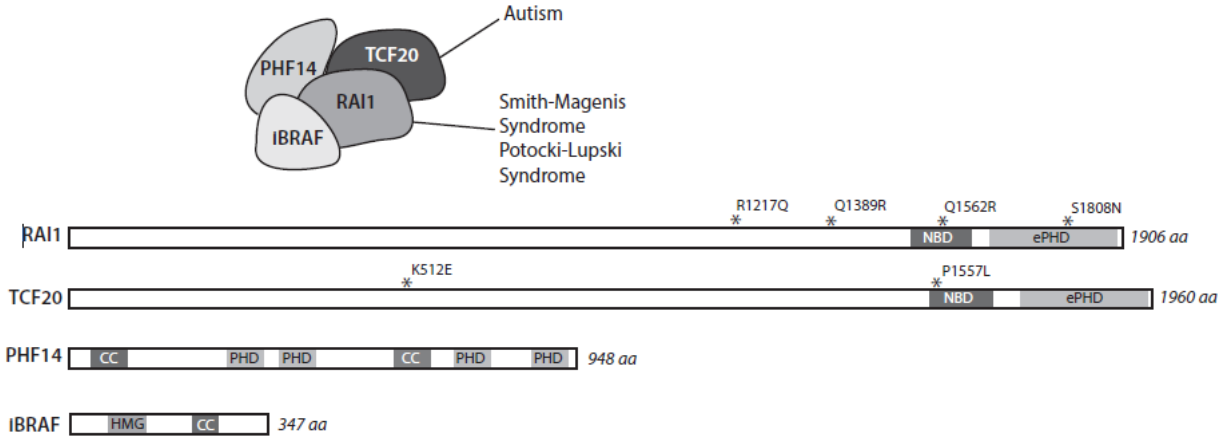

Figure 3-11. Putative RAI1 complex. The RAI1 complex may consist of four non-enzymatic histone- and DNA-binding proteins[3,4]. NBD=nucleosome binding domain. ePHD= extended plant homeodomain. CC: coiled coil. HMG= high mobility group box.

Unlike typical chromatin regulatory machineries, the RAI1 complex lacks histone-modifying enzymes. Notably, PHF14, RAI1, and its paralogue TCF20 (SPBP) carry putative methyl-histone recognition modules: PHDs and extended PHDs (ePHDs) (Figure 3-11) [87], suggesting reader function of the complex. The present work demonstrates that RAI1 can both activate and repress transcription depending on the target genes (Fig. 3-5). I speculate that RAI1 functions to recruit distinct histone modifying proteins in the baseline state to activate TTX-downregulated genes and to repress TTX-upregulated genes. Which protein? We previously reviewed the potential interaction of RAI1 and the histone methyltransferase MLL1/KDM2A across early neurodevelopment [3]. RAI1 may interact with MLL1 in the context of synaptic plasticity, as both RAI1 and MLL1 are expressed in mature neurons. Alternatively, like RAI1, TET3 and EHMT1/2 have been demonstrated to have important roles in homeostatic upscaling [21,22]. While TET3 positively regulates transcription by removing CpG methylation [88], EHMT1/2 generally acts as a transcriptional repressor by placing the repressive histone H3K9 methylation mark [89]. Thus, the two facets of RAI1's role in transcriptional dynamics could be through interactions with positive and negative transcriptional regulators, such as TET3 and EHMT1/2. An interaction with TET3 at baseline is a tempting explanation, as loss of TET3 in neurons appears to not only regulate TTX and BIC-responsive scaling, it also upregulates baseline synaptic strength, similar to RAI1 [21]. (It should be noted that the authors did not statistically test for this.) Therefore, in this model, RAI1 may recruit TET3 at baseline, then departs the chromatin in response to low or high activity, while other histone recognition complexes recruit TET3 to other loci important for the scaling process.

Another aspect of the RAI1 complex to consider is the current evidence of its association with distinct histone modifications. The RAI1 complex binds to unmethylated H3K4, whereas H3K4me3 repels RAI1 [4], which suggests that methyl-recognition may be correlated with the dynamics of RAI1 chromatin binding in response to activity. Previous studies have shown that H3K4me3 increases globally in response to picrotoxin, a GABA-A receptor antagonist which increases neural activity levels like BIC. Similarly, H3K4me3 trends towards a global increase in response to TTX [22]. This is consistent with RAI1's dramatic repellence from the chromatin under BIC, and somewhat less strong repellence after TTX. Therefore, RAI1 may serve to recruit

H3K4me3 methyltransferases, thus concurrently displacing itself, in a read-recruit-leave mechanism.

However, RAI1 also has been shown to be associated with H2A.Z, which is found to be enriched at both active and repressed gene promoters [90,91]. In the cerebellar cortex, H2A.Z has been shown to be integrated, via the NuRD complex, into the promoters of activity-response genes after cessation of neural stimulation [92]. Upon returning to normal baseline levels of activity, H2A.Z is incorporated into activity-dependent promoters, and it appears to prevent too dramatic a reduction in expression. That is, loss of H2A.Z reduces post-stimulation expression of activity-dependent genes. This suggests H2A.Z may help to regulate baseline transcription set points. As a mediator of baseline transcription of activity-dependent genes and a potential binder of H2A.Z, RAI1 may take part in this mechanism of set point establishment through H2A.Z binding. This could be analyzed by examining RAI1-chromatin interactions before and after baseline states have been achieved during synaptic plasticity.

In sum, future analyses of RAI1's molecular interactions, through biochemical binding assays and mass spectrometry, will help to determine the mechanisms by which RAI1 regulates baseline transcription of activity-dependent genes.

Potential Lessons

Often, initial examination of a protein of interest's function involves RNA-sequencing of control/WT and KD/KO cells, with the selection of differentially expressed genes as the next step to highlight pathways of interest. However, this may obscure trends in transcription that are unknowable unless directly compared with other states. For example, RAI1 dependent genes at baseline showed mild fold changes, and were composed of numerous TTX and BIC responsive genes, with enrichment in broad gene ontologies that did not indicate a likely mechanistic pathway. However, by comparing *Rai1*-KD genes with gene sets known to be associated with neuronal inactivity and hyperactivity, a clear hypothesis could be formed: loss of RAI1 pushed cellular state towards an inactivity-like transcriptome. This potentiated further analysis of downstream phenotypes. In this sense, RNA-sequencing studies can be designed to include "reference states" as comparison; for example, the study of loss of a neurodevelopmental gene at

E16 can be compared with the transcriptome of E12 vs E18 brains to search whether the gene aberrantly delays or accelerates the developmental transcriptome. Alternatively, the transcriptome resulting from loss of a gene of interest can be compared to the transcriptomes resulting from loss of genes with other known phenotypes. This approach would be useful in the case of a confident hypothesis or pursuit of a specific mechanism of interest. Also, since gene expression may be disrupted in only a subset of cells, relying on trends instead of significant genes may allow sensitivity to cell-subtypes specific changes without relying on more technically challenging techniques such as single-cell RNA sequencing or cell-type specific nuclei isolation.

Similarly, sole reliance on significant gene expression changes can lead to missed mechanisms, especially when examining chromatin regulators, which regulate high numbers of genes, or profiling dynamic gene expression at a single time point across development or after a stimulus, since the time point chosen may not represent the most robust differential expression. Therefore, examining sub-significant gene expression changes allows further gene-network-level analysis. For example, we found that *Rai1*-KD mildly upregulated *Per2* by 25%, which is undetectable by typical qPCR and was not be detectable at the protein level through Western blot analysis. However, examination of sub-significant trends revealed that many circadian genes were altered by *Rai1*-KD. This interaction is described in the following chapter.

CHAPTER 4.

Potential Roles of RAI1 in Circadian Rhythms

Introduction

Circadian rhythms represent an internal clock for animals to adapt their physiology to the day and night cycle. Recent transcriptome studies using all major organs in mice revealed that approximately 45% of protein-coding genes show circadian expression in at least one organ, and that 10% of genes oscillate in a given cell type [93,94]. This suggests pervasive yet cell-type and tissue-specific variations in circadian gene regulations. The core of circadian oscillatory gene expression is a transcriptional negative-feedback mechanism, whereby a heterodimer of the transcription factors CLOCK and BMAL activates transcription of their negative regulators *PER1/2* and *CRY1/2* in a 24 hour cycle [95].

Circadian gene regulation is associated with periodic relaxing and compacting of chromatin structure at gene promoters [96]. Several chromatin regulators, including CLOCK itself as a histone acetyltransferase, have been shown to contribute to the circadian transcriptional program [97]. In reminiscence of activity-dependent gene expression, chromatin regulators that are associated with neurodevelopmental disorders also appear to be critical for circadian gene expression. These include RAI1, the histone methyltransferase MLL, the histone demethylases LSD1 and KDM5A [95,96,98-100]. Therefore, sleep disturbance observed in the neurodevelopmental conditions associated with these genes may be a consequence of impaired circadian transcription.

In the case of RAI1, clinical analyses first implicated its role in circadian rhythms. Every reported individual with SMS experienced subjective sleep disturbances such as daytime sleepiness and frequent nighttime awakenings [101]. The production of melatonin appears to be a primary factor in the observed sleep abnormalities of SMS. Melatonin is a key hormone secreted

by the pineal gland during the night, thereby synchronizing the circadian clock throughout the body [102]. While most individuals with SMS display an inverted secretion pattern of melatonin, in rare cases, a normal melatonin secretion pattern accompanies sleep disturbance [103,104]. This raises the possibility that melatonin-independent mechanisms underlie the sleep abnormalities in SMS. Indeed, heterozygous *Rai1* ablation in C57/BL6 mice, which are known to lack melatonin secretion, is sufficient to impair circadian behaviors[74].

Mechanistic studies further support the role of RAI1 in intrinsic circadian regulation, independent of melatonin-mediated endocrine system. *RAI1* knockdown in cultured cell lines led to reduced and shortened oscillation of CLOCK target genes [105]. The reduced expression of circadian genes was also observed in fibroblasts derived from individuals with SMS [105]. Furthermore, RAI1 was found to directly occupy an intron of the *CLOCK* gene and promote its transcription [105]. However, a comprehensive understanding of RAI1's role regulating key circadian genes and neuronal function remain undiscovered.

Loss of RAI1 alters genes associated with CLOCK and PER2 Regulation

Intriguingly, our dataset supports the hypothesis that RAI1 interacts with the circadian transcriptome. In the Bru-seq dataset, the top gene upregulated by *Rai1*-KD is *Per2*, which encodes a key circadian regulator. PER2 antagonizes the function of CLOCK, a histone acetyltransferase responsible for activating circadian genes[106]. Electrophysiological recordings from cortical slices derived from *Clock*-mutant mice display increased synaptic strength, suggesting CLOCK activity represses synaptic strengthening [107]. As PER2 antagonizes CLOCK, I hypothesized that PER2 may function to induce synaptic strengthening. Bru-seq revealed that in TTX-treated cultures, *Rai1*-KD decreases *Per2* expression (Fig.4-1). At baseline activity, *Rai1*-KD increases *Per2* transcription. At high activity, *Rai1*-KD does not affect *Per2* transcription. I hypothesized that RAI1 switches in an activity-dependent manner from an activator to repressor of *Per2* to respectively block or induce CLOCK's repression of synaptic strengthening (Fig.4-2).

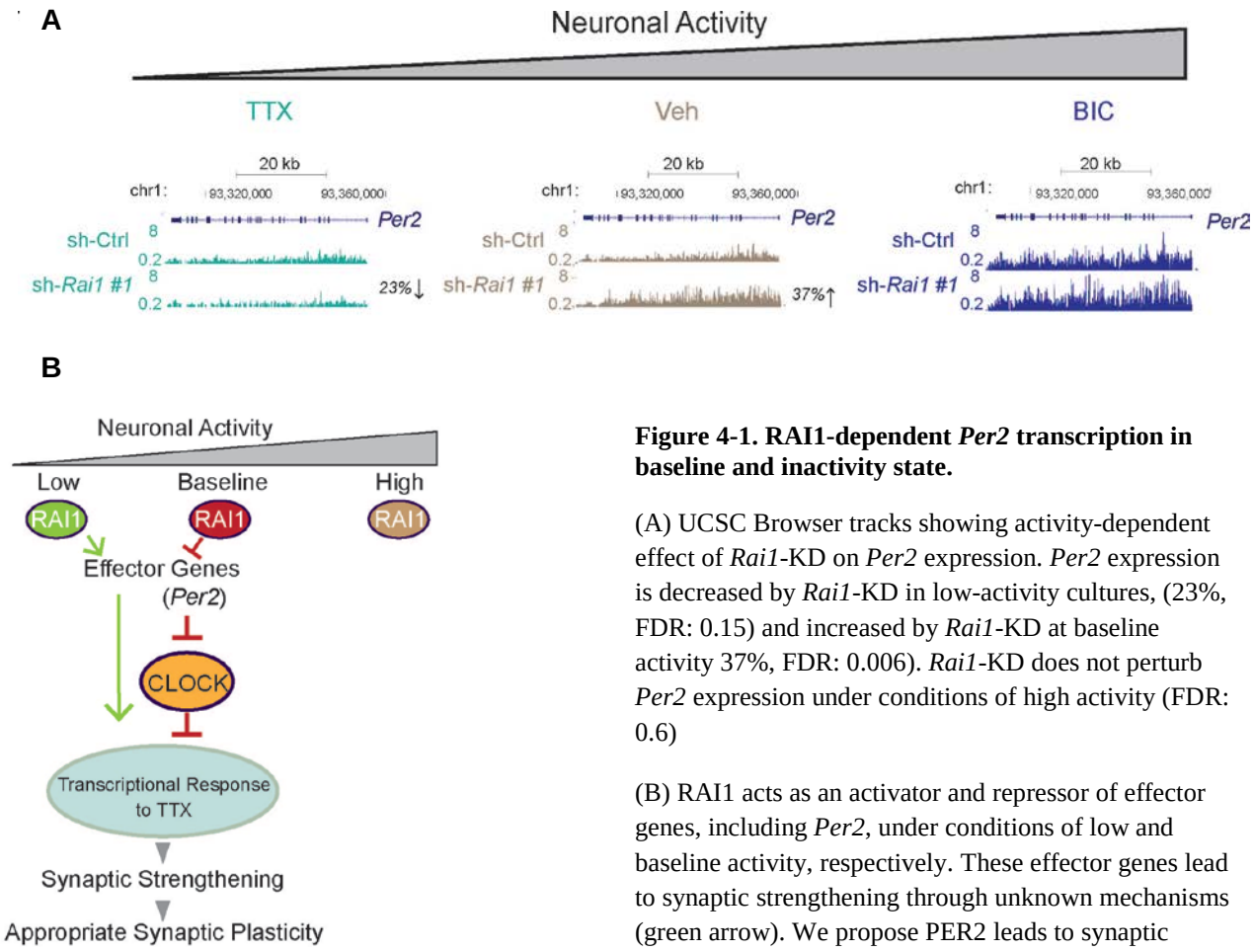

Figure 4-1. RAI1-dependent *Per2* transcription in baseline and inactivity state.

(A) UCSC Browser tracks showing activity-dependent effect of *Rai1*-KD on *Per2* expression. *Per2* expression is decreased by *Rai1*-KD in low-activity cultures, (23%, FDR: 0.15) and increased by *Rai1*-KD at baseline activity 37%, FDR: 0.006). *Rai1*-KD does not perturb *Per2* expression under conditions of high activity (FDR: 0.6)

(B) RAI1 acts as an activator and repressor of effector genes, including *Per2*, under conditions of low and baseline activity, respectively. These effector genes lead to synaptic strengthening through unknown mechanisms (green arrow). We propose PER2 leads to synaptic strengthening by blocking the function of CLOCK, a repressor of synaptic strength. High activity inactivates RAI1's role as a regulator of synaptic strength.

If RAI1 dysregulates *Per2* transcription, does it affect PER2 protein levels? While tested antibodies appeared non-specific (data not shown), it would be predicted that PER2-target genes would be disrupted by *Rai1*-KD. Therefore, I took a list of genes upregulated be *Per2*-KD in human embryonic stem cells [6]. These are putative PER2-upregulated genes. If my model were correct, Per2-upregualted genes would be expected to be downregulated by *Rai1*-KD at baseline. When plotting the effect of *Rai1*-KD on these genes, I found indeed that these genes predominately trended towards downregulation, in support of the model (Figure 4-3).

Since another CLOCK-target gene, *Cry1*, was dysregulated by *Rai1*-KD at baseline, I searched to see whether CLOCK-target genes were enriched in *Rai1*-KD genes. Using the 2016 ChIP-X

Enrichment Analysis software, I found that RAI1-dependent baseline genes are significantly enriched for CLOCK binding sites [108]. Although this experiment was performed in human 293T cells, this provides evidence that RAI1 may more broadly regulate CLOCK-target genes, either through suppression of *Per2* transcription or through direct recruitment of CLOCK.

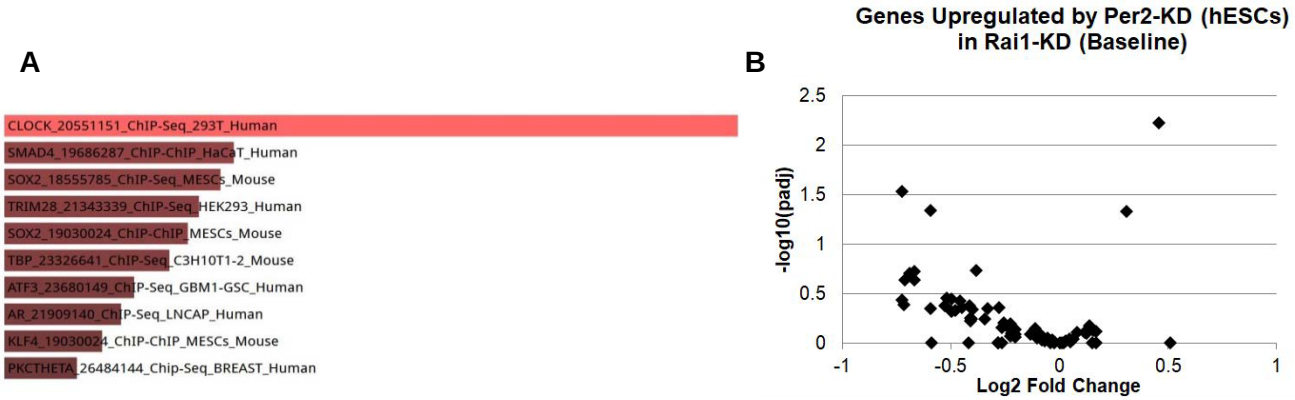

Figure 4-2. RAI1-target genes are regulated by PER2 and CLOCK

(A) ChEA 2016, Enricher Software outputs a significant enrichment for CLOCK binding motifs based on Human 293T ChIP-seq experiment.[1]

(B) Genes upregulated by *Per2*-KD in human embryonic stem cells (hESCs)[6] are downregulated by *Rai1*-KD at baseline.

Discussion

Our work and previous studies have implicated RAI1 in circadian gene regulation, activity-dependent gene regulation, and synaptic scaling. Further experiments are required to establish how RAI1's roles in these processes interact. RAI1 may play independent roles in each of these processes, or one or more pairs of processes may be functionally linked. Circadian clocks in cultured non-neuronal cells are synchronized by serum shock or chemical agents such as dexamethasone, hydrogen peroxide, or forskolin [109]. These treatments intersect with pathways important for neuronal activity, e.g. forskolin phosphorylates CREB. The intersection between metabolic and neuronal activity pathways suggests that treatment of TTX or BIC may also serve to synchronize circadian clocks in neurons, though this has not yet been published.

Since the RAI1 chromatin binding phenotype is strong, it would be interesting to test if RAI1 chromatin binding is altered across circadian time and/or sleep/wake cycles *in vivo*. Since

daytime/wake is associated with higher inputs from environment, it may be analogous to BIC treatment; in this sense, RAI1 may be dispensable for this time of the circadian clock. However, nighttime/sleep may be analogous to TTX treatment. Although RAI1 departs the chromatin at 4 hours post TTX treatment, RAI1 appears essential to achieve the full amplitude of TTX-response genes, suggesting RAI1 may be necessary for this state or this time of the circadian clock. Therefore, loss of RAI1 may interfere with the circadian nighttime state. In cultured neurons, loss of RAI1 led to net increase in neuronal firing. If RAI1 has cyclic binding to the chromatin that peaks at the transition between day and night (CT12) but diminishes by CT16 (4 hours post TTX) and remains low throughout CT4 (4 hours post BIC) , this may coincide with our data. This leads to the hypothesis that loss of RAI1 would cause aberrant synaptic strengthening and increased neuronal firing at the nighttime state.

By what mechanism might RAI1 exert circadian influence on the chromatin? Many histone marks, including H3K4me3, shows circadian cycling [110]. We have previously identified a putative interaction between RAI1 and known H3K4me regulators LSD1 and MLL [3]. Briefly, RAI1 is part of a complex that appears to counteract LSD1/REST's inhibition of neuronal genes across neurodevelopment by recruiting MLL. This potential interaction may be at play in the circadian clock. LSD1 appears to be directly involved in the core CLOCK-BMAL machinery of circadian transcription. LSD1 can be phosphorylated by PKCα at a specific serine residue (S112) in a circadian manner [100] (Figure 4C). The phosphorylation of LSD1-S112 directly recruits and/or stabilizes CLOCK-BMAL on chromatin, which in turn activates CLOCK-target genes. Replacement of wildtype LSD1 with the phosphorylation-deficient p.Ser112Ala mutant in mice resulted in impaired circadian rhythmicity at molecular and behavioral levels [100]. The circadian role of LSD1 is independent of its demethylase activity [100,111].

In contrast to the catalysis-independent roles of the demethylases, MLL1 appears to govern circadian oscillation by trimethylating H3K4 [99]. MLL1 was shown to be recruited to promoters via the CLOCK-BMAL complex, in turn activating circadian gene expression in mouse embryonic fibroblasts. In principle, rhythmic expression of genes requires gene activation followed by transcriptional repression. A more recent study showed that MLL1 can be acetylated at several lysine residues, and that the acetylation can be removed by the deacetylase SIRT1 in a

circadian manner [112] (Figure 4D). SIRT1-mediated deacetylation of MLL1 from residues K1130 and K1133 appears to diminish the H3K4 methyltransferase activity of MLL1. MLL1 regulates thousands of genes with broad functions, thus this work raised an exciting possibility that MLL1 generates circadian oscillation of the H3K4me landscape genome-wide, thereby controlling broader physiology in a circadian manner. RAI1's involvement in circadian rhythms may be in part related to its recruitment or stabilization of MLL1 on the chromatin. However, alternative interactions may be possible.

The drastic symptom of inverted sleep patterns in individuals with Smith-Magenis syndrome (SMS) makes this a particularly interesting molecular axis to examine with relevant applications in therapeutics. Furthermore, as the role of synaptic scaling in sleep begins to be more thoroughly tested, SMS models may prove valuable given the known human symptoms and the known effect of RAI1 on synaptic upscaling.

CHAPTER 5.

Neuronal Activity-Dependent Promoter Selection

Introduction

Neuronal activity does not only alter gene expression levels, but alters transcriptional processing and post-transcriptional modifications. For example, genome wide-analyses have shown activity-dependent alternative splicing [113], including use of microexons [114], activity-dependent A→U editing [115-118] and activity-dependent enhancer usage [119,120]. Therefore, observing activity-dependent transcriptional mechanisms beyond up- and down-regulation of genes may give insight into how neurons alter the transcriptome and proteome.

One mechanism that has been relatively unexplored is the use of alternative promoters or transcription start sites (TSS) in response to neuronal activity. Activity-dependent promoter/TSS usage has been observed in specific neuronal genes. For example, the gene BDNF contains four promoters, two of which are known to be activity-dependent [36,121]. Interestingly, the protein products from each of these four promoters are identical [122,123]. It has been suggested that the untranslated region results in differential localization of mRNA in the neuron [124,125]. However, estimates of the number of mammalian genes with multiple transcription start sites have been as high as 56% [126-128]. Many propose that distinct transcription start sites are essential for development and/or cell-type specific expression. Indeed, whole-genome analyses of promoter usage suggest that in the cerebellum, alternative promoters are used differentially across developmental time[129].

The limited knowledge about activity-dependent TSS is in part due to the specific sequencing methods required for TSS profiling. Standard RNA-sequencing often depletes 5' ends of genes, preventing robust detection of changes in TSS [130]. Often, cap-analysis of gene expression (CAGE) coupled with sequencing, or transcription-start-site-sequencing (TSS-seq) have been

used to analyze the usage of transcription start sites. These techniques are effective, but they do not profile whole gene expression, and have not yet been used in combination with nuclear or nascent RNA-sequencing in order to analyze dynamic activity-dependent gene expression.

However, our use of Bru-seq by chance potentiated the discovery of activity-dependent promoter usage. The Bru-seq method produced abundant intronic reads which allowed the first intron to prove as a much more robust signal of TSS usage. For RNA-sequencing analyses to corroborate our studies, we used the DLAF method, developed in the Iwase lab to enrich for 5' reads that allowed analysis of switches in promoter usage while examining mRNAs [131]. I developed the DLAF protocol for low-input RNA allowing sequencing of TSS usage from RNA derived from *in vivo* experiments to find whole-tissue and excitatory neuron-specific examples of activity-dependent promoter usage. Promoter usage predominately appears to switch protein level changes, including the presence of N-terminal localization signals. We demonstrate that the switch in localization signal of a phosphodiesterase PDE2A is essential for the localization of PDE2A to the mitochondria and for electrophysiological properties of neurons. In sum, the role of differentially regulated activity-dependent promoters may be important for synaptic plasticity more broadly.

A minority of expressed genes contain multiple active promoters in neuronal cultures

In our Bru-seq study (Fig 2-1), the top gene upregulated by TTX (*Prkag2*) showed an interesting pattern of activity-dependent expression (Fig. 5-1A). The upregulation appeared due to the activation of an upstream promoter in response to TTX treatment. ChIP-seq for H3K4me3 and H3K4me1 from mouse cortical neuronal cultures supported that this was an active neuronal promoter [132]. To determine if other genes displayed this phenomenon, I developed a custom pipeline to detect more instances of alternative promoter usage in neuronal cultures (Fig. 5-1C). I found that of the 12,260 genes expressed over a threshold in neuronal cultures, 909 (7.4%) show multiple active promoters. Activity-dependent genes are significantly enriched for genes with multiple active promoters, 9-13% compared to 4% of non-responsive genes, when examined by a Chi-square test (Fig 5-1C). Genes with multiple promoters showed gene ontology enrichment for neuron development and nervous system development, suggesting neuron-associated genes are

well-represented in the cohort of multi-promoter genes (Fig. 5-1D).

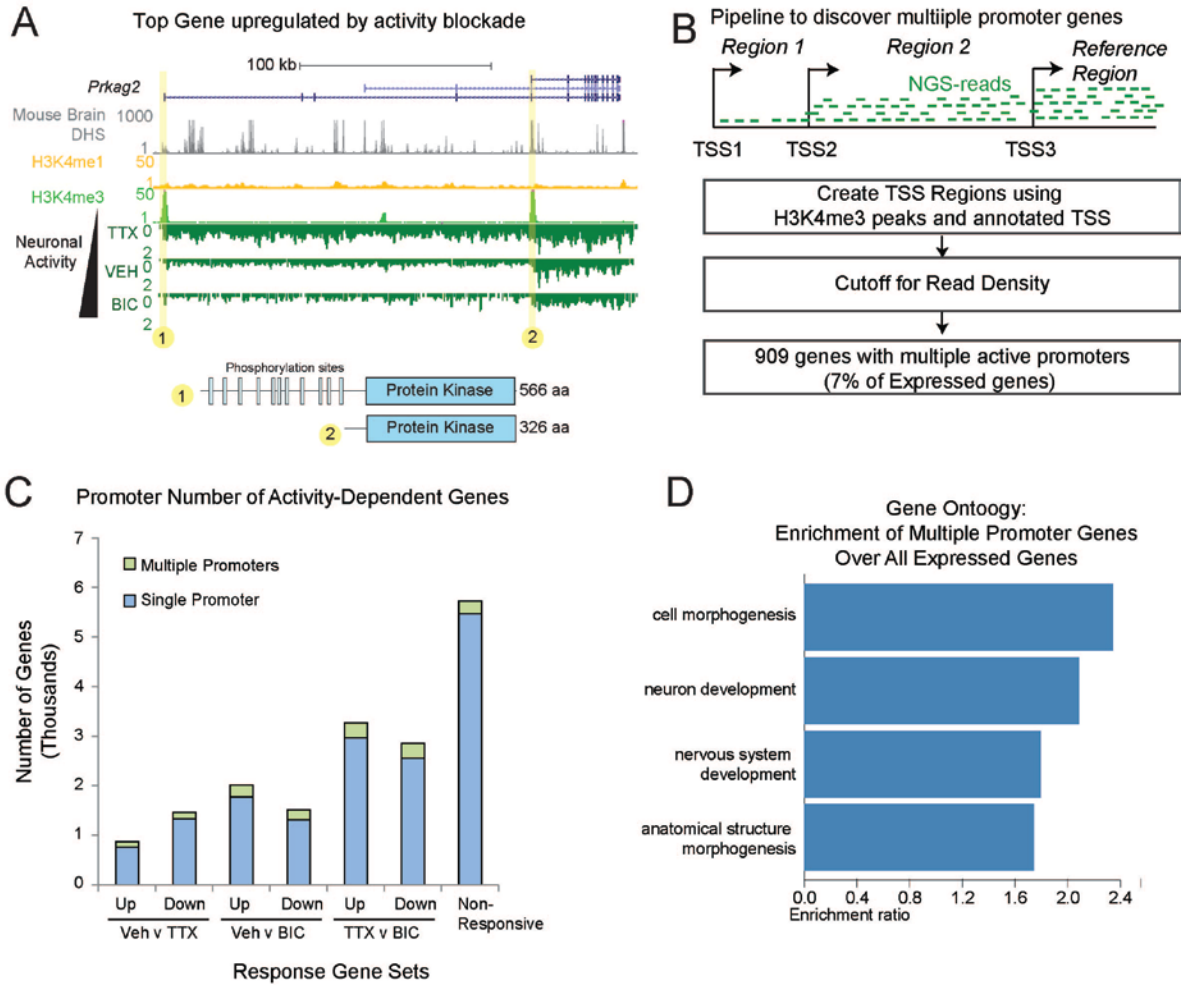

Figure 5-1. Multiple promoter genes expressed in mixed *in vitro* neuronal cultures.

(A) *Prkag2*, the top gene upregulated by TTX, shows upregulation of the upstream promoter.

(B) Pipeline to discover genes with multiple active promoters yielded 909 genes (7% of expressed genes).

(C) Genes differentially expressed between TTX and BIC treatment conditions are enriched in multi-promoter genes.

(D) Multi-promoter genes are enriched for neuronal gene ontologies compared to all expressed genes.

A subset of multi-promoter genes show differential usage of each promoter in response to activity shifts

To assess whether multi-promoter genes regulated promoter usage distinctly as in the case of *Prkag2,* I designed a pipeline to assess the ratio of reads in each TSS region compared to a downstream reference region (Fig. 5-2A). I used a linear model with a dummy variable for the treatment of Veh vs BIC, Veh vs TTX, or TTX vs BIC to detect the genes with activity-dependent alterative TSS usage. Using a false discovery rate of 0.1 and a minimum absolute correlation of 0.1, I found 102/909 genes (11%) of all genes with multiple promoters show differential usage above these cutoffs (Fig. 5-2A). Top most significant genes are shown in Fig. 5-2B and included *Prkag2* and the synaptic genes *Nrxn2* and *Dlgap1*. To examine whether multi-promoter genes with activity-dependent differential usage of promoters (ADDUP) are enriched in activity-dependent genes, we calculated the proportion of activity dependent genes by examining significantly regulated genes between the TTX and Vehicle condition, the BIC and Vehicle condition, and the TTX and BIC condition. The genes upregulated by BIC are significantly enriched for ADDUP genes, suggesting whole-gene induction of transcription by activity is correlated with differential usage. The ADDUP genes, compared to all multi-promoter genes are enriched in gene ontology terms for calcium-mediated signaling, amine transport, voltage-gated calcium channel complex, and cyclic nucleotide binding, suggesting critical signaling processes may be regulated by these genes.

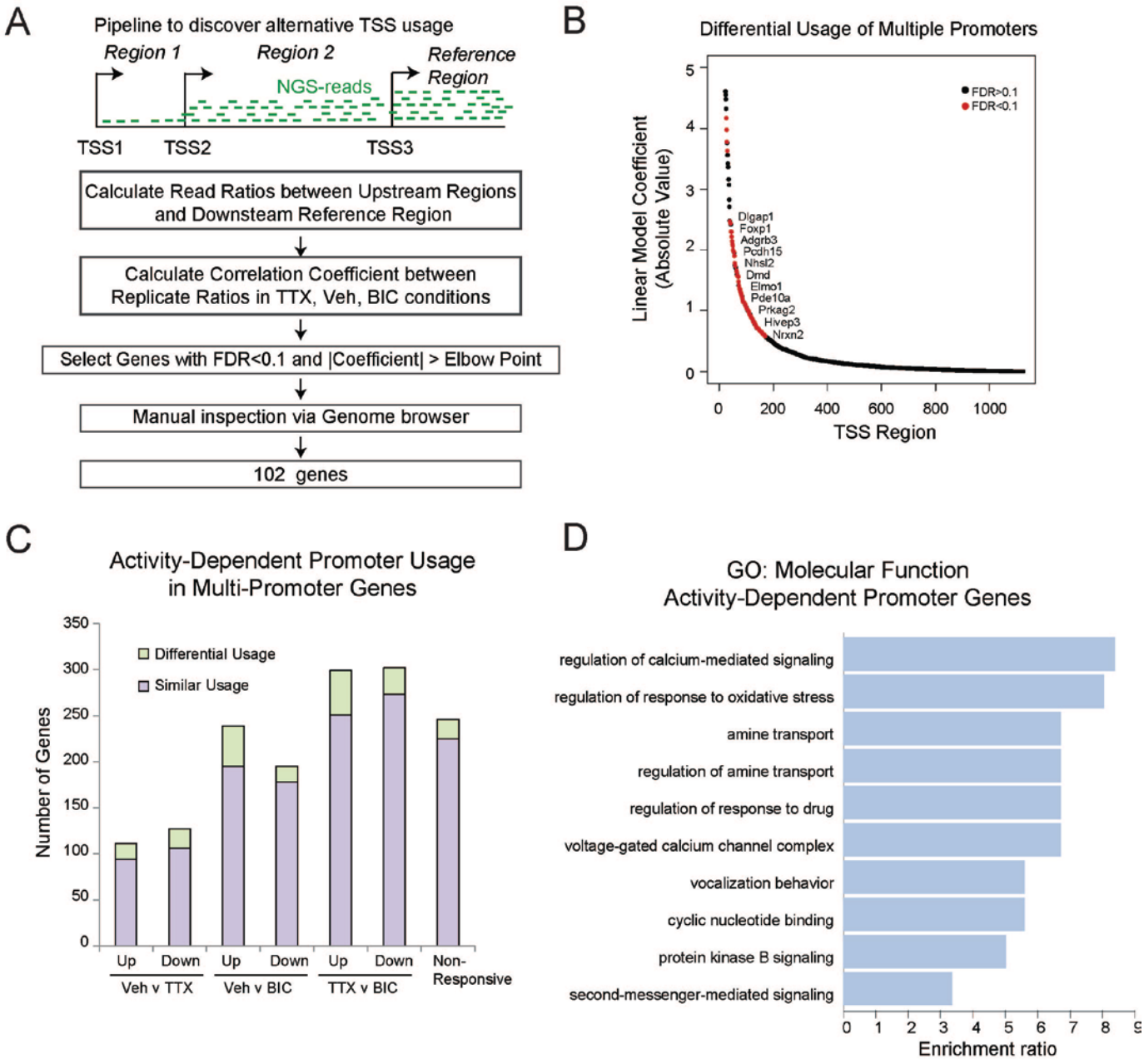

Figure 5-2. Activity-dependent differential usage of promoters (ADDUP) occurs in a minority of multi-promoter genes.

(A) Pipeline revealed 102/909 (11%) of genes show differential usage of promoters in response to neural activity shifts.

(B) Multi-promoter genes that achieve an FDR <0.1 and a coefficient greater than the elbow point when comparing TTX v BIC read ratios.

(C) Genes upregulated by BIC are enriched for differential usage of promoters.

(D) Genes with differential usage of multiple promoters are enriched for calcium signaling related gene ontologies.

In vivo *stimulation of mouse visual cortex yields ADDUP genes*

To examine whether alternative promoter usage occurs *in vivo* in response to physiological stimuli, we used a light-stimulation paradigm in adult mice[47]. Light stimulation is not only successful at inducing changes in neuronal activity in a reasonable proportion of neurons , but it has been associated with synaptic scaling[133,134]. We exposed a cohort of 6 adult female mice (8 week) to 72 hr darkness, then re-exposed 3 mice to bright light for 4 hr (Fig 5-3A). We then sacrificed the mice, dissected the V1 visual cortices and the S1 somatosensory cortices. We utilized a modified form of direct ligation of adaptors to the first-strand cDNA (DLAF) method to enrich for 5' end of genes [130], and performed deep sequencing. We used the identical pipeline to analyze activity-dependent promoter usage *in vivo* and found 26 genes with ADDUP (Fig. 5-3B). 11/26 genes (42%) were also found to be significant in the *in vitro* experiment (Fig 5-3B, inset Venn). However, there was a significant positive correlation between the linear model coefficients of *in vitro* and *in vivo* data, between all potential ADDUP genes (Fig 5-4C). The *in vivo* ADDUP genes were enriched for calcium channel gene ontologies, similar to the *in vitro* study (Fig 5-3D).

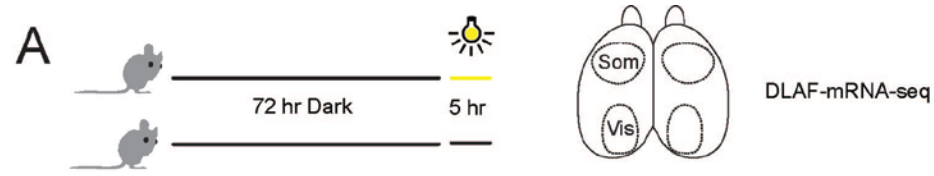
A
72 hr Dark
5 hr
Som
Vis
DLAF-mRNA-seq

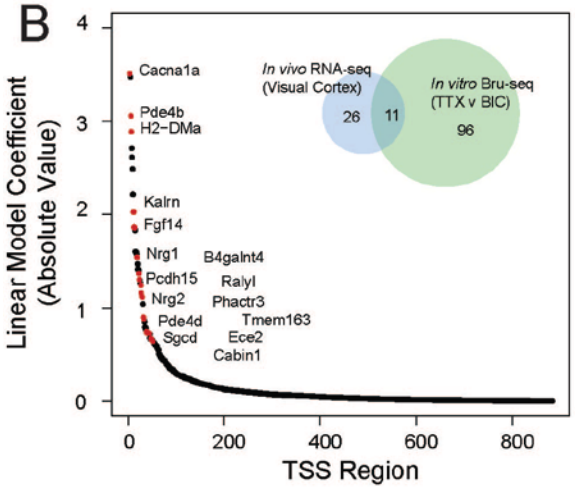
B
Linear Model Coefficient
(Absolute Value)
TSS Region
Cacna1a
Pde4b
H2−DMa
Kalrn
Fgf14
Nrg1
Pcdh15
Nrg2
Pde4d
Sgcd
B4galnt4
Ralyl
Phactr3
Tmem163
Ece2
Cabin1
In vivo RNA-seq
(Visual Cortex)
In vitro Bru-seq
(TTX v BIC)
26
11
96

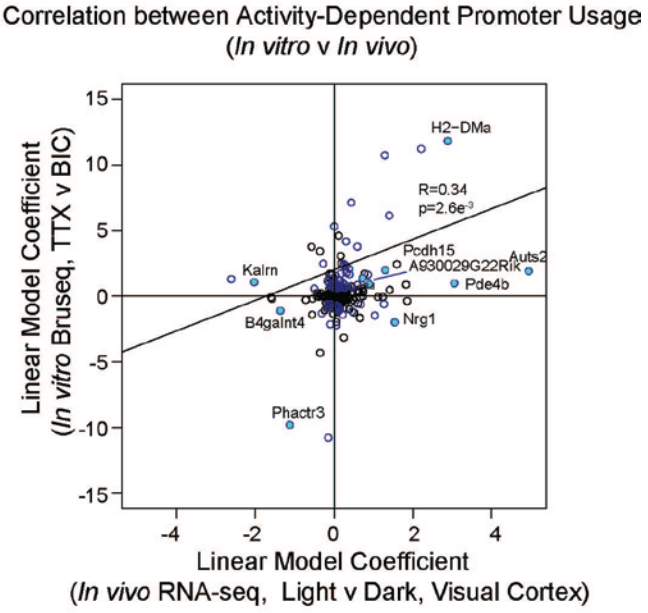
C
Correlation between Activity-Dependent Promoter Usage
(In vitro v In vivo)
Linear Model Coefficient
(In vitro Bruseq, TTX v BIC)
Linear Model Coefficient
(In vivo RNA-seq, Light v Dark, Visual Cortex)
H2−DMa
R=0.34
p=2.6e-3
Pcdh15
A930029G22Rik
Auts2
Pde4b
Kalrn
B4galnt4
Nrg1
Phactr3

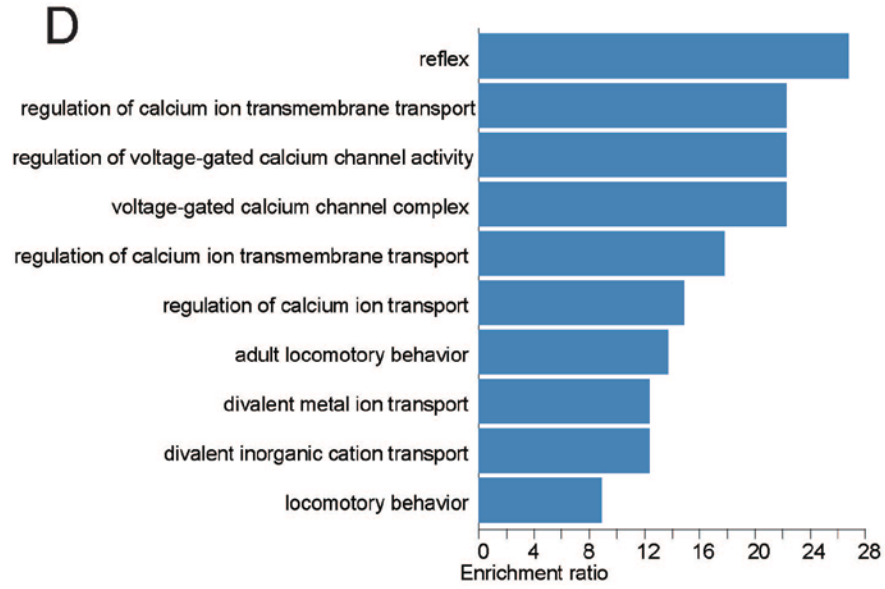
D
reflex
regulation of calcium ion transmembrane transport
regulation of voltage-gated calcium channel activity
voltage-gated calcium channel complex
regulation of calcium ion transmembrane transport
regulation of calcium ion transport
adult locomotory behavior
divalent metal ion transport
divalent inorganic cation transport
locomotory behavior
Enrichment ratio

Figure 5-3. *In vivo* brain tissue reveals differential promoter usage in response to physiological neural stimulation.

(A) Experimental paradigm. Adult mice were placed into darkness for 72 hr, then either exposed to light or retained in darkness an additional 5 hours. Mice were sacrificed, and the visual cortices (and somatosensory cortices as control) were dissected and prepared for DLAF-mRNA sequencing.

(B) Utilizing the pipeline in Figure 5-2, 26 genes were discovered to show differential promoter usage in multi-promoter genes in the light-induced condition. Eleven Genes overlapped with those found in *in vitro* Bru-seq experiment.

(C) There is a significant correlation between coefficients of genes found in *in vitro* and *in vivo* datasets.

(D) Significant genes *in vivo* are enriched for calcium signaling gene ontologies.

Cell-type specificity of alternative promoter usage

To ascertain whether distinct promoters were induced differentially through cell-type specific regulation and whether transcripts were stably associated with ribosomes to be translated, we crossed Ribotag mice [135] with *Neurod6*-Cre mice to express an HA-tagged ribosomal subunit Rpl22 exclusively in excitatory neurons [136,137]. We then repeated the experiment, this time immunoprecipitating excitatory neuron-specific ribosome-associated RNA (Fig. 5-5A). Visual cortex showed a robust response in activity-dependent gene expression, while somatosensory cortex showed only one gene differentially regulated, validating the region-specific activation of neurons (Fig. 5-5B.) Analysis of whole-gene expression showed strong depletion of non-excitatory neuronal genes, demonstrating the efficacy of Ribotag immunoprecipitation (Fig 5-5C).

After running the identical pipeline to capture ADDUP, we found no genes passed the threshold of significance after multiple comparisons corrections. However, once we relaxed the threshold to an uncorrected p-value <0.1, we found 23 genes that showed ADDUP , including the Rac GTPase-activator *Elmo1*, the nuclear-receptor binding protein *Lrif1*, and the phosphodiesterase *Pde10a*, which were found in the other datasets. These genes were enriched for metabolic process and stimulus response gene ontologies.

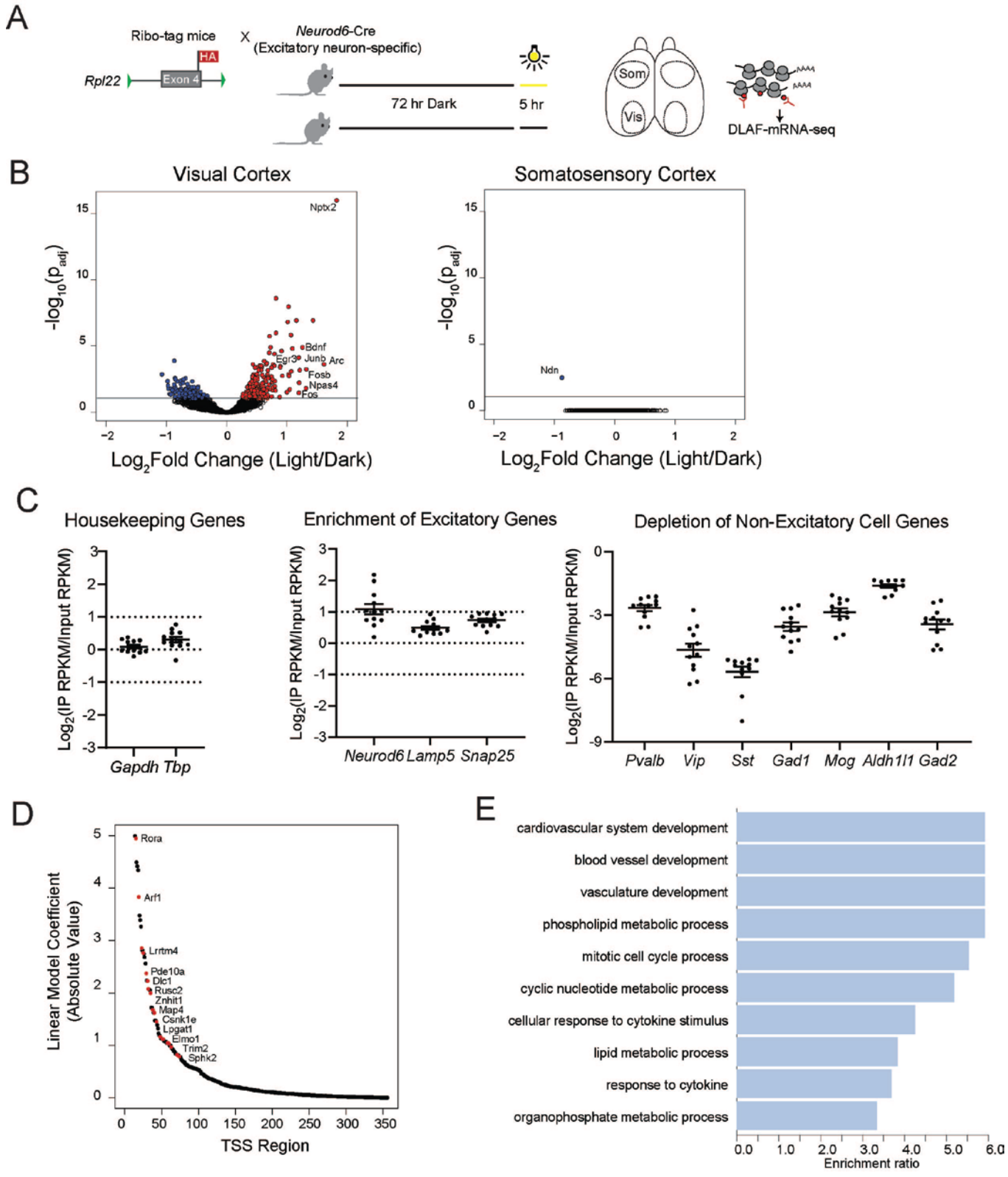
A
Ribo-tag mice
X
Neurod6-Cre
(Excitatory neuron-specific)
HA
Rpl22
Exon 4
72 hr Dark
5 hr
Som
Vis
DLAF-mRNA-seq
B
Visual Cortex
Somatosensory Cortex
-log10(padj)
Log2Fold Change (Light/Dark)
Nptx2
Bdnf
Egr3
Junb
Arc
Fosb
Npas4
Fos
Ndn
C
Housekeeping Genes
Enrichment of Excitatory Genes
Depletion of Non-Excitatory Cell Genes
Log2(IP RPKM/Input RPKM)
Gapdh Tbp
Neurod6 Lamp5 Snap25
Pvalb Vip Sst Gad1 Mog Aldh1l1 Gad2
D
Linear Model Coefficient
(Absolute Value)
TSS Region
Rora
Arf1
Lrrtm4
Pde10a
Dlc1
Rusc2
Znhit1
Map4
Csnk1e
Lpgat1
Elmo1
Trim2
Sphk2
E
cardiovascular system development
blood vessel development
vasculature development
phospholipid metabolic process
mitotic cell cycle process
cyclic nucleotide metabolic process
cellular response to cytokine stimulus
lipid metabolic process
response to cytokine
organophosphate metabolic process
Enrichment ratio

Figure 5-4. Excitatory-cell specific, ribosome-associated mRNA transcripts reveal alternative promoter usage *in vivo*.

(A) Ribotag mice were crossed with Neurod6-Cre mice and submitted to same activation of visual cortex. After dissection of cortices, ribosomes were immunoprecipitated and associated RNAs prepared with DLAF-mRNA-seq.

(B) Whole-gene analysis reveals induction of activity-dependent genes exclusively in visual cortex.

(C) Whole-gene validation of Ribotag immunoprecipitation from excitatory neurons.

(D) Genes above the previous cutoff for coefficient and passing a relaxed cutoff of unadjusted $p<0.1$.

(E) Genes with potential ADDUP are enriched in metabolism, cyclic nucleotide binding, and development.

Protein sequence is altered by promoter usage

Since alternative promoter selection can affect transcription and translation on multiple levels, we first examined whether alternative promoter selection altered the predicted peptide sequence of the encoded protein. In 88% of genes, protein coding sequence was altered by promoter selection (Fig 5-5A, top Venn). Many genes showed loss of annotated domains (Fig 5-5B), indicating altered function. However, a great many genes showed shorter or unannotated changes in peptide. Since a majority of genes are membrane-bound synaptic proteins, we examined whether signal peptide presence was altered in the list of genes with predicted protein-level changes due to promoter use. N-terminal signal peptides are short (~15 aa long) sequences which target a newly synthesized protein to the lumen of the endoplasmic reticulum. N-terminal peptides also are known to target proteins to the mitochondria. We used TargetP [5] to search for differential presence of signal peptides and mitochondrial localization signals in the N-terminal region of the protein isoforms found in Bru-seq, RNA-seq, and Ribotag-RNA-seq. 9% of protein level changes resulted in a predicted change to localization signal, either a signal peptide or a mitochondrial localization signal (Fig 5-5A, bottom Venn). One of these predicted changes included the phosphodiesterase PDE2A, a cyclic GMP and cyclic AMP cleavage protein found in neurons [138]. Interestingly, *Pde2a* is one of the few ADDUP genes that respond to both TTX and BIC by preferentially activating the same promoter (Fig. 5-5C). The long isoform is relatively upregulated in the TTX and BIC conditions, while the shorter, mitochondrial localization signal containing isoform is relatively upregulated in the baseline condition. To assess whether these protein isoforms localized to the predicted location in our cultures, we

overexpressed V5-tagged exogenous PDE2A isoforms in neurons and imaged their co-localization with mitochondrial marker TOMM20 (Fig. 5-5C). We found indeed that the short isoform, but not the long isoform, correlated in localization with TOMM20 (Fig 5-5D).

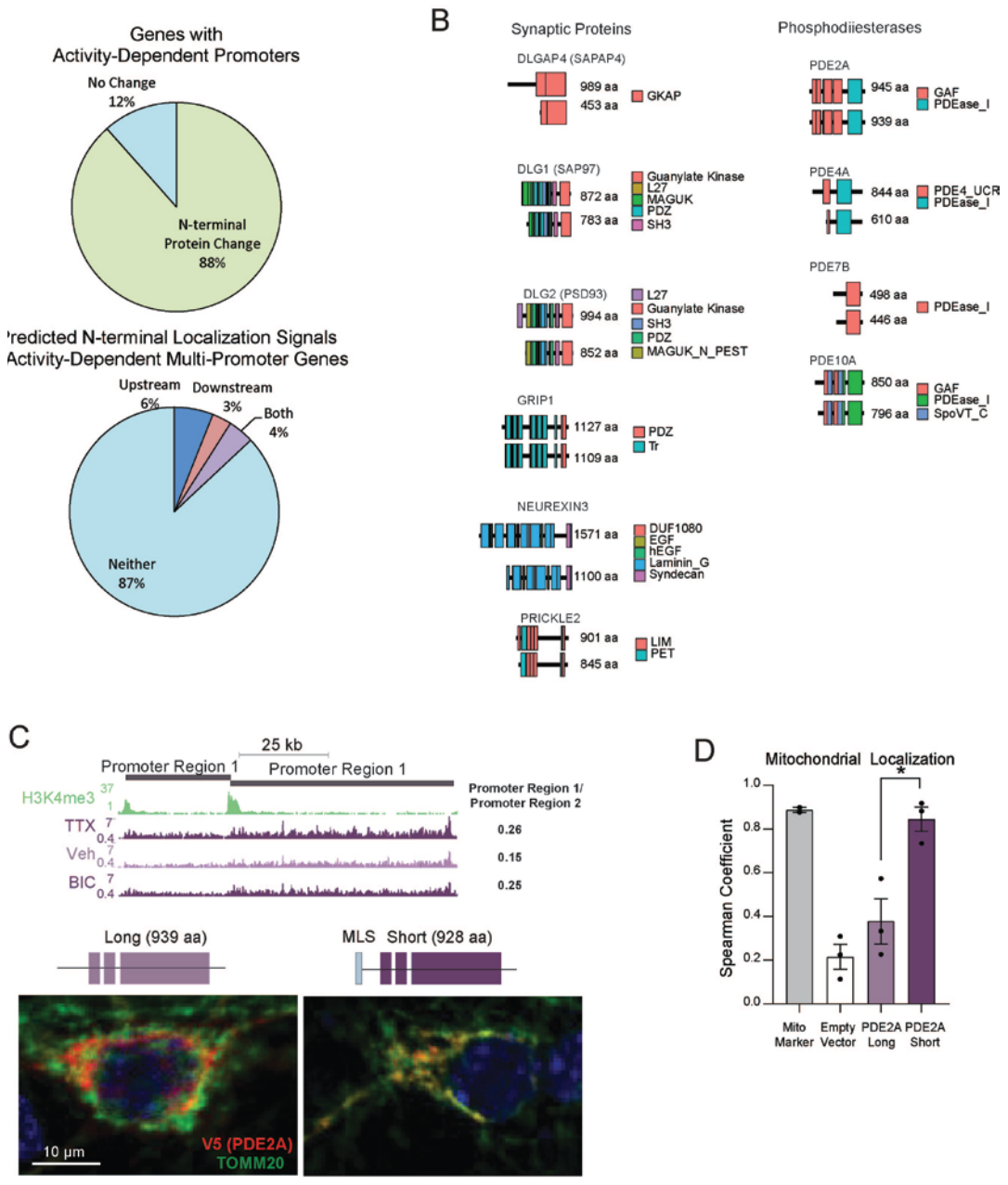

Figure 5-5. Activity-dependent differential usage of promoters yields predicted protein N-terminal changes. A. 88% of ADDUP genes show a predicated N-terminal isoform change, while 9% show potential differential presence of N-terminal localization signal, as predicted by TargetP software[5]. B. Genes overrepresented in gene ontologies include synaptic genes and phosphodiesterases. C. Phosphodiesterase PDE2A shows altered ratio of usage in response to activity, with differential preference for the long *Pde2a* isoform after both BIC and TTX treatment. The short isoform contains a mitochondrial localization signal, and is preferentially used in baseline state. Exogenous expression of the long and short PDE2A isoforms in mouse neurons demonstrates the preferred mitochondrial localization of the short (baseline) isoform.

Promoter-dependent subcellular localization drives synaptic changes in PDE2A

Very few (9%) ADDUP gene promoter-dependent protein products show a change in the predicted signal peptide or mitochondrial peptide-targeting sequences (Figure 5-5A), suggesting promoter usage may not be solely to alter signal peptide sequences. However, previous literature demonstrates that the N-terminus can be a site of post-translational modifications that direct protein isoforms to distinct subcellular locations even without a signal peptide. For example, glutamate-interacting protein1 (GRIP1), which was found in our *in vitro* and *in vivo* dataset to display ADDUP, has two promoters that result in the production of two proteins distinct only by 19 N-terminal residues. One of these residues is a site of palmitoylation [139]. This post-translational modification targets one isoform of GRIP1 to the synapse [140]. Thus, it appears promoter usage can direct protein localization even in the absence of a change in signal peptide.

Overexpression of differential promoter isoforms of PDE2A alters electrophysiology

Lastly, we wanted to determine experimentally the importance of the promoter switch to function of neurons. We therefore overexpressed the two isoforms of PDE2A, the long cytoplasmic form (Cyto-Pde2a) or the short mitochondrial-targeted form (Mito-Pde2a). We found that there was a significant difference in mEPSC amplitude between the Cyto-Pde2a and the Mito-Pde2a (Fig. 5-6A). Cumulative probability plot showed a significant difference between control-transfected neurons and both isoforms. However, the Mito-Pde2a is closer to the baseline level cumulative probability, which is consistent with its predominate expression at baseline. However, the Mito-Pde2a shows a striking increase in mEPSC frequency (Fig 5-6C), suggesting it may mediate synaptic regulation through multiple mechanisms, and that its concentration at baseline levels is critical for normal mEPSC frequency.

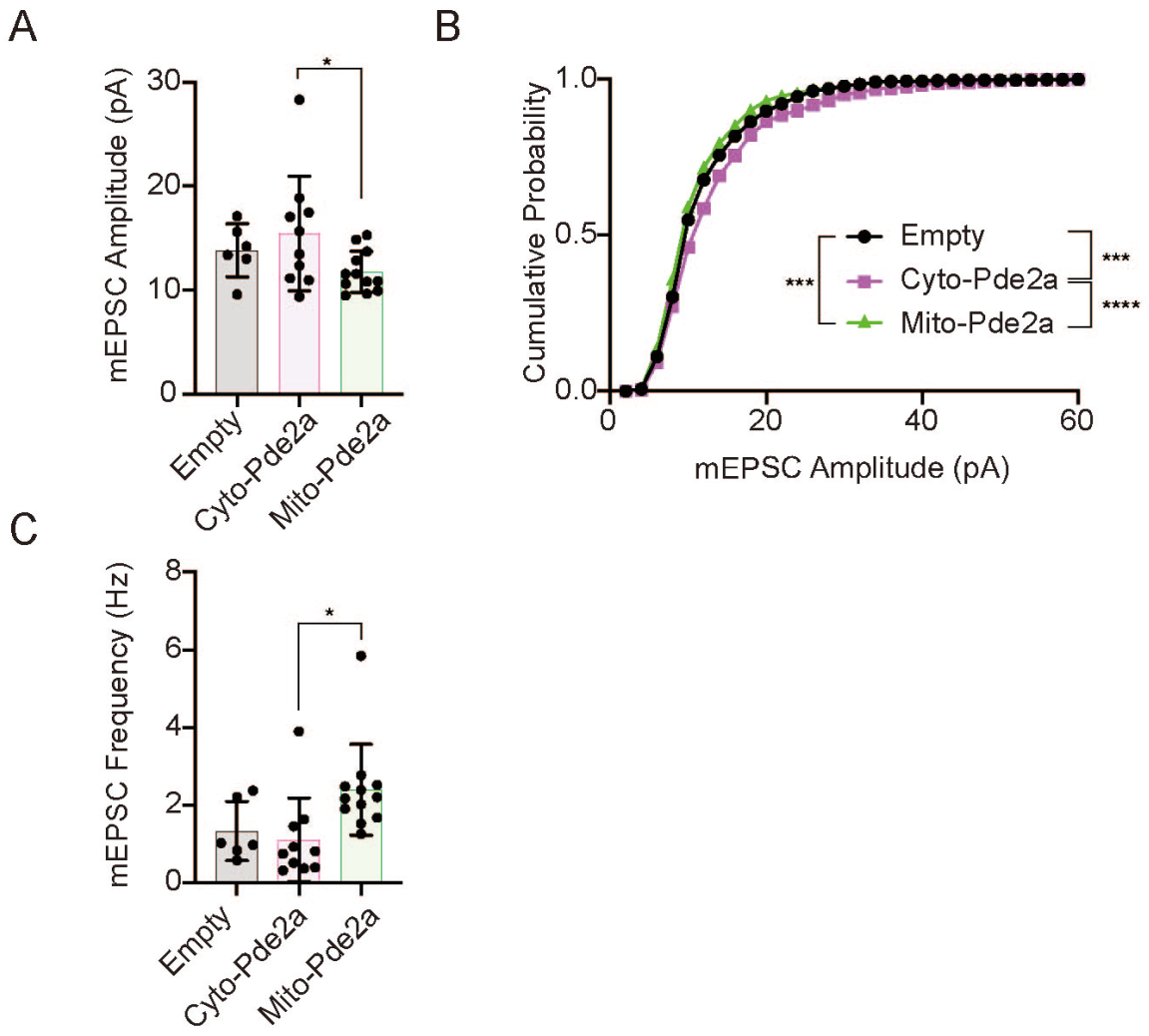

Figure 5-6. Exogenous expression of promoter-dependent isoforms of ADDUP gene *Pde2a* alters mEPSC amplitude and frequency

(A) Mito-PDE2A expression leads to a reduced mEPSC amplitude compared to the cyto-PDE2A isoform.

(B) Cumulative probability of mESPC amplitude reveals significant shift of the cytoplasmic isoform towards higher amplitude.

Discussion

Our data show that ~7% of the brain's transcriptome arises from multi-promoter genes, and that these multi-promoter genes are enriched in the activity-dependent gene set. Around 10% of these MGP display activity-dependent differential usage of promoters (ADDUP) at the timepoints tested. In the *in vivo* whole tissue and Ribotag data, both gene expression and ADDUP appeared more highly variable. However, there were similar examples in ADDUP *in vivo*, and exclusively in excitatory neurons. Experiments using more biological replicates *in vivo*, using nuclear RNA-sequencing (e.g. conditional SUN1-expressing mice[141,142]) crossed with other cell-type specific promoters (e.g. from excitatory neuronal subtypes or layer 4 cells) may more robustly reveal ADDUP. As evidenced by our data analysis, ADDUP appears to be a method of increasing the cellular proteome. While many genes' promoter-specific isoforms possess distinct functional domains, many show unannotated polypeptide changes. These N-terminal sites are therefore of interest to determine their role in protein function, localization, interaction, and degradation.

Comparing multi-promoter genes with gene list of autism-associated genes from SFARI demonstrated a significant enrichment of autism spectrum genes compared to all expressed genes (18% vs 7%, Chi-square test, p=2.2x10-16 [143]. However, ADDUP genes were not enriched for autism spectrum genes compared to all multi-promoter genes (22% vs 18%, Chi-square test, p=0.2). This suggests that multi-promoter genes are associated with autism spectrum genes. Although promoter usage itself may or may not underlie these genes association with autism, understanding promoter usage in autism-associated genes is important, as promoter usage of these genes may be a target for therapeutics. While many of the multi-promoter genes found display homologous H3K4me3 peaks in human brain tissue, the ADDUP of the genes we found may be mouse-specific. Therefore, pluripotent-cell derived human neurons should be analyzed for ADDUP to determine functional conservation across species.

The distinction between ADDUP and shifts in stable, translated mRNA remains to be determined. Because alternative promoters allow for distinct 5' leader regions to be transcribed, miRNA silencing or translation initiation regulation mechanisms may be at work to either normalize or enhance the distinct production. While many experimental variables may cause the difference in ADDUP gene lists between Bru-seq and Ribotag experiments, alternative 5' leader

processing may be behind the genes labeled ADDUP in our Ribotag experiment but not found to show ADDUP in Bru-seq.

In sum, these activity-dependent promoters may be a key to mechanisms of plasticity and should be taken into account when designing qPCR primers, RNA-seq experiments, and antibody-probe design. The roles of non-protein level effects of promoter usage have yet to be explored as well, as 5' UTR regulation is essential to RNA translation and neuronal function. Additionally, the transcription termination sites of these promoters, and alternative splicing, should be more deeply examined, as promoter usage may directly affect these processes as well.

Broader perspectives

Multi-promoter genes, whether their promoters are coordinately or differentially regulated, have broad potential for cellular regulation. The appearance of secondary promoters in these genes evolved to simultaneously express two forms of the protein: e.g. to produce a dominant-negative isoform to counterbalance the original isoform under all cellular conditions, or to produce isoforms targeted to distinct locations or binding partners. This was the case in the study on light-induced promoter usage in plants, where 78% of genes with alternative promoters encoded distinct protein isoforms, and 25% of these were predicted to alter subcellular localizations [144].

However, since many multi-promoter genes contain very distal promoters, the energy and time required to transcribe the isoforms may be very distinct between promoters. This may itself function to direct differential time expression of isoforms, which could affect mRNA or protein product regulation [145], or to conserve ATP usage for purposes of cellular homeostasis.

How would differential usage evolve? It may be that ADDUP are more likely to evolve when established multiple promoters were spaced distantly enough that transcriptional and chromatin-level regulation could differentially regulate the two promoters. Indeed, the distance between promoters in ADDUP genes are significantly longer than the promoters in non-ADDUP multi-promoter genes. However, enough ADDUP genes are shorter than other multi-promoter genes, suggesting promoters that do not show differential usage upon neuronal activity shifts have the potential to be used differentially in response to other stimuli or cellular contexts (e.g. circadian time).

As evidenced by our data analysis, ADDUP appears to be a method of increasing the cellular proteome. However, we have not definitively demonstrated that ADDUP occurs intracellularly. Therefore, it could also be a way of diversifying cell types within the brain. For example, a subset of excitatory neurons receiving light stimulation in the visual cortex may respond by initiating transcription from an alternative promoter that acts to produce a protein isoform that enhances synaptic responses to the stimuli. This may be a mechanism through which distinct neuronal circuits can respond differently to sensory stimuli. To address this question, single-cell analysis of ADDUP genes will likely require techniques such as *in situ* hybridization and imaging. Single-cell sequencing methods are not currently adapted to the read coverage required to analyze promoter usage, though this is advancing with such protocols as RamDA-seq[146].

In addition to the effect of ADDUP on protein isoform expression, evidence shows that transcription start site usage can be correlated with alternative exon usage through exon-mediated activation of transcription starts (EMATS). Proximal alternative exons may upregulate the use of weak alternative promoters through splicing-factor-mediated recruitment or stabilization of transcriptional machinery [147]. Genes with such internal exons are enriched in brain development, neuron projection, and synapse organization. This phenomenon occurs mostly when the induced transcription start site is within 2 kb of the included exon. It is possible that neuronal activity activates downstream exon usage, which in turn activates a weak intragenic promoter.

Many of our ADDUP genes occur in genes with long first exons (e.g. greater than 30 kb in length, data not shown). Genes with long first exons have been identified to exhibit recursive splicing, in which stepwise splicing events occur across the intron [148]. These splicing factors may in turn take part in the activation, maintenance, or repression of promoter usage in these genes. Alternatively, ADDUP and recursive splicing could have co-evolved with first intron lengthening without having causal interaction with one another mechanistically.

In contrast, there is evidence from plant studies that upstream promoter usage can inhibit downstream promoter usage [149]. It was found that this was dependent on the FACT chromatin complex. The FACT complex is conserved in mammals and Supt16 and Ssrp1 are expressed ubiquitously in the brain [47]. Furthermore, *SUPT16* mutations have been associated with a neurodevelopmental disorder [150]. Whether or not FACT chromatin complexes are functioning in

the brain similar to their function in plants remains an open question. Furthermore, how this phenomenon and the EMATS mechanism interact is relevant to understanding the multiple mechanisms at play in ADDUP.

Despite the potential importance of ADDUP, our data demonstrate that the majority of these promoters are used coordinately at this stage of activity-dependent transcription *in vitro*, and with greater variability *in vivo*. It is likely that ADDUP genes found to robustly switch in our datasets (e.g. *Elmo1*) occurs more uniformly across many cells compared to less robust ADDUP genes which may switch promoter usage only in a distinct cell subtype. Alternatively, we may find that ADDUP occurs stochastically across cell types as a side effect of other cellular states. Examining ADDUP across cell types may pave the way towards understanding more broadly how common ADDUP is intracellularly versus across a population of cells.

Remaining questions include the mechanism of switching these promoters. It is likely that these genes evolved to have stimulus-response promoters in a manner similar to the evolution of single-promoter genes. Therefore, it is not surprising to find known activity-dependent TF motifs enriched in ADDUP promoters. However, epigenetic and chromosome conformation may also control these promoters. The evolution of these promoters suggests these may play important roles in stimulus-dependent processes in other cell types, specifically other calcium-signaling cell types such as cardiomyocytes.

CRE elements are enriched in BIC-upregulated and TTX-downregulated genes. CREB has been found to bind to activity-induced genes such as *Fos* and *Jun* at baseline activity level and in response to TTX. However, CRE sites appear to require TATA boxes to recruit CREB-regulated transcription coactivator 1 (CRTC1) in response to activity or reduce CRTC1 occupancy in response to TTX. [151]. CRE-containing promoters absent of TATA boxes, however, do not recruit CRTC1 and are not stimulus dependent. Therefore, examination of activity-dependent genes can include examination for the presence of CRE elements and differential TATA box presence. CREB is, however, recruited by neuronal activity to enhancer regions, suggesting enhancers may guide neuronal activity-dependent transcription. [151]

Synthetic biology approaches can illuminate some of the questions underlying alternative promoter selection. For example, fluorescent reporter genes under the control of drug-inducible

synthetic alternative promoters[152] can be used to examine the interaction between inter-promoter distance and differential regulation, 5' leader regulation, and the importance of cis and trans elements or coordinated cellular treatments (e.g. high vs. low activity states). In this way, questions of mechanism can be directly answered at the level of single-cells and cell population.

To test these hypotheses on mechanism, alternative TSS usage can be assessed in cultured neurons treated with lentiviral knockdown of transcription factors, splicing factors and FACT complex members. In this way we may reveal the underlying mechanisms that guide promoter selection.

CONCLUSION

The model of activity-dependent transcription and synaptic scaling is a useful tool to explore the interacting functions of chromatin regulators, and the interacting mechanisms of alternative promoter usage, alternative splicing, alternative 3' ends, enhancer activation, and others. In this work, I demonstrated the utility of a nascent RNA method to detect more precisely the expression trends in the transcriptomes between high- and low-activity states. Nascent transcription analysis had the advantage of identifying with certainty that the effects analyzed came from transcriptional mechanisms.

Interestingly, we discovered, as is the case with RAI1 chromatin binding and PDE2A promoter usage, times when shifts to either high or low activity states show similar changes compared to the baseline state. This suggests that the baseline state retains an identity beyond a midpoint between the two states, and requires a specific transcriptome in order to maintain its state. This perspective may help to unravel new mechanisms controlling synaptic scaling, LTP, and LTD, especially if all three activity states are simultaneously examined.

Alternatively, our analysis with RAI1 underlines a link between neural activity-dependent transcription and circadian rhythms. The intersection between these two phenomena remains relatively unexamined in analyses of activity-dependent neuronal function, despite ample evidence of transcriptional regulatory mechanisms and protein pathways shared between them. The initiation of hyperactivity and inactivity may serve to synchronize neuronal cultures' circadian clocks similar to zeitgeibers of light or eating in living animals. In this case, the cultures at baseline represent not a specific cellular state but a population of neurons with unsynchronized clocks. Therefore, any distinction between baseline state and inactivity or hyperactivity may be due to neurons at distinct timepoints in their circadian cycles. In this interpretation, RAI1 likely oscillates on the chromatin in a circadian manner, with peak occupancy at a time that does not correlate with 4 hours post TTX or BIC. Loss of RAI1, then,

may push cells transcriptome towards not (only) an inactivity-like state, but a different circadian time. Casting neuronal activity in terms of its effect on circadian time may reveal better how neuronal activity-dependent transcription and thus synaptic plasticity functions at the transcriptional level. Furthermore, expanding the set of enzymes that intersect with neuronal function and neurodevelopment, allows for an expanded toolbox of drugs that can be used to address neurodevelopmental disorders and sleep. A deeper understanding of circadian time and synaptic plasticity can also inform which compounds may impact either system with maximal efficacy and safety.

While bulk analysis of diverse cellular populations obscures cell-specific changes, assessing correlations between genome-wide characteristics may allow the detection of interesting trends, as was the case with the discovery of alternative promoters and with *Rai1*-KD's trend towards a TTX-like state. Small correlations may reveal the mechanisms of cell-subtype specific changes. This broad view can be augmented by a cell-type and single-cell approach. That is, the immunocytochemistry and electrophysiology used in this dissertation can be complimented by methods to isolate cell subtypes from bulk tissue/culture (e.g. INTACT), or single cell methods such as *in situ* hybridization, live-imaging, or single-cell sequencing methods.

Genes associated with neurodevelopmental disorders allow us to identify pathways of interest that are relevant for cognition. For example, the striking sleep patterns of individuals with SMS bolster the hypothesis of RAI1's interaction with circadian genes. Drawing more ties between human behavior and characteristics in a given monogenic NDD and the molecular and cellular functions of its associated gene will accelerate both our understanding of pathways and processes like synaptic scaling and our ability to produce the most relevant therapeutics.

APPENDICES

Appendix A. Development of Low-Input DLAF RNA-seq Library Preparation Protocol

The discovery of alternative promoter usage after activity shifts was possible due to abundant intronic reads from Bru-seq protocol. However, to profile mature RNAs, we needed to use an mRNA sequencing protocol. However, many conventional mRNA sequencing protocols deplete read coverage at the 5' end of genes, making transcription start site identification difficult. The Direct Ligation of Adaptors to First-strand cDNA protocol developed in the Iwase lab actually enriches the 5' end of genes [130]. However, the protocol was developed for RNA inputs ~ 1-4 mg. Neurod6-Cre Ribotag immunoprecipitation of ribosome-associated RNAs from the visual and somatosensory cortices often yielded RNA mass <100 µg. Initial experiments using the original DLAF protocol resulted in poor library complexity and over-representation of adaptors. I aimed to adapt the DLAF protocol to achieve a shorter, more streamlined protocol that retained maximal RNA for robust sequencing results.

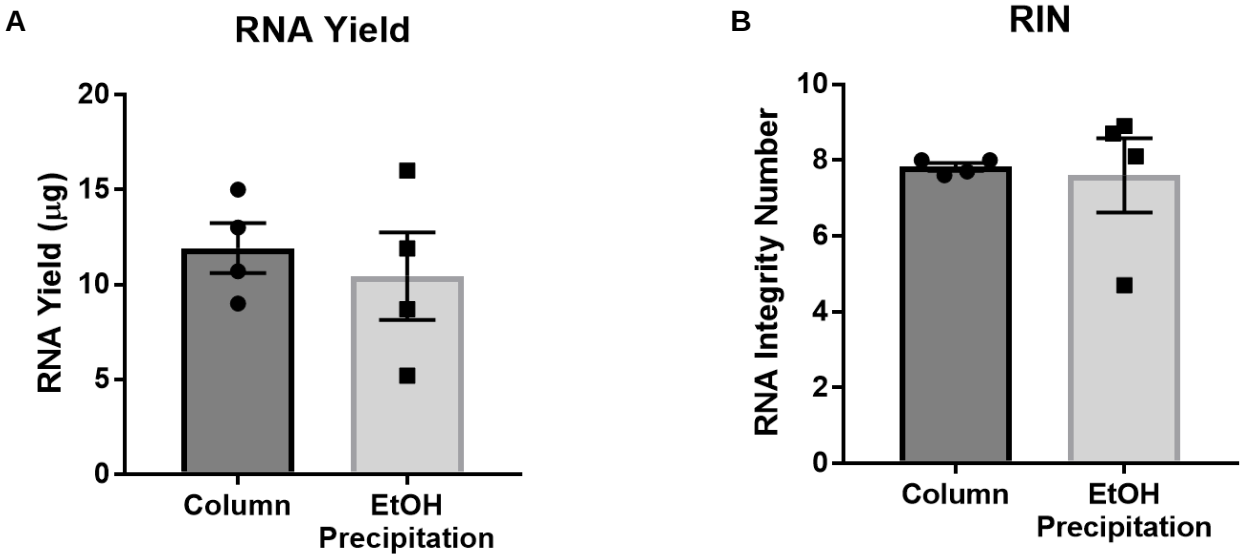

Figure A-1. Effect of Post-Trizol Purification Method on RNA yield and integrity. Column Purification achieves similar RNA yield (A) and RNA integrity number (RIN, B) as EtOH purification, with less variability.

Examination of purification and RNA fragmentation steps

After ribosome immunoprecipitation, RNAs must be separated from ribosomal proteins through Trizol phase separation. Since column purification can retain much RNA in the column, I first examined whether the critical purification step after Trizol phase separation was distinctly different between column purification and ethanol precipitation. Phase separated RNA from one whole-tissue sample was divided into 8 equal volumes and 4 replicates per purification method was tested and examined using Bioanalyzer RNA concentration and RNA integrity analysis. I found that while column purification and ethanol precipitation resulted in similar mean yields and RNA integrity numbers, column purification resulted in lower variability (Fig. A-1). Therefore, I proceeded with column purification as the standard method.

Another critical step in library purification is RNA fragmentation, which determines the size of library fragments. Too long of RNA fragments fail to adhere to the Illumina chip, and too short of fragments prevent size-separation with adaptors, leading to adaptor contamination. Since my initial run of the DLAF protocol resulted in high adaptor proportions, I wanted to optimize the fragmentation protocol to the ideal RNA fragment length of ~200-300 nucleotides. First, I examined whether RNA fragmentation was concentration-dependent, as different samples may yield quite varying concentrations of RNA as input to the fragmentation step. I compared identical RNA diluted to 8 ng/µL, 2 ng/µL, and 0.8 ng/µL, and subjected it to fragmentation in high-magnesium Tris-HCl buffer for 4, 8, or 12 minutes. I found that there was little drastic difference in the efficacy of the fragmentation protocol for each concentration, suggesting RNA fragmentation is concentration-independent within this relevant range (Fig. A-2). However, when examining the time-dependence of RNA fragmentation, 12 minutes outperformed 8 and 4 minutes, as there remained many high-molecular-weight, unfragmented RNAs in the 4 and 8 minute samples. Therefore, I selected 12 minutes as the standard fragmentation time.

Next, I tested the temperature dependence of RNA fragmentation. Using the same concentration of 8 ng/µL (400 ng total), I tested temperatures between 65 and 90° C. There was a clear increase in 200-400 nt size RNAs at 90° C, so I proceeded with this temperature. (Fig. A-3).

I then tested whether magnesium concentration was critical for RNA fragmentation. The current protocol stated the use of a commercial fragmentation buffer that contained 2.8 mM Mg^{2+}. I fragmented 8 ng/μL RNA for 12 minutes at 90 ° C under Mg^{2+} concentrations ranging from 0.7-5.5 mM. There was a clear shift in RNA fragment size above 1.4 mM Mg^{2+}, including RNAs shorter than 200 nt, overlapping with the predicted adaptor length of 150 nt (Fig. A-4). This also explained the potential low yield in library size, as RNAs in this size range were likely to be size-selected away. Therefore, I selected 1.4 mM as the standard Mg^{2+} concentration.

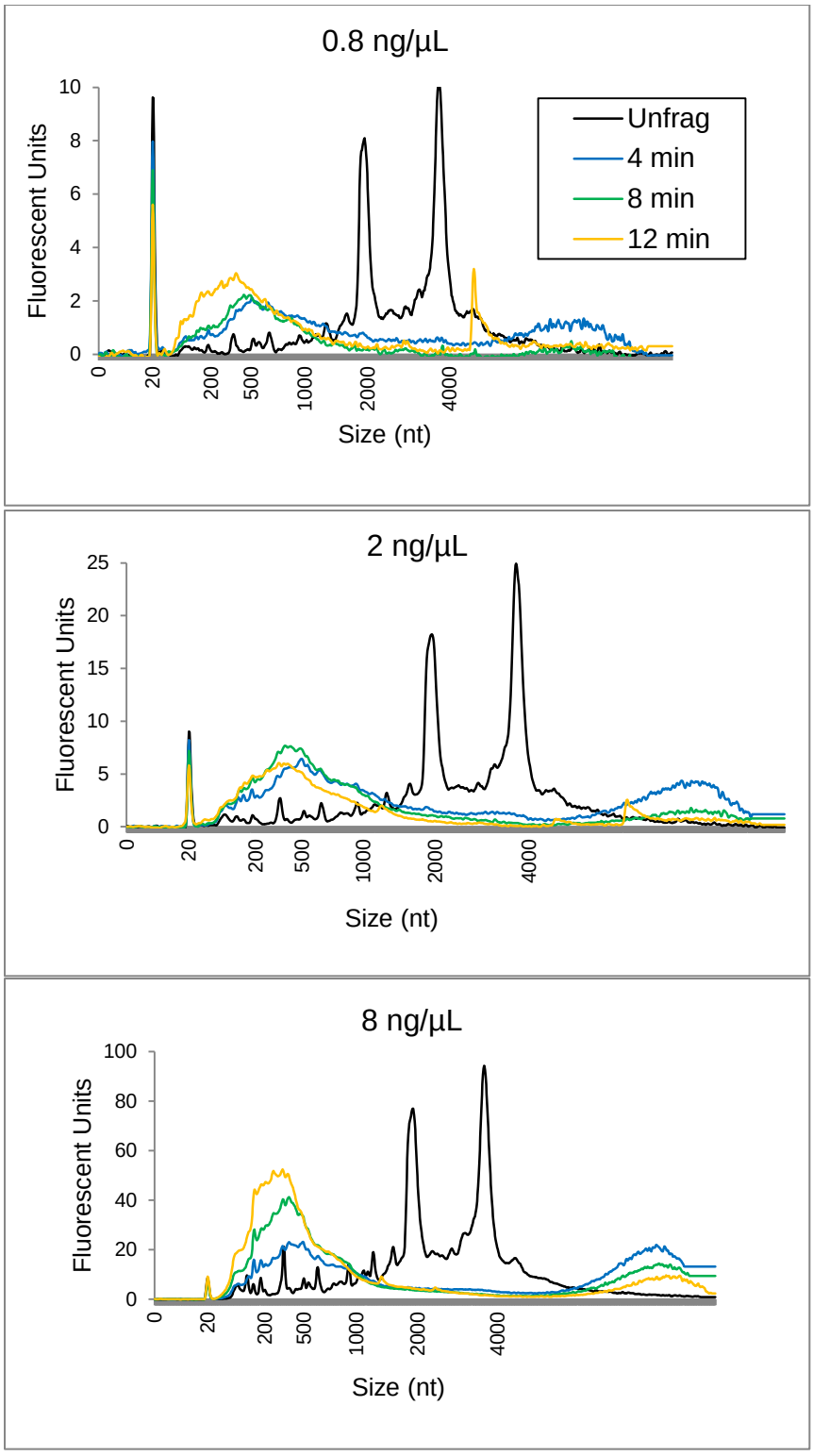

Figure A-2. Effect of Time and Concentration on Fragmentation. RNA at 0.8, 2, and 8 ng/µL show robust fragmentation after 4 min at 80˚ C. However, at all concentrations, 12 min yielded higher intensity between 200-300 nt (target size).

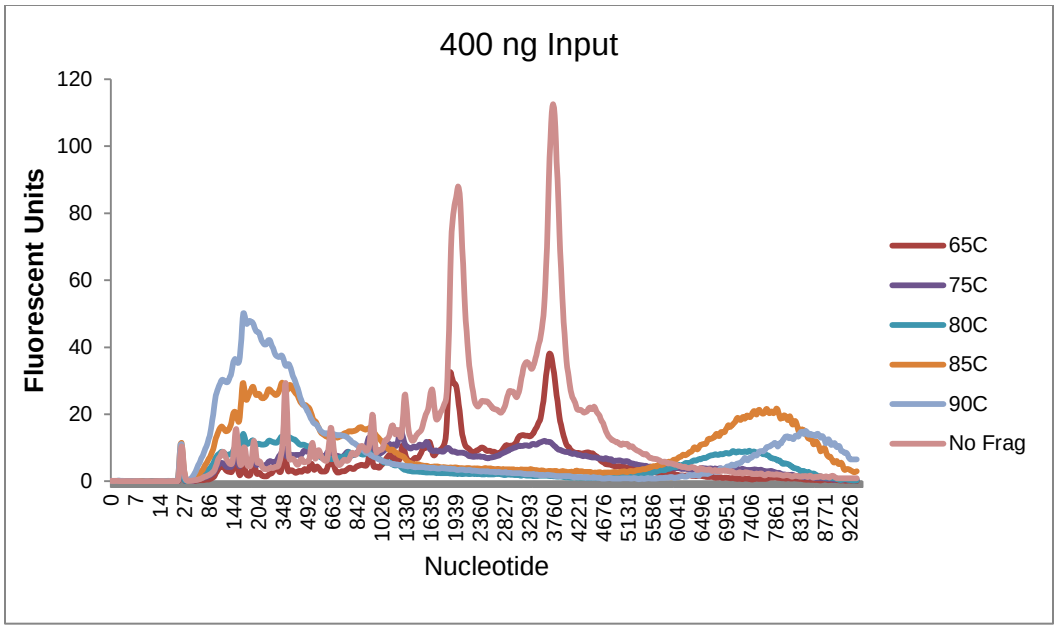

Figure A-3. Effect of Temperature on RNA fragmentation. Temperatures of 85-90˚ C show most robust fragmentation, while lower temperatures show remaining long RNA.

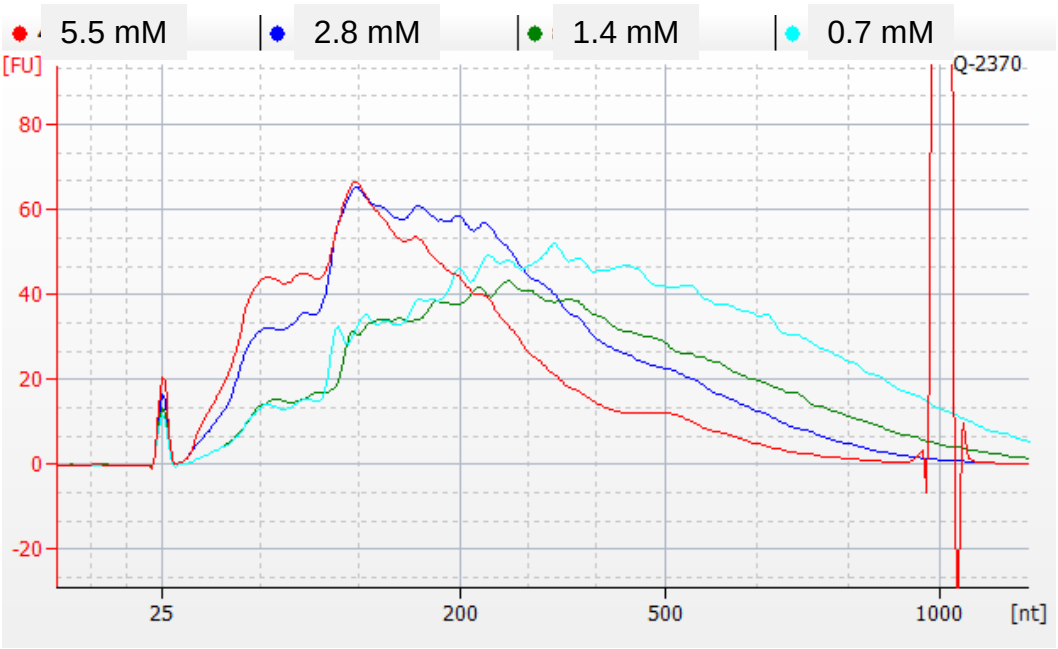

Figure A-4. Effect of Magnesium Concentration on RNA fragmentation. Magnesium Concentration greater than 1.4 µM shows shift towards over-fragmented RNA.

Lastly, I tested the robustness of Ampure bead RNA purification to slight changes in protocol. There are many warnings that state that incubation time, bead drying time, and elution time are critical for efficient purification. Since during library preparation I handle many samples, this could be a source of variability, as different samples receive different times for each step. Therefore, I sought to determine critical factors of Ampure bead purification. I varied initial RNA: bead incubation time from 5-15 minutes; I varied dry time from 2 to 10 minutes (at which point the beads were very dry and light brown), and I varied elution time from 5 to 10 minutes. I used column purification of RNA as a control, which is known to yield lower amounts of RNA. Using 2 replicates for each sample, I found that surprisingly, all conditions showed similar yields (ranging from 90% yield to 70% yield) (Fig A-5). This is significant, but not as drastic as presumed. The long dry samples did have an overall lower yield than the short dry samples (Fig. A-6), but this was not drastic, especially as 10 minute dry time is an extreme length of time unlikely to occur even with dozens of samples. Other conditions did not show any evidence of being critical. Meanwhile, the column purification performed much worse, with only 10% yield (likely so low due to low 100 ng input). Therefore, going forward, small modifications to Ampure protocol are likely not to affect yield, excepting very long bead dry times.

Lastly, I wanted to assess whether use of the more precise, but more time consuming Qubit was superior to the Nanodrop. I therefore measured 16 samples in both Nanodrop and Qubit and observed correlation between measurements (Fig. A-7A). However, there was a consistent trend in Nanodrop measuring higher concentrations of RNA by ~20% (Fig. A-7B). Therefore, Qubit was used to determine the initial concentrations of RNA in the subsequent low-DLAF input experiment in order to input sufficient RNA.

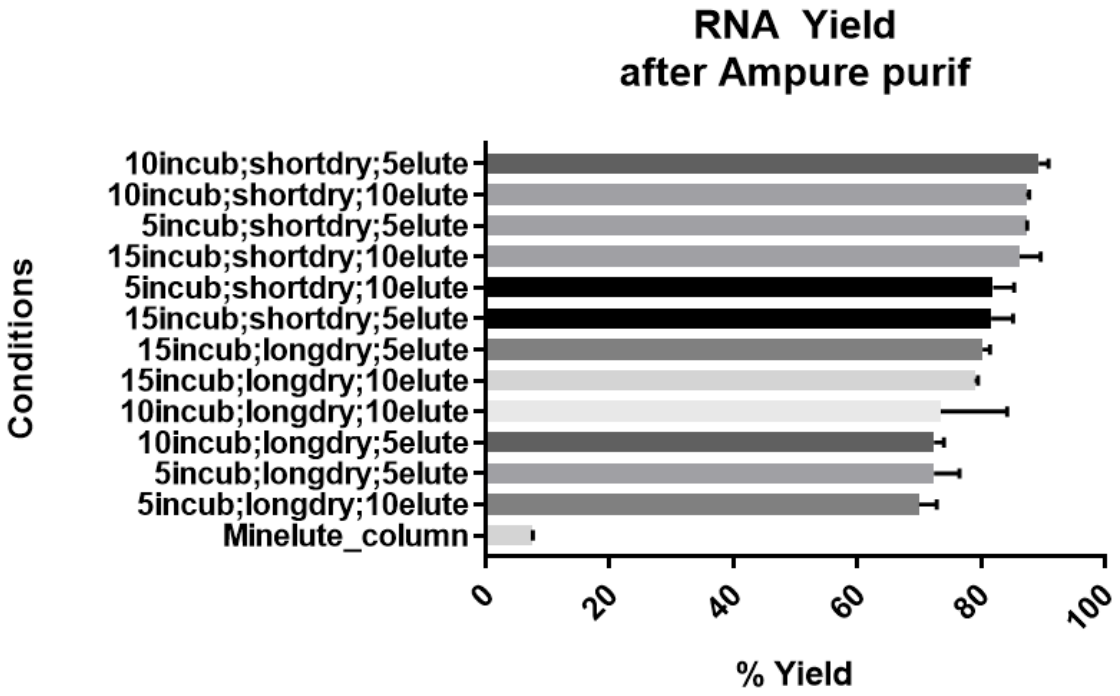

Figure A-5. Ampure purification protocol is robust to small changes in protocol

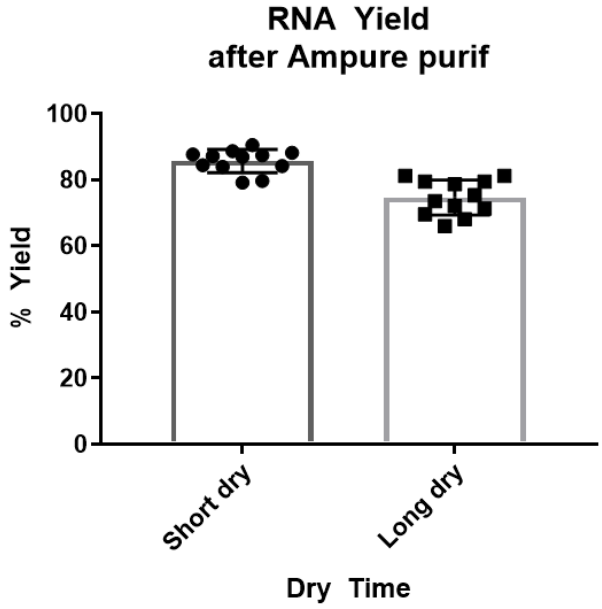

Figure A-6. Effect of Dry Time on RNA Yield in Ampure purification. Extra-long dry time (15 min) shows minor reduction in yield compared to short dry time (2 min)

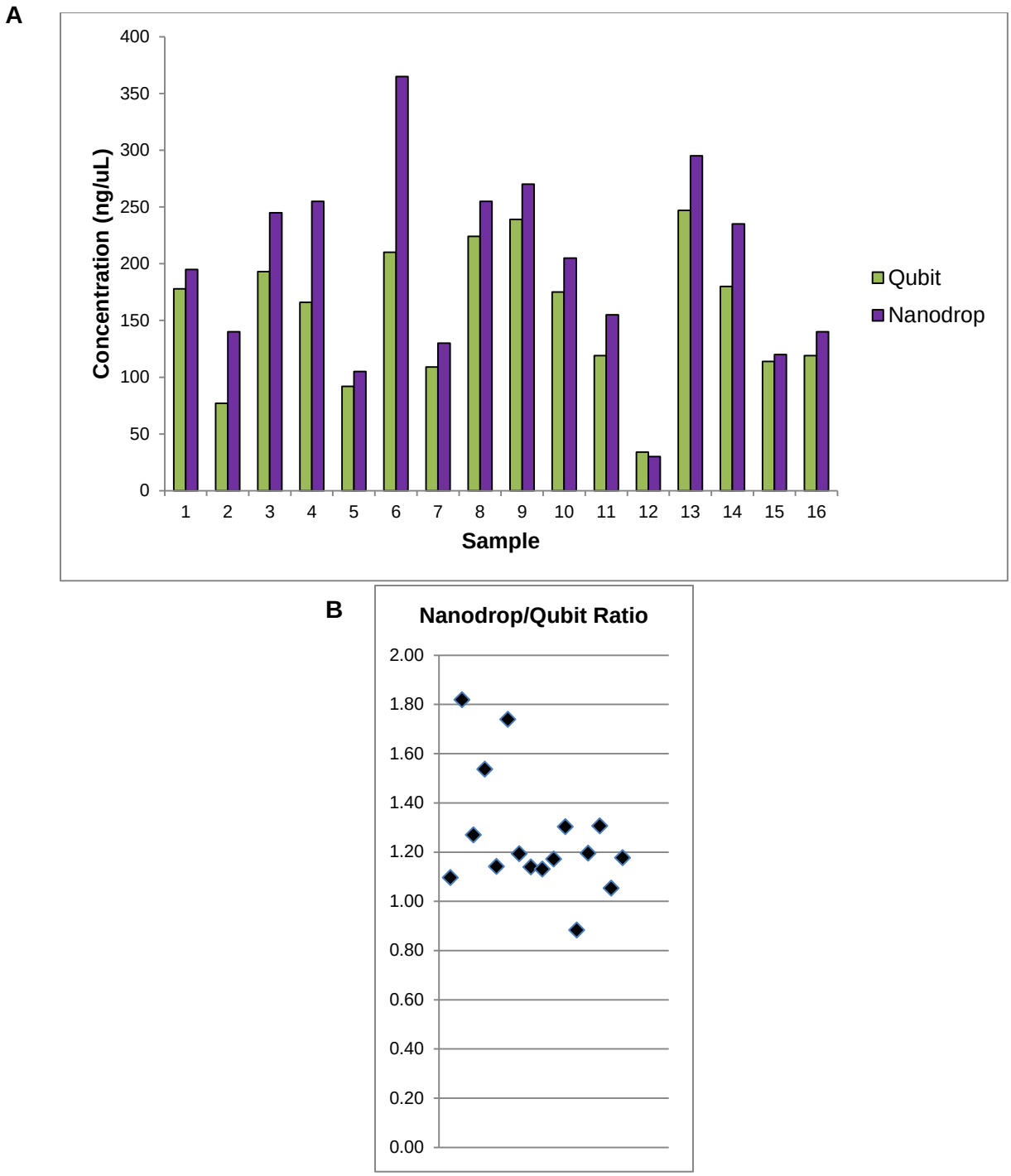

Figure A-7. Comparison of Nanodrop and Qubit measurements of RNA concentration in water. Sample concentrations correlate between the two methods (A), though Nanodrop predicts ~20% higher concentration (B).

I therefore ran the adapted Low-DLAF protocol with RNA inputs of 4 µg, 1 µg, 250 µg, and 62.5 µg, then submitted them to Illumina sequencing. I found that all samples (N=1) had similar reads

assigned to mouse mm9 genome. Lower input RNA had less adaptor contamination, likely as total adaptor mass was reduced for lower RNA input. However, there was a clear increase in the percentage of ribosomal reads in the low-input samples, suggesting these may be preferentially retained and amplified, and more stable in lower concentrations than non-ribosomal RNAs. However, the genes that were uniquely mapped were of similar percentage, and the overall percentage of good reads (those uniquely assigned to one genomic location in the mm9 genome) decreased only from 53% to 48% from 4 µg input to 62.5 µg input. Similarly, the genes mapped to mm9, ~70% were assigned to gene bodies (Fig. A-8).

Interestingly, while there were a similar number of reads input from each sample, the median read count/gene was significantly higher for higher RNA input 4 µg sample. This suggests there were a few genes with an overabundance of reads in the lower samples (e.g. contaminating ribosomal RNAs). This same trend was seen examining the read counts at TSS region (TSS + 1kb downstream (ds)). However, even low input retained similar coverage at TSS compared to total gene read count, suggesting the 5' end coverage is not disproportionately compromised with low RNA input.

Lastly, I examined the correlation of read counts across the gene or TSS region between the 4 µg input and lower inputs. Predictably, the rho correlation was highest for 250 ng input, and lower for lower inputs (Fig. A-10). However, there was a clear positive correlation across all inputs excepting the negative 0 input control.

Discussion

These data give evidence that although there is a significant reduction in quality reads/gene or reads/TSS region for each sample, much lower input samples can be assessed, although deeper sequencing and removal of ribosomal reads may be necessary to achieve quality differential expression results.

Input	Reads	Adaptor Reads	% Adaptors	Uniquely Mapped	% Uniquely Mapped	Ribosomal	% Ribo	Mitochondrial	% Mito	Good Reads	% Good of Mapped	% Good overall	Assigned to Gene	Reads Assigned to Gene (M)	% Assigned from Good	% Assigned	Norm Factor
4 ug	10,152,461	1,577,558	16%	5915751	58%	352961	6%	135358	2%	5427432	92%	53%	3758221	3.7582	69.24%	37%	1.8425
1 ug	10,940,881	1865642	17%	5620378	51%	816391	15%	105369	2%	4698618	84%	43%	3373802	3.3738	71.80%	31%	2.1283
250 ng	11,062,037	218,576	2%	6852978	62%	1238187	18%	187932	3%	5426859	79%	49%	4094342	4.0943	75.45%	37%	1.8427
63ng	9,413,143	840,291	8%	5608004	60%	1025812	18%	164268	3%	4417924	79%	47%	3345677	3.3457	75.73%	36%	2.2635
0 ng	1,127,998	767,188	68%	5639	0.50%	726	13%	143	3%	4770	85%	0%	2882	0.0029	60.42%	0%	2096.4

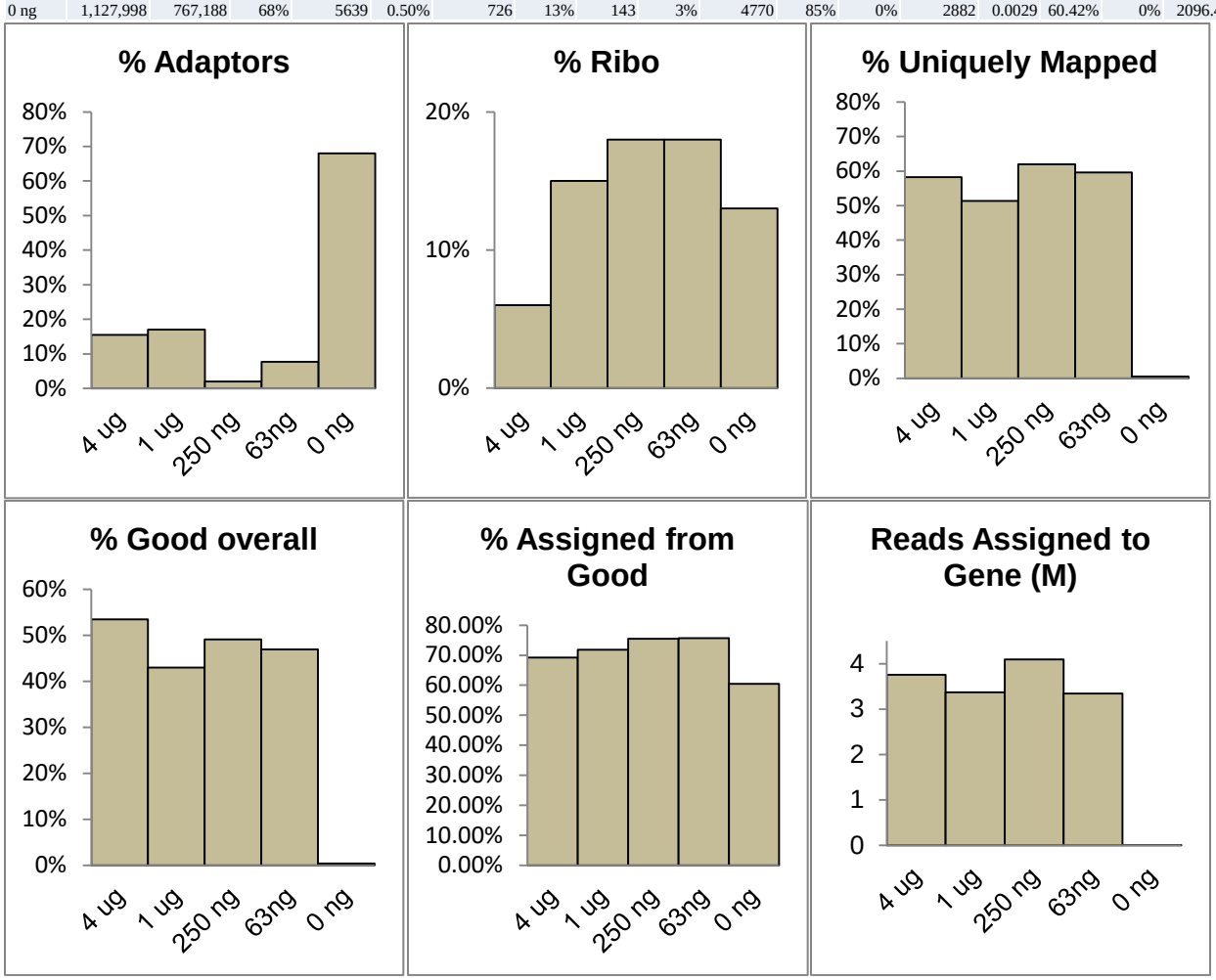

Figure A-8. RNA Input's effect on filtered and unfiltered read counts.

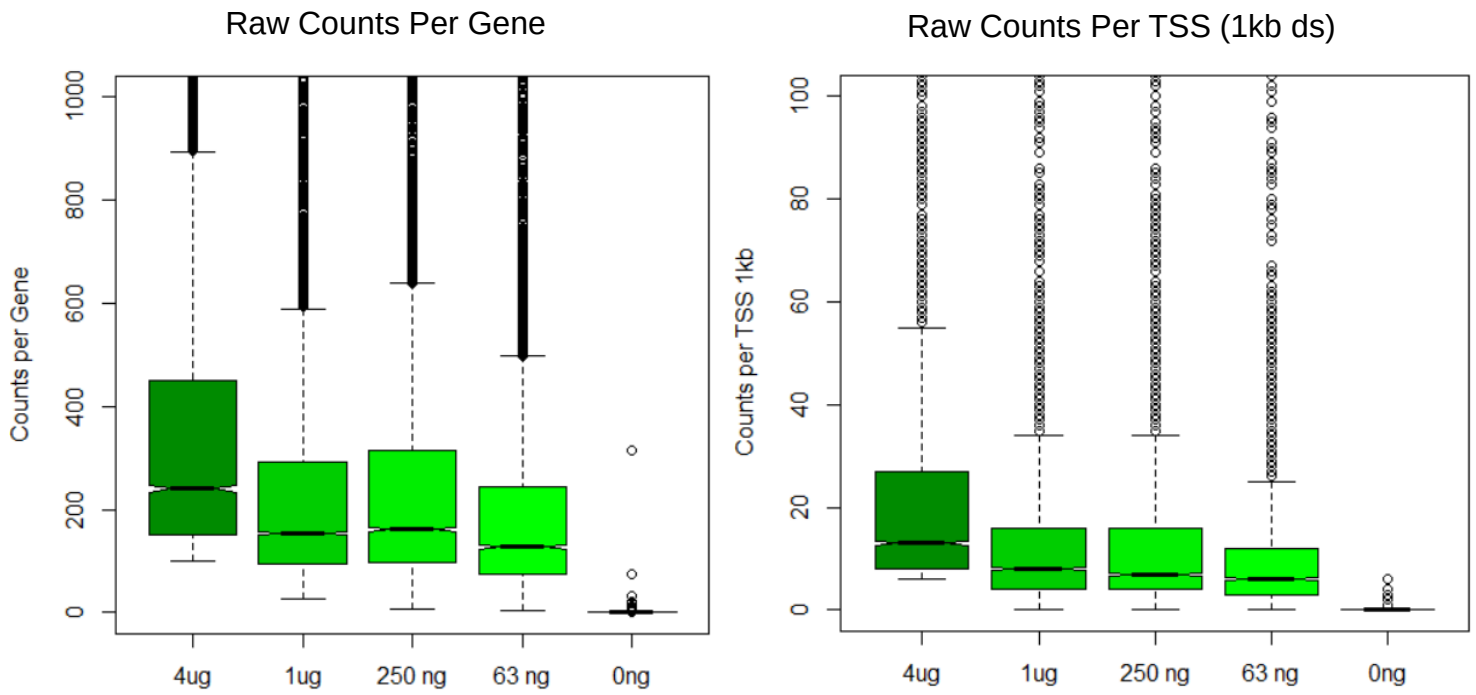

Figure A-9. RNA Input's effect on normalized read counts

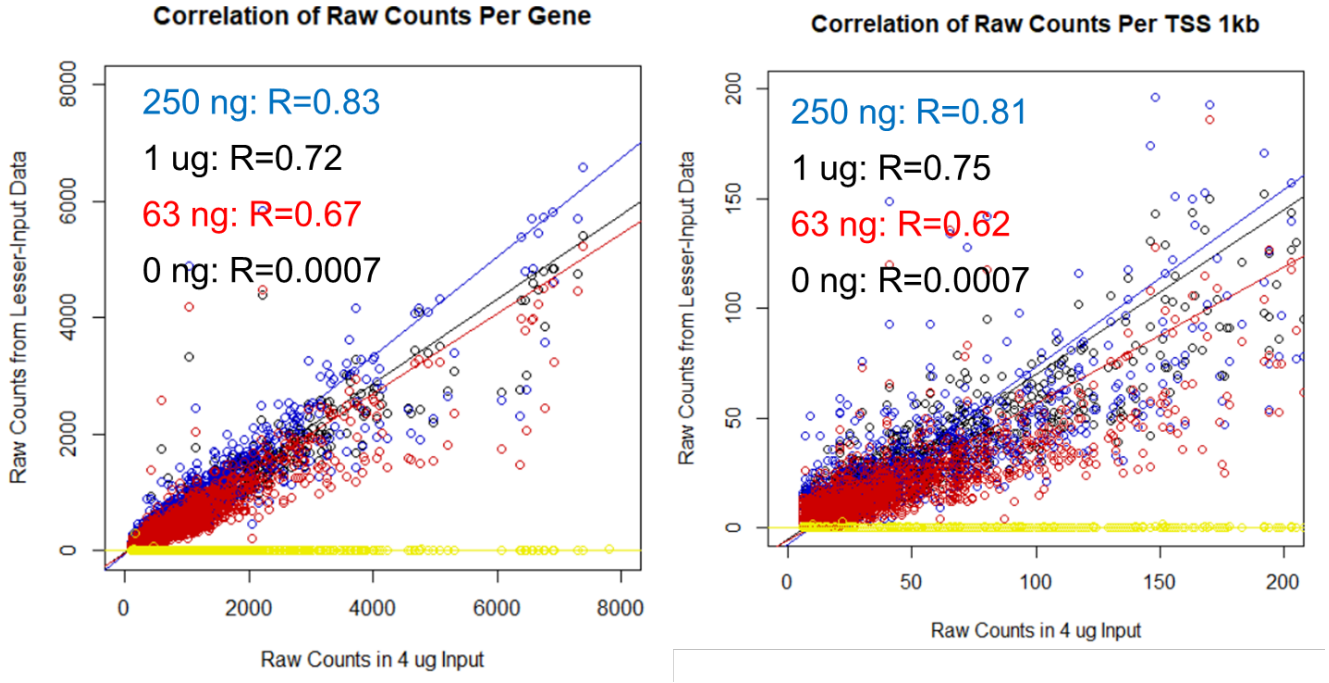

Figure A-10. Mapping reads to gene and TSS regions from low-input samples

Appendix B. Materials and Methods

Primary neuron culture and shRNA-mediated Rai1*-KD*

The cortices and hippocampi from E18.5 mouse pups were pooled into biological replicates with identical female-male ratios. Sex of the pups was determined by PCR using primers for the *ZFY* gene (Table S6). Primary culture of neurons was carried out as previously described [132 153]. Briefly, dissociated tissues were plated at 4 million cells/6 cm poly-D-lysine-coated plate (Sigma) grown in Neurobasal Media supplemented with B27 (Gibco, #17504044). No mitotic inhibitors were added, allowing the growth of non-neuronal cells. Half the culture medium was freshened every 3-5 days. On DIV 14, cells were infected with lentiviral shRNA as previously described [153]. Lentivirus were generated using co-transfection into HEK-293t cells of psPAX2 (Addgene, 12260), pMD2.G (Addgene, 12259) and pLKO plasmids containing shRNA against *Rai1* untranslated region (*Rai1*-shRNA #1: Sigma, TRCN0000124984) or coding region (*Rai1*-shRNA #2: Sigma, TRCN0000328334) or scramble shRNA (Sigma, SHC202). For Bru-seq experiments, we used SHC202 and *Rai1*-shRNA #1. For electrophysiology, we used SHC202, *Rai1*-shRNA #1 and #2, whose target sequences are identical between mouse and rat. The conditioned media containing lentiviruses was collected, concentrated with Lenti-X concentrator (Takara, 631232), and resuspended in Neurobasal medium, and stored at −80°C. The titer of lentivirus was determined by survival of transduced 293 cells under puromycin and a comparable amount of virus that result in >90% survival of infected neurons was used for all biological replicates. Puromycin was not added to cultured neurons for experiments.

Network activity alterations and Bru-seq experiments

On DIV17, cells were treated with bicuculline-methiodide (Abcam, ab120108, 20 μM), TTX (Tocris, 1069, 1 μM), or vehicle (sterile water), for 4 hours. 3 hours and 40 minutes post treatment, bromouridine (Bru, Sigma, dissolved in PBS) was added to cultures at 2 mM final

concentration. Cultures were harvested in Tri-reagent BD (Sigma, T3809) and frozen immediately. RNA was purified using phenol-chloroform extraction and isopropanol precipitation, treated with DNAse I (NEB) then fragmented by high-magnesium, high temperature incubation. From 1 µg of total RNA, enrichment of Bru-containing RNA and library preparation were performed as previously described [44,45] with minor modifications. We designed custom adaptors (Table S6) which were directly ligated to the 3' ends of RNA using RNA ligase 1 (NEB Cat. No. M0437) and truncated RNA ligase KQ (NEB M0373). Bromouridine-labeled RNAs were immunoprecipitated using anti-BrdU antibody (Santa Cruz Biotechnology, sc-32323). Enriched RNAs were reverse transcribed using a primer complementary to the RNA adaptor (Table S6). Adaptor duplexes with 5- or 6-base pair random nucleotide overhangs were ligated to the 3' end of the cDNA (Table S6). The cDNA libraries were amplified using primers that carry Illumina indices, then 180-400 bp DNA fragments were isolated using by an agarose gel. The nucleotide sequences of primers used for library amplification are found in Table S6. The libraries were subjected to single-end 50-bp sequencing using Illumina HiSeq 2000 platform. We performed 2 to 3 biological replicates for all drug treatment and knockdown conditions.

Sequencing data analysis

After confirming the quality of sequencing data by FastQC, reads were mapped to mm9 reference genome using Bowtie2 [154] and annotated with Tophat2 [155]. Adaptors were trimmed using BBDUK (http://jgi.doe.gov/data-and-tools/bb-tools/), when 2-30 bp on the left of the read matched the predicted adaptor (k=30, mink=2, minlength=15, hdist=1). Bru-seq signals were quantified by FeatureCounts [156]. We excluded *Rn45s*, *Lars2*, *Rn4.5s*, *Cdk8*, *Zc3h7a* and the mitochondrial chromosome to avoid counts of over-amplified genes that may skew RPKM normalization. DE-genes were identified using DESeq2 [46] using the same parameters for the Bru-seq data and three published mRNA-seq datasets of neuron culture and *Rai1*-KO mice [2,21,43]. We also used DESeq2 to calculate RPKM expression values across the entire genic regions, including introns. Gene ontology was examined using RNA-Enrich [80]. Significance cutoff for reporting Sig-genes was an unadjusted p value< 0.05. We only presented GO terms that contain 5 to 250 genes.

Western blot

To validate *Rai1*-KD in mouse forebrain neuron culture, *Rai1*-KD and control cultures were harvested at 3 days after lentiviral transduction and subjected to Western blot analysis as described previously [132]. RAI1 antibodies were generated by immunizing rabbits with a synthesized RAI1 peptide (aa 28 to 42, ENYRQPGQAGLSCDR, Thermo Fisher Scientific), followed by affinity purification using the peptide as the affinity ligand (Thermo Fisher Scientific). Anti-PCNA antibody (Santa Cruz sc-56, 1:1000) was used for a loading control. For analysis of RAI1 level during activity shifts, the cortices from E18.5 rat pups were dissected, dissociated, and plated at 700,000 cells/well in a PDL-coated 6-well dish. Neurons were grown in Neurobasal/B27 medium for 14 DIV. Vehicle (1% water), TTX (1 μM) or BIC (20 μM) were added to the culture and cells were harvested with a 1:1 mixture of 2X Laemmeli buffer (BioRad, 1610737, 1:20 beta-mercaptoethanol) and radioimmunoprecipitation assay (RIPA) buffer supplemented with 50 mM BGP and 1 mM Na3VO4. Protein samples were boiled for 10 minutes at 100°C. 10-15 μg of each sample was loaded per lane, separated by 7.5% SDS-PAGE, and transferred onto PVDF membrane (Millipore IPVH00010). Membranes were then blocked with 5% skim milk or 3% blotting-grade blocker (BioRad 1706404) for 1 hr, probed overnight with the following primary antibodies diluted in 3% BSA (Fisher Scientific BP1600): RAI1 (1:1000), beta-actin (Sigma A5441, 1:20,000). Horseradish peroxide (HRP)-conjugated secondary IgG antibodies (EMD Millipore AP132P or AQ160P) were also diluted in 3% BSA, and the HRP signal was developed with various chemiluminescent substrates from Thermo Fisher Scientific (34080 or 34095) and Li-COR Biosciences (926-95000). Protein band intensity was visualized and quantified in the linear range using LI-COR C-Digit and Image Studio software. Results were compared using one-way ANOVA.

Immunocytochemistry

Two biological replicates of forebrain neuron cultures were obtained from E17.5 mouse embryos. On DIV19, they were fixed with 4% paraformaldehyde in 16% sucrose/PBS, permeabilized with 0.25% Triton-X in 1X PBS, blocked for 30 minutes with 10% bovine albumin serum (Sigma A2153), and overnight incubation of antibodies in 3% BSA at 4°C.Primary antibodies used in the study are following. anti-NeuN (EMD Millipore, MAB377, 1:1000), anti-GFAP (NeuroMab N206A/8, 1:1000), anti-MAP2 (EMD Millipore, AB5543,

1:1000), anti-OLIG2 (EMD Millipore, AB9610, 1:1000), anti-CD11b (Abcam, ab133357, 1:500), anti-GAD67 (Santa Cruz, sc-5602, 1:1000). Secondary antibodies (Invitrogen Alexa Fluor 488, 555, or 647) were applied for 45 min at room temperature. Fluorescence images were acquired using an Olympus BX61 fluorescence microscope (60X oil-immersion lens) and CellSense software. Immunoreactivity was quantified semi-automatedly using a custom ImageJ script after confirming specific staining by visual inspection.

Electrophysiology

All animal use followed NIH guidelines and was in compliance with the University of Michigan Committee on Use and Care of Animals. Dissociated postnatal (P0-2) rat hippocampal neuron cultures were prepared as previously described (Henry et al., 2012). Neurons were transfected with 1.0 µg of either non-targeting sh-RNA (sh-Ctrl) or *Rai1*-shRNA at DIV 12. For the rescue experiments RNAi resistant Rai1 expressing plasmids or its empty vector was co-transfected with the above sh-RNA expressing plasmids. For the Pde2a experiments, empty vector or mouse Pde2a constructs were transfected. Transfections were performed using CalPhos Transfection kit (ClonTech) or Lipofectamine 2000 (ThermoFisher Scientific) according to the manufacturer's protocols. All experiments were performed 48 hours after transfection. To induce synaptic scaling, neurons were treated with either 1 µM TTX, 10 µM bicuculline or vehicle for 24hr prior to recording. mEPSCs were recorded from a holding potential of – 70 mV with an Axopatch 200B or Multiclamp 700B amplifier from neurons bathed in HEPES buffered saline (HBS) containing: 119 mM NaCl, 5 mM KCl, 2 mM CaCl2, 2 mM MgCl2, 30 mM Glucose, 10 mM HEPES (pH 7.4) plus 1 µM TTX and 10 µM bicuculline; mEPSCs were analyzed with Synaptosoft MiniAnalysis software. Whole-cell pipette internal solutions contained: 100 mM cesium gluconate, 0.2 mM EGTA, 5 mM MgCl2, 2 mM ATP, 0.3 mM GTP, 40 mM HEPES (pH 7.2). Statistical differences between experimental conditions were determined by unpaired Student's t-tests (Fig. 6) or one-way ANOVA followed by post-hoc Fisher's LSD test (Fig. 3).

Surface GluA1 expression analysis

Surface GluA1 staining was conducted as previously described with slight modification (Henry et al., 2012). On DIV12, rat cultured hippocampal cells were infected either with lentivirus carrying sh-Ctrl or sh-*Rai1* as described above. After 72 hours of incubation, cultured cells were

live-labeled with rabbit anti-GluA1 antibody (10 µg/ml, EMD Biosciences) for 20 min at 37°C, fixed with 2% paraformaldehyde, and further labeled with mouse anti-PSD-95 (EMD Millipore, MAB1596, 1:1000). Goat anti-mouse Alexa 488 and Goat anti-rabbit Alexa 555 secondary antibodies (Abcam, 1:500) were applied for 60 min at room temperature to visualize PSD-95 and GluA1 staining. Images of PSD-95 and GluA1 were aquired using an inverted Olympus FV1000 laser-scanning confocal microscope using a Plan-Apochromat 63 X /1.4 oil objective. Then, synaptic GluA1 was defined as a particle that occupied > 10% of the PSD-95 positive area, and the average integrated intensity of synapatic GluA1 was calculated using a custom macro for ImageJ. Statistical differences between experimental conditions were determined by unpaired Student's t-tests.

Culturing on MEAs and Single Unit Recordings

Dissociated postnatal (P0-3) rat hippocampal neurons were plated onto sterile multi-electrode arrays chips (MEAs) (60MEA200/30IR–TI; Multichannel Systems, Reutlingen, Germany) at a density of ~350 cells/mm2. MEAs were coated with 0.05% polyethyleneimine and laminin (1 µg/µL). MEAs were transferred to the incubator for at least 3 hours to allow for cell adhesion. Once adhered, media was added to each MEA to achieve a total volume of 1 ml per MEA. Media used was composed of Neurobasal Plus Medium with 1X B-27 Plus supplement, 1X GlutaMax and 50 U/ml of Pen/Strep (ThermoFisher, Waltham, MA). MEAs were covered with a gas permeable, ethlylene propylene membrane (MEA-MEM, Multichannel Systems, Reutlingen, Germany). Half volume media exchanges were done every 3-4 days. We evaluated the health of the neuronal cultures on DIV 10. Cultures that exhibited spontaneous spiking activity on ≥ 10 electrodes were considered healthy and included in the study. On DIV 11, neurons were transfected with lentivirus encoding scrambled or Rai1- by performing a half-media change. On DIV 14, Local Field Potential (LFP) recordings were acquired at 20 kHz using a MEA2100-System (Multichannel Systems, Reutlingen, Germany). MEA chips were secured to the headstage of the amplifier and maintained in a controlled environment (37°C, 5% CO2) for the duration of the recording. Prior to recording, we left the MEAs undisturbed for eight min to allow for acclimation after handling. Spontaneous activity was captured during five min epochs. Data was imported into MATLAB (MathWorks, Natick, MA) and analyzed using custom written scripts. The LFP signal was high pass filtered at 100 Hz using a Butterworth filter. Spikes were

detected using amplitude thresholds set at five times the root mean square of the noise. Neuronal units were identified by spike sporting using principal component analysis of the detected spike and manually identifying clusters. A spike was defined by the signal 1 ms before the peak to 3 ms after the peak. The inter spike interval was defined as the time between two adjacent spikes. Mean firing frequency was calculated by dividing the total number of spikes detected for each neuronal unit by the recording duration. Statistical analyses were done in MATLAB and GraphPad Prism (GraphPad Software, San Diego, CA).

RAI1 ChIP-seq

ChIP was performed as previously described [157]. We dissociated E18 mouse forebrains and culture them for 14 DIV, infected with lentivirus containing sh-*Rai1* #1 or sh-Ctrl. On DIV17, we treated cultures with 2 □M BIC, or water vehicle for 4 hours, harvested the cells, fixed with 1% formaldehyde in HBSS for 30 minutes at room temperature, and prepared chromatin samples. We digested chromatin first with MNase for 20 min at 25°C. We then spiked, *Drosophila* chromatin, which contains fly-specific histone variant H2Av (Active Motif Cat. No. 53083). Samples were then further sheared by sonication using Qsonica Q800R3 at 70% amplitude 15 sec pulse with 20 sec interval for 30 min (total time: 70 min). The antibodies applied were the abovementioned anti-RAI1 polyclonal and anti-*Drosophila* H2Av antibodies (2.5 μg/sample). Antibody-antigen complex that formed at 4°C overnight were precipitated with Dynabeads Protein A/G mixture (1:1, Invitrogen 10001D, 10003D). We isolated the pulled down DNA and made sequencing libraries with NEBNext reagents (E7645S) and sequenced them on the Illumina HiSeq4000 platform to generate 50 bp single-end reads.

Raw reads were demultiplexed and filtered according to the standard Illumina analysis pipeline. Reads from sequencing libraries were then mapped to the mouse (mm9) and fruit fly (dm6) genome assemblies using Bowtie1 [158] allowing up to 2 mismatches. Only uniquely-mapped reads were used for analysis. We used MACS2 (version 2.1.0.20140616, FDR < 0.01) to identify RAI1 peaks using pooled input samples as a control [159]. For visualization in the UCSC browser, bigwig files were generated with coverage normalized using the number of mapped reads to the *Drosophila* genome (reads mapped per reference genome per million reads) [160,161]. ChIPseeker [162] annotated RAI1 peaks to promoters, genic, or intergenic regions. We integrated following publically available epigenomic datasets: DNase I hypersensitive sites (DHS) of whole brain

samples (E14.5: GSM1014197, 8 week adult: GSM1014151), H3K4me1: whole brain (8 week: GSM769022, E14.5: GSM1000096), H3K4me3: whole brain (8 week: GSM769026, E14.5: GSM1000095): H3K27ac (E14.5 whole brain: GSM1000094, 8 week forebrain: GSM3666438): and H3K27me (E14.5 H3K27me2 whole-brain: GSM1000143, 8 week H3K27me3 forebrain, GSM3666437). Putative transcriptional enhancers were defined as DHS-positive RAI1 peaks (± 500 bp) that overlap with H3K4me1 but not H3K4me3.

Alternative promoter analysis

A custom pipeline using bedtools (v2.25.0) [163] and R (3.6.1) was developed to discover genes with alternative TSS usage (accessible at https://github.com/pmgaray). Briefly, coordinates for H3K4me3 broadpeaks in mouse cortical neuron cultures were selected if they overlapped with the coordinates of Refseq or GENCODE mouse mm10 annotated TSS. This list of promoter regions was then intersected with gene bodies to attribute gene name to each putative promoter. These were converted to TSS Regions and Featurecounts (1.5.0) [156] was used to attribute read counts to each TSS region. TSS regions with RPKM <0.003 and RPM < 1 were filtered out based on the point of maximum curvature of ranked RPKM/RPMs (akmediods:::elbowPoint, github.com/agentlans) . Genes with more than one TSS region that passed these thresholds were counted as multiple promoter genes. The most downstream promoter region was defined as the reference region. Raw read ratios for each replicate were calculated by dividing read count of upstream TSS regions by the read count of the downstream reference region. A linear model was constructed using the default R lm command; QR decomposition solution to linear least squares problem (lm(value ~ Treatment, data=Array of ratios)). TTX, vehicle, or BIC were used as the dummy variable to determine if a correlation existed between treatment and the relative ratio of upstream and downstream promoter usage. P-values for the hypothesis test Correlation=0 were adjusted by Benjamini-Hochberg adjustment (p.adj, method="BH") and a cutoff of 0.1 was selected to define ADDUP genes.

In vivo validation

Mice were raised in 12 hour/12 hour light dark cycles until post-natal day 60. Mice were maintained in a 24 hour dark cycle, and then half the mice returned to light for 4 hours. Mice were sacrificed, and the visual cortex and somatosensory cortices of each hemisphere dissected.

Brains were dissociated, cells lysed, and tagged-ribosomes immunoprecipitated. Resulting RNA/ribosome mix was resuspended in Trizol.

RNA-seq Library Preparation

RNA was prepared according to an adapted version of the DLAF protocol [130] to accommodate lower input mass. NEBNext rRNA-depletion kit was utilized with 10 ng of RNA as input.

RNA-seq Sequencing and Analysis

Reads were mapped to the mouse mm10 genome by STAR (2.5.3a). BED file of First exons was created by taking annotated Refseq mm10 transcripts, selecting out the first exon, and intersecting with gene names in order to attribute exon number and gene name to each exon**.** Featurecounts was used to quantify read count/exon. Exons with counts >100 reads were selected. Potential genes were examined visually to corroborate changes. Gene ontology enrichment was analyzed with WebGestalt (2019) [164]

Immunocytochemistry and Image Analysis

Two biological replicates of cortex and hippocampus from E17 mouse pups were collected and plated onto PDL-coated glass coverslips. At DIV 14 they were infected with lentiviral shRNA. On DIV19, they were fixed with 4% paraformaldehyde in sucrose/PBS. Slips were stained with anti-NeuN, anti-GFAP, anti-Map2, anti-Olig2, anti-microglia, anti-Vglut, anti-Vgat and anti-Pdgrfa. Antibody was incubated overnight at 4 ° C. Secondary antibodies (Alexafluor 488, 555, and 647) were applied for 45 minutes at room temperature. Slips were affixed with Prolong Gold with DAPI. Slips were imaged using a Nikon X microscope and Olympus CellSense software at 20X magnification. Cells were quantified using a custom ImageJ script.

Data Availability

Sequencing data generated for this study have been submitted to the NCBI Gene Expression Omnibus (GEO; http://www.ncbi.nlm.nih.gov/geo/) under accession number GSE121749.

REFERENCES

1 Kuleshov, M. V. *et al.* Enrichr: a comprehensive gene set enrichment analysis web server 2016 update. *Nucleic Acids Res.* **44**, W90-W97, doi:10.1093/nar/gkw377 (2016).

2 Huang, W. H. *et al.* Molecular and Neural Functions of Rai1, the Causal Gene for Smith-Magenis Syndrome. *Neuron* **92**, 392-406, doi:10.1016/j.neuron.2016.09.019 (2016).

3 Garay, P. M., Wallner, M. A. & Iwase, S. Yin–yang actions of histone methylation regulatory complexes in the brain. *Epigenomics* **8**, 1689-1708, doi:10.2217/epi-2016-0090 (2016).

4 Eberl, H. C., Spruijt, C. G., Kelstrup, C. D., Vermeulen, M. & Mann, M. A map of general and specialized chromatin readers in mouse tissues generated by label-free interaction proteomics. *Mol. Cell* **49**, 368-378, doi:10.1016/j.molcel.2012.10.026 (2013).

5 Emanuelsson, O., Nielsen, H., Brunak, S. & von Heijne, G. Predicting Subcellular Localization of Proteins Based on their N-terminal Amino Acid Sequence. *J. Mol. Biol.* **300**, 1005-1016, doi:*https://doi.org/10.1006/jmbi.2000.3903* (2000).

6 Muter, J. *et al.* The clock protein period 2 synchronizes mitotic expansion and decidual transformation of human endometrial stromal cells. *FASEB journal : official publication of the Federation of American Societies for Experimental Biology* **29**, 1603-1614, doi:10.1096/fj.14-267195 (2015).

7 West, A. E., Griffith, E. C. & Greenberg, M. E. Regulation of transcription factors by neuronal activity. *Nat. Rev. Neurosci.* **3**, 921-931 (2002).

8 Benito, E. & Barco, A. The neuronal activity-driven transcriptome. *Mol. Neurobiol.* **51**, 1071-1088, doi:10.1007/s12035-014-8772-z (2015).

9 Saha, R. N. *et al.* Rapid activity-induced transcription of Arc and other IEGs relies on poised RNA polymerase II. *Nat. Neurosci.* **14**, 848-856, doi:10.1038/nn.2839 (2011).

10 Hong, S. J., Li, H., Becker, K. G., Dawson, V. L. & Dawson, T. M. Identification and analysis of plasticity-induced late-response genes. *Proc. Natl. Acad. Sci. U. S. A.* **101**, 2145-2150, doi:10.1073/pnas.0305170101 (2004).

11 Ebert, D. H. & Greenberg, M. E. Activity-dependent neuronal signalling and autism spectrum disorder. *Nature* **493**, 327-337, doi:10.1038/nature11860 (2013).

12 Loebrich, S. & Nedivi, E. The function of activity-regulated genes in the nervous system. *Physiol. Rev.* **89**, 1079-1103, doi:10.1152/physrev.00013.2009 (2009).

13 Turrigiano, G. G. The self-tuning neuron: synaptic scaling of excitatory synapses. *Cell* **135**, 422-435, doi:10.1016/j.cell.2008.10.008 (2008).

14 Abbott, L. F. & Nelson, S. B. Synaptic plasticity: taming the beast. *Nat. Neurosci.* **3**, 1178, doi:10.1038/81453 (2000).

15 Miller, K. D. & MacKay, D. J. C. The Role of Constraints in Hebbian Learning. *Neural Comput.* **6**, 100-126, doi:10.1162/neco.1994.6.1.100 (1994).

16 Turrigiano, G. G. The dialectic of Hebb and homeostasis. *Philosophical Transactions of the Royal Society B: Biological Sciences* **372**, doi:10.1098/rstb.2016.0258 (2017).

17 Yee, A. X., Hsu, Y.-T. & Chen, L. A metaplasticity view of the interaction between homeostatic and Hebbian plasticity. *Philosophical Transactions of the Royal Society B: Biological Sciences* **372** (2017).

18 Fernandes, D. & Carvalho, A. L. Mechanisms of homeostatic plasticity in the excitatory synapse. *J. Neurochem.*, doi:10.1111/jnc.13687 (2016).

19 de Vivo, L. *et al.* Ultrastructural evidence for synaptic scaling across the wake/sleep cycle. *Science* **355**, 507 (2017).

20 Sultan, F. A. & Day, J. J. Epigenetic mechanisms in memory and synaptic function. *Epigenomics* **3**, 157-181, doi:10.2217/epi.11.6 (2011).

21 Yu, H. *et al.* Tet3 regulates synaptic transmission and homeostatic plasticity via DNA oxidation and repair. **18**, 7-9, doi:10.1038/nn.4008 (2015).

22 Benevento, M. *et al.* Histone Methylation by the Kleefstra Syndrome Protein EHMT1 Mediates Homeostatic Synaptic Scaling. *Neuron* **91**, 341-355, doi:10.1016/j.neuron.2016.06.003 (2016).
23 Mao, W. *et al.* Activity-Induced Regulation of Synaptic Strength through the Chromatin Reader L3mbtl1. *Cell Reports* **23**, 3209-3222, doi:*https://doi.org/10.1016/j.celrep.2018.05.028* (2018).
24 De Rubeis, S. *et al.* Synaptic, transcriptional and chromatin genes disrupted in autism. *Nature* **515**, 209-215, doi:10.1038/nature13772 (2014).
25 Iwase, S. *et al.* Epigenetic Etiology of Intellectual Disability. *The Journal of Neuroscience* **37**, 10773, doi:10.1523/JNEUROSCI.1840-17.2017 (2017).
26 Gupta, S. *et al.* Histone methylation regulates memory formation. *J. Neurosci* **30**, 3589-3599, doi:10.1523/JNEUROSCI.3732-09.2010 (2010).
27 Jakovcevski, M. *et al.* Neuronal Kmt2a/Mll1 histone methyltransferase is essential for prefrontal synaptic plasticity and working memory. *J. Neurosci.* **35**, 5097-5108, doi:10.1523/JNEUROSCI.3004-14.2015 (2015).
28 Wang, J. *et al.* LSD1n is an H4K20 demethylase regulating memory formation via transcriptional elongation control. *Nat. Neurosci.* **18**, 1256-1264, doi:10.1038/nn.4069 (2015).
29 Gupta-Agarwal, S. *et al.* G9a/GLP histone lysine dimethyltransferase complex activity in the hippocampus and the entorhinal cortex is required for gene activation and silencing during memory consolidation. *J. Neurosci.* **32**, 5440-5453, doi:10.1523/JNEUROSCI.0147-12.2012 (2012).
30 Wijayatunge, R. *et al.* The histone lysine demethylase Kdm6b is required for activity-dependent preconditioning of hippocampal neuronal survival. *Mol. Cell. Neurosci.* **61**, 187-200, doi:10.1016/j.mcn.2014.06.008 (2014).
31 Widagdo, J. & Anggono, V. The m6A-epitranscriptomic signature in neurobiology: from neurodevelopment to brain plasticity. *J. Neurochem.* **0**, doi:10.1111/jnc.14481 (2018).
32 Cohen, J. E., Lee, P. R. & Fields, R. D. Systematic identification of 3'-UTR regulatory elements in activity-dependent mRNA stability in hippocampal neurons. *Philos. Trans. R. Soc. Lond. B Biol. Sci.* **369**, doi:10.1098/rstb.2013.0509 (2014).
33 Notaras, M. *et al.* UPF2 leads to degradation of dendritically targeted mRNAs to regulate synaptic plasticity and cognitive function. *Mol. Psychiatry*, doi:10.1038/s41380-019-0547-5 (2019).
34 Glock, C., Heumüller, M. & Schuman, E. M. mRNA transport & local translation in neurons. *Curr. Opin. Neurobiol.* **45**, 169-177, doi:*https://doi.org/10.1016/j.conb.2017.05.005* (2017).
35 Kim, J. *et al.* Developmental and degenerative modulation of brain-derived neurotrophic factor transcript variants in the mouse hippocampus. *Int. J. Dev. Neurosci.* **38**, 68-73, doi:*https://doi.org/10.1016/j.ijdevneu.2014.08.001* (2014).
36 Pruunsild, P., Sepp, M., Orav, E., Koppel, I. & Timmusk, T. Identification of cis-elements and transcription factors regulating neuronal activity-dependent transcription of human BDNF gene. *The Journal of neuroscience : the official journal of the Society for Neuroscience* **31**, 3295-3308, doi:10.1523/JNEUROSCI.4540-10.2011 (2011).
37 Treutlein, B., Gokce, O., Quake, S. R. & Südhof, T. C. Cartography of neurexin alternative splicing mapped by single-molecule long-read mRNA sequencing. *Proc. Natl. Acad. Sci. U. S. A.* **111**, E1291-E1299, doi:10.1073/pnas.1403244111 (2014).
38 Sim, S. E., Bakes, J. & Kaang, B. K. Neuronal activity-dependent regulation of MicroRNAs. *Mol. Cells* **37**, 511-517, doi:10.14348/molcells.2014.0132 (2014).
39 Sanjana, N. E., Levanon, E. Y., Hueske, E. A., Ambrose, J. M. & Li, J. B. Activity-dependent A-to-I RNA editing in rat cortical neurons. *Genetics* **192**, 281-287, doi:10.1534/genetics.112.141200 (2012).
40 Karlsson, K., Lönnerberg, P. & Linnarsson, S. Alternative TSSs are co-regulated in single cells in the mouse brain. *Mol. Syst. Biol.* **13**, 930-930, doi:10.15252/msb.20167374 (2017).
41 Fogarty, E. A. *et al.* SOX10 regulates an alternative promoter at the Charcot-Marie-Tooth disease locus MTMR2. *Hum. Mol. Genet.* **25**, 3925-3936, doi:10.1093/hmg/ddw233 (2016).

42 Pal, S. *et al.* Alternative transcription exceeds alternative splicing in generating the transcriptome diversity of cerebellar development. *Genome Res.* **21**, 1260-1272, doi:10.1101/gr.120535.111 (2011).
43 Schaukowitch, K. *et al.* An Intrinsic Transcriptional Program Underlying Synaptic Scaling during Activity Suppression. *Cell Rep* **18**, 1512-1526, doi:10.1016/j.celrep.2017.01.033 (2017).
44 Paulsen, M. T. *et al.* Use of Bru-Seq and BruChase-Seq for genome-wide assessment of the synthesis and stability of RNA. *Methods (San Diego, Calif.)* **67**, 45-54, doi:10.1016/j.ymeth.2013.08.015 (2014).
45 Paulsen, M. T. *et al.* Coordinated regulation of synthesis and stability of RNA during the acute TNF-induced proinflammatory response. *Proceedings of the National Academy of Sciences* **110**, 2240-2245, doi:10.1073/pnas.1219192110 (2013).
46 Love, M. I., Huber, W. & Anders, S. Moderated estimation of fold change and dispersion for RNA-seq data with DESeq2. *Genome Biol.* **15**, 550, doi:10.1186/s13059-014-0550-8 (2014).
47 Hrvatin, S. *et al.* Single-cell analysis of experience-dependent transcriptomic states in the mouse visual cortex. *Nat. Neurosci.* **21**, 120-129, doi:10.1038/s41593-017-0029-5 (2018).
48 Hasel, P. *et al.* Neurons and neuronal activity control gene expression in astrocytes to regulate their development and metabolism. *Nat Commun* **8**, 15132, doi:10.1038/ncomms15132 (2017).
49 Risher, W. C. & Eroglu, C. Thrombospondins as key regulators of synaptogenesis in the central nervous system. *Matrix Biol.* **31**, 170-177, doi:10.1016/j.matbio.2012.01.004 (2012).
50 Zhang, Y. *et al.* An RNA-sequencing transcriptome and splicing database of glia, neurons, and vascular cells of the cerebral cortex. *J. Neurosci.* **34**, 11929-11947, doi:10.1523/JNEUROSCI.1860-14.2014 (2014).
51 Okuno, H. Regulation and function of immediate-early genes in the brain: Beyond neuronal activity markers. *Neurosci. Res.* **69**, 175-186, doi:*https://doi.org/10.1016/j.neures.2010.12.007* (2011).
52 Schanzenbächer, Christoph T., Sambandan, S., Langer, Julian D. & Schuman, Erin M. Nascent Proteome Remodeling following Homeostatic Scaling at Hippocampal Synapses. *Neuron* **92**, 358-371, doi:10.1016/j.neuron.2016.09.058 (2016).
53 Müller, F., Zaucker, A. & Tora, L. Developmental regulation of transcription initiation: more than just changing the actors. *Curr. Opin. Genet. Dev.* **20**, 533-540, doi:10.1016/j.gde.2010.06.004 (2010).
54 Pennington, K. L., Marr, S. K., Chirn, G.-W. & Marr, M. T., 2nd. Holo-TFIID controls the magnitude of a transcription burst and fine-tuning of transcription. *Proc. Natl. Acad. Sci. U. S. A.* **110**, 7678-7683, doi:10.1073/pnas.1221712110 (2013).
55 Hurst, S. E. *et al.* A novel variant in TAF1 affects gene expression and is associated with X-linked TAF1 intellectual disability syndrome. *Neuronal Signal* **2**, NS20180141-NS20180141, doi:10.1042/NS20180141 (2018).
56 El-Saafin, F. *et al.* Homozygous TAF8 mutation in a patient with intellectual disability results in undetectable TAF8 protein, but preserved RNA polymerase II transcription. *Hum. Mol. Genet.* **27**, 2171-2186, doi:10.1093/hmg/ddy126 (2018).
57 Gropman, A. L., Duncan, W. C. & Smith, A. C. Neurologic and developmental features of the Smith-Magenis syndrome (del 17p11.2). *Pediatr. Neurol.* **34**, 337-350, doi:10.1016/j.pediatrneurol.2005.08.018 (2006).
58 Elsea, S. H. & Williams, S. R. Smith-Magenis syndrome: haploinsufficiency of RAI1 results in altered gene regulation in neurological and metabolic pathways. *Expert Rev. Mol. Med.* **13**, e14-e14, doi:10.1017/S1462399411001827 (2011).
59 Lucas, R. E., Vlangos, Christopher N, Das, Parimal, Patel, Pragna I, and Elsea, Sarah H. Genomic organisation of the ~1.5 Mb Smith-Magenis syndrome critical interval: Transcription map, genomic contig, and candidate gene analysis. *Europ. J. Hum. Genet.* **9**, 892-902 (2001).
60 Carmona-Mora, P. *et al.* RAI1 Transcription Factor Activity Is Impaired in Mutants Associated with Smith-Magenis Syndrome. *PLoS One* **7**, doi:10.1371/journal.pone.0045155 (2012).

61 Carmona-Mora, P. & Walz, K. Retinoic Acid Induced 1, RAI1: A Dosage Sensitive Gene Related to Neurobehavioral Alterations Including Autistic Behavior. *Curr. Genomics* **11**, 607-617, doi:10.2174/138920210793360952 (2010).
62 Potocki, L. *et al.* Molecular mechanism for duplication 17p11.2- the homologous recombination reciprocal of the Smith-Magenis microdeletion. *Nat. Genet.* **24**, 84-87, doi:10.1038/71743 (2000).
63 Potocki, L. *et al.* Characterization of Potocki-Lupski syndrome (dup(17)(p11.2p11.2)) and delineation of a dosage-sensitive critical interval that can convey an autism phenotype. *Am. J. Hum. Genet.* **80**, 633-649, doi:10.1086/512864 (2007).
64 Zhang, F. *et al.* Identification of uncommon recurrent Potocki-Lupski syndrome-associated duplications and the distribution of rearrangement types and mechanisms in PTLS. *Am. J. Hum. Genet.* **86**, 462-470, doi:10.1016/j.ajhg.2010.02.001 (2010).
65 van der Zwaag, B. *et al.* Gene-network analysis identifies susceptibility genes related to glycobiology in autism. *PLoS One* **4**, doi:10.1371/journal.pone.0005324 (2009).
66 Toulouse, A., Rochefort, D., Roussel, J., Joober, R. & Rouleau, G. a. Molecular cloning and characterization of human RAI1, a gene associated with schizophrenia. *Genomics* **82**, 162-171, doi:10.1016/S0888-7543(03)00101-0 (2003).
67 Haybaeck, J. *et al.* Increased expression of retinoic acid-induced gene 1 in the dorsolateral prefrontal cortex in schizophrenia, bipolar disorder, and major depression. *Neuropsychiatr. Dis. Treat.* **11**, 279-289, doi:10.2147/NDT.S72536 (2015).
68 Williams, S. R. *et al.* Haploinsufficiency of HDAC4 causes brachydactyly mental retardation syndrome, with brachydactyly type E, developmental delays, and behavioral problems. *Am. J. Hum. Genet.* **87**, 219-228, doi:10.1016/j.ajhg.2010.07.011 (2010).
69 Mullegama, S., Alaimo, J., Chen, L. & Elsea, S. Phenotypic and Molecular Convergence of 2q23.1 Deletion Syndrome with Other Neurodevelopmental Syndromes Associated with Autism Spectrum Disorder. *Int. J. Mol. Sci.* **16**, 7627-7643, doi:10.3390/ijms16047627 (2015).
70 Bi, W. *et al.* Rai1 deficiency in mice causes learning impairment and motor dysfunction, whereas Rai1 heterozygous mice display minimal behavioral phenotypes. *Human Molecular Genetics* **16**, 1802-1813, doi:10.1093/hmg/ddm128 (2007).
71 Burns, B. *et al.* Rai1 haploinsufficiency causes reduced Bdnf expression resulting in hyperphagia, obesity and altered fat distribution in mice and humans with no evidence of metabolic syndrome. *Hum. Mol. Genet.* **19**, 4026-4042, doi:10.1093/hmg/ddq317 (2010).
72 Tahir, R., Kennedy, A., Elsea, S. H. & Dickinson, A. J. Retinoic acid induced-1 (Rai1) regulates craniofacial and brain development in Xenopus. *Mech. Dev.* **1**, 1-14, doi:10.1016/j.mod.2014.05.004 (2014).
73 Molina, J. *et al.* Abnormal social behaviors and altered gene expression rates in a mouse model for Potocki-Lupski syndrome. *Hum. Mol. Genet.* **17**, 2486-2495, doi:10.1093/hmg/ddn148 (2008).
74 Lacaria, M., Gu, W. & Lupski, J. R. Circadian abnormalities in mouse models of smith-magenis syndrome: Evidence for involvement of RAI1. *American Journal of Medical Genetics, Part A* **161**, 1561-1568, doi:10.1002/ajmg.a.35941 (2013).
75 Girirajan, S. & Elsea, S. H. Abnormal maternal behavior, altered sociability, and impaired serotonin metabolism in Rai1-transgenic mice. *Mamm. Genome* **20**, 247-255, doi:10.1007/s00335-009-9180-y (2009).
76 Allen Institute for Brain Science. *Allen Developing Mouse Brain Atlas [Internet]. Available from http://developingmouse.brain-map.org*, 2015).
77 Bi, W. *et al.* Inactivation of Rai1 in mice recapitulates phenotypes observed in chromosome engineered mouse models for Smith-Magenis syndrome. *Hum. Mol. Genet.* **14**, 983-995, doi:10.1093/hmg/ddi085 (2005).
78 Huang, W.-H. *et al.* Early adolescent Rai1 reactivation reverses transcriptional and social interaction deficits in a mouse model of Smith–Magenis syndrome. *Proceedings of the National Academy of Sciences* **115**, 10744, doi:10.1073/pnas.1806796115 (2018).

79 Fragoso, Y. D. *et al.* Expression in the human brain of retinoic acid induced 1, a protein associated with neurobehavioural disorders. *Brain structure & function*, doi:10.1007/s00429-014-0712-1 (2014).
80 Lee, C., Patil, S. & Sartor, M. A. RNA-Enrich: a cut-off free functional enrichment testing method for RNA-seq with improved detection power. *Bioinformatics* **32**, 1100-1102, doi:10.1093/bioinformatics/btv694 (2016).
81 Kim, J. H. *et al.* LRpath analysis reveals common pathways dysregulated via DNA methylation across cancer types. *BMC Genomics* **13**, 526, doi:10.1186/1471-2164-13-526 (2012).
82 Vierstra, J. *et al.* Mouse regulatory DNA landscapes reveal global principles of cis-regulatory evolution. *Science* **346**, 1007-1012, doi:10.1126/science.1246426 (2014).
83 Creyghton, M. P. *et al.* Histone H3K27ac separates active from poised enhancers and predicts developmental state. *Proceedings of the National Academy of Sciences* **107**, 21931, doi:10.1073/pnas.1016071107 (2010).
84 Zajaczkowski, E. L. *et al.* Bioorthogonal Metabolic Labeling of Nascent RNA in Neurons Improves the Sensitivity of Transcriptome-Wide Profiling. *ACS Chem. Neurosci.* **9**, 1858-1865, doi:10.1021/acschemneuro.8b00197 (2018).
85 Meier, K. & Brehm, A. Chromatin regulation: how complex does it get? *Epigenetics* **9**, 1485-1495, doi:10.4161/15592294.2014.971580 (2014).
86 Lan, F. *et al.* Recognition of unmethylated histone H3 lysine 4 links BHC80 to LSD1-mediated gene repression. *Nature* **448**, 718-722, doi:10.1038/nature06034 (2007).
87 Musselman, C. A. & Kutateladze, T. G. Handpicking epigenetic marks with PHD fingers. *Nucleic Acids Res.* **39**, 9061-9071, doi:10.1093/nar/gkr613 (2011).
88 Ito, S. *et al.* Role of Tet proteins in 5mC to 5hmC conversion, ES-cell self-renewal and inner cell mass specification. *Nature* **466**, 1129, doi:10.1038/nature09303

https://www.nature.com/articles/nature09303#supplementary-information (2010).
89 Tachibana, M. *et al.* Histone methyltransferases G9a and GLP form heteromeric complexes and are both crucial for methylation of euchromatin at H3-K9. *Genes Dev.* **19**, 815-826 (2005).
90 Pünzeler, S. *et al.* Multivalent binding of PWWP2A to H2A.Z regulates mitosis and neural crest differentiation. *The EMBO Journal* **36**, 2263-2279, doi:10.15252/embj.201695757 (2017).
91 Subramanian, V., Fields, P. A. & Boyer, L. A. H2A.Z: a molecular rheostat for transcriptional control. *F1000Prime Rep* **7**, 01-01, doi:10.12703/P7-01 (2015).
92 Yang, Y. *et al.* Chromatin remodeling inactivates activity genes and regulates neural coding. *Science (New York, N.Y.)* **353**, 300-305, doi:10.1126/science.aad4225 (2016).
93 Zhang, R., Lahens, N. F., Ballance, H. I., Hughes, M. E. & Hogenesch, J. B. A circadian gene expression atlas in mammals: implications for biology and medicine. *Proc. Natl. Acad. Sci. U. S. A.* **111**, 16219-16224, doi:10.1073/pnas.1408886111 (2014).
94 Patel, V. R., Eckel-Mahan, K., Sassone-Corsi, P. & Baldi, P. How pervasive are circadian oscillations? *Trends Cell Biol.* **24**, 329-331, doi:10.1016/j.tcb.2014.04.005 (2014).
95 Liu, C. & Chung, M. Genetics and epigenetics of circadian rhythms and their potential roles in neuropsychiatric disorders. *Neurosci. Bull.* **31**, 141-159, doi:10.1007/s12264-014-1495-3 (2015).
96 Ripperger, J. A. & Schibler, U. Rhythmic CLOCK-BMAL1 binding to multiple E-box motifs drives circadian Dbp transcription and chromatin transitions. *Nat. Genet.* **38**, 369-374, doi:10.1038/ng1738 (2006).
97 Masri, S. & Sassone-Corsi, P. The circadian clock: a framework linking metabolism, epigenetics and neuronal function. *Nature Reviews Neuroscience* **14**, 69+ (2013).
98 Najmabadi, H. *et al.* Deep sequencing reveals 50 novel genes for recessive cognitive disorders. *Nature* **478**, 57-63, doi:10.1038/nature10423 (2011).
99 Katada, S. & Sassone-Corsi, P. The histone methyltransferase MLL1 permits the oscillation of circadian gene expression. *Nat. Struct. Mol. Biol.* **17**, 1414-1421, doi:10.1038/nsmb.1961 (2010).

100 Nam, Hye J. *et al.* Phosphorylation of LSD1 by PKCα Is Crucial for Circadian Rhythmicity and Phase Resetting. *Mol. Cell* **53**, 791-805, doi:10.1016/j.molcel.2014.01.028 (2014).
101 Boone, P. M. *et al.* Abnormal circadian rhythm of melatonin in Smith-Magenis syndrome patients with RAI1 point mutations. *Am. J. Med. Genet. A* **155A**, 2024-2027, doi:10.1002/ajmg.a.34098 (2011).
102 Pevet, P. & Challet, E. Melatonin: both master clock output and internal time-giver in the circadian clocks network. *J. Physiol. Paris* **105**, 170-182, doi:10.1016/j.jphysparis.2011.07.001 (2011).
103 Potocki, L. *et al.* Circadian rhythm abnormalities of melatonin in Smith-Magenis syndrome. *J. Med. Genet.* **37**, 428-433, doi:10.1136/jmg.37.6.428 (2000).
104 Boudreau, E. A. *et al.* Review of disrupted sleep patterns in Smith-Magenis syndrome and normal melatonin secretion in a patient with an atypical interstitial 17p11.2 deletion. *Am. J. Med. Genet. A* **149A**, 1382-1391, doi:10.1002/ajmg.a.32846 (2009).
105 Williams, S. R., Zies, D., Mullegama, S. V., Grotewiel, M. S. & Elsea, S. H. Smith-magenis syndrome results in disruption of CLOCK gene transcription and reveals an integral role for RAI1 in the maintenance of circadian rhythmicity. *Am. J. Hum. Genet.* **90**, 941-949, doi:10.1016/j.ajhg.2012.04.013 (2012).
106 Ye, R. *et al.* Dual modes of CLOCK:BMAL1 inhibition mediated by Cryptochrome and Period proteins in the mammalian circadian clock. *Genes Dev.* **28**, 1989-1998 (2014).
107 Hayashi, Y. *et al.* The intrinsic microglial molecular clock controls synaptic strength via the circadian expression of cathepsin S. *Sci. Rep.* **3**, 2744-2744, doi:10.1038/srep02744 (2013).
108 Lachmann, A. *et al.* ChEA: transcription factor regulation inferred from integrating genome-wide ChIP-X experiments. *Bioinformatics* **26**, 2438-2444, doi:10.1093/bioinformatics/btq466 (2010).
109 Xie, Y. *et al.* New Insights Into the Circadian Rhythm and Its Related Diseases. *Front. Physiol.* **10**, 682 (2019).
110 Vollmers, C. *et al.* Circadian Oscillations of Protein-Coding and Regulatory RNAs in a Highly Dynamic Mammalian Liver Epigenome. *Cell Metab.* **16**, 833-845, doi:10.1016/j.cmet.2012.11.004 (2012).
111 DiTacchio, L. *et al.* Histone lysine demethylase JARID1a activates CLOCK-BMAL1 and influences the circadian clock. *Science* **333**, 1881-1885, doi:10.1126/science.1206022 (2011).
112 Aguilar-Arnal, L., Katada, S., Orozco-Solis, R. & Sassone-Corsi, P. NAD(+)-SIRT1 control of H3K4 trimethylation through circadian deacetylation of MLL1. *Nat. Struct. Mol. Biol.*, doi:10.1038/nsmb.2990 (2015).
113 Hermey, G., Blüthgen, N. & Kuhl, D. Neuronal activity-regulated alternative mRNA splicing. *The International Journal of Biochemistry & Cell Biology* **91**, 184-193, doi:*https://doi.org/10.1016/j.biocel.2017.06.002* (2017).
114 Quesnel-Vallières, M. *et al.* Misregulation of an Activity-Dependent Splicing Network as a Common Mechanism Underlying Autism Spectrum Disorders. *Mol. Cell* **64**, 1023-1034, doi:10.1016/j.molcel.2016.11.033.
115 Sanjana, N. E., Levanon, E. Y., Hueske, E. A., Ambrose, J. M. & Li, J. B. Activity-Dependent A-to-I RNA Editing in Rat Cortical Neurons. *Genetics* **192**, 281-287, doi:10.1534/genetics.112.141200 (2012).
116 Balik, A., Penn, A. C., Nemoda, Z. & Greger, I. H. Activity-regulated RNA editing in select neuronal subfields in hippocampus. *Nucleic Acids Res.* **41**, 1124-1134, doi:10.1093/nar/gks1045 (2013).
117 Gurevich, I., Englander, M. T., Adlersberg, M., Siegal, N. B. & Schmauss, C. Modulation of Serotonin 2C Receptor Editing by Sustained Changes in Serotonergic Neurotransmission. *The Journal of Neuroscience* **22**, 10529 (2002).
118 Orlandi, C. *et al.* AMPA Receptor Regulation at the mRNA and Protein Level in Rat Primary Cortical Cultures. *PLoS One* **6**, e25350, doi:10.1371/journal.pone.0025350 (2011).

119 Malik, A. N. *et al.* Genome-wide identification and characterization of functional neuronal activity-dependent enhancers. *Nat. Neurosci.* **17**, 1330-1339, doi:10.1038/nn.3808 (2014).
120 Kim, T. K. *et al.* Widespread transcription at neuronal activity-regulated enhancers. *Nature* **465**, 182-187, doi:10.1038/nature09033 (2010).
121 Timmusk, T. *et al.* Identification of brain-derived neurotrophic factor promoter regions mediating tissue-specific, axotomy-, and neuronal activity-induced expression in transgenic mice. *The Journal of Cell Biology* **128**, 185 (1995).
122 Pruunsild, P., Kazantseva, A., Aid, T., Palm, K. & Timmusk, T. Dissecting the human BDNF locus: Bidirectional transcription, complex splicing, and multiple promoters(). *Genomics* **90**, 397-406, doi:10.1016/j.ygeno.2007.05.004 (2007).
123 Liu, Q.-R. *et al.* Human brain derived neurotrophic factor (BDNF) genes, splicing patterns, and assessments of associations with substance abuse and Parkinson's Disease. *American Journal of Medical Genetics Part B: Neuropsychiatric Genetics* **134B**, 93-103, doi:10.1002/ajmg.b.30109 (2005).
124 Pattabiraman, P. P. *et al.* Neuronal activity regulates the developmental expression and subcellular localization of cortical BDNF mRNA isoforms in vivo. *Mol. Cell. Neurosci.* **28**, 556-570, doi:*https://doi.org/10.1016/j.mcn.2004.11.010* (2005).
125 Chiaruttini, C. *et al.* Dendritic trafficking of BDNF mRNA is mediated by translin and blocked by the G196A (Val66Met) mutation. *Proc. Natl. Acad. Sci. U. S. A.* **106**, 16481-16486, doi:10.1073/pnas.0902833106 (2009).
126 Singer, G. A. C. *et al.* Genome-wide analysis of alternative promoters of human genes using a custom promoter tiling array. *BMC Genomics* **9**, 349, doi:10.1186/1471-2164-9-349 (2008).
127 Kim, T. H. *et al.* A high-resolution map of active promoters in the human genome. *Nature* **436**, 876, doi:10.1038/nature03877

https://www.nature.com/articles/nature03877#supplementary-information (2005).
128 The, F. C., the, R. P. & Clst. A promoter-level mammalian expression atlas. *Nature* **507**, 462, doi:10.1038/nature13182

https://www.nature.com/articles/nature13182#supplementary-information (2014).
129 Zhang, P. *et al.* Relatively frequent switching of transcription start sites during cerebellar development. *BMC Genomics* **18**, 461, doi:10.1186/s12864-017-3834-z (2017).
130 Agarwal, S., Macfarlan, T. S., Sartor, M. A. & Iwase, S. Sequencing of first-strand cDNA library reveals full-length transcriptomes. *Nat Commun* **6**, 6002, doi:10.1038/ncomms7002 (2015).
131 Agarwal, S. *et al.* LSD1/KDM1A Maintains Genome-wide Homeostasis of Transcriptional Enhancers. *bioRxiv* (2017).
132 Iwase, S. *et al.* A Mouse Model of X-linked Intellectual Disability Associated with Impaired Removal of Histone Methylation. *Cell Rep* **14**, 1000-1009, doi:10.1016/j.celrep.2015.12.091 (2016).
133 Goel, A. & Lee, H. K. Persistence of experience-induced homeostatic synaptic plasticity through adulthood in superficial layers of mouse visual cortex. *J. Neurosci.* **27**, 6692-6700, doi:10.1523/JNEUROSCI.5038-06.2007 (2007).
134 O'Herron, P., Levy, M., Woodward, J. J. & Kara, P. An Unexpected Dependence of Cortical Depth in Shaping Neural Responsiveness and Selectivity in Mouse Visual Cortex. *eneuro* **7**, ENEURO.0497-0419.2020, doi:10.1523/ENEURO.0497-19.2020 (2020).
135 Sanz, E. *et al.* Cell-type-specific isolation of ribosome-associated mRNA from complex tissues. *Proceedings of the National Academy of Sciences* **106**, 13939, doi:10.1073/pnas.0907143106 (2009).
136 Goebbels, S. *et al.* Genetic targeting of principal neurons in neocortex and hippocampus of NEX-Cre mice. *Genesis* **44**, 611-621, doi:10.1002/dvg.20256 (2006).

137 Wu, S.-X. *et al.* Pyramidal neurons of upper cortical layers generated by NEX-positive progenitor cells in the subventricular zone. *Proc. Natl. Acad. Sci. U. S. A.* **102**, 17172-17177, doi:10.1073/pnas.0508560102 (2005).
138 Xu, Y., Zhang, H.-T. & O'Donnell, J. M. in *Phosphodiesterases as Drug Targets* (eds Sharron H. Francis, Marco Conti, & Miles D. Houslay) 447-485 (Springer Berlin Heidelberg, 2011).
139 Yamazaki, M. *et al.* Differential palmitoylation of two mouse glutamate receptor interacting protein 1 forms with different N-terminal sequences. *Neurosci. Lett.* **304**, 81-84, doi:*https://doi.org/10.1016/S0304-3940(01)01766-9* (2001).
140 Hanley, L. J. & Henley, J. M. Differential roles of GRIP1a and GRIP1b in AMPA receptor trafficking. *Neurosci. Lett.* **485**, 167-172, doi:*https://doi.org/10.1016/j.neulet.2010.09.003* (2010).
141 Deal, R. B. & Henikoff, S. The INTACT method for cell type–specific gene expression and chromatin profiling in Arabidopsis thaliana. *Nat. Protoc.* **6**, 56-68, doi:10.1038/nprot.2010.175 (2011).
142 Mo, A. *et al.* Epigenomic Signatures of Neuronal Diversity in the Mammalian Brain. *Neuron* **86**, 1369-1384, doi:10.1016/j.neuron.2015.05.018 (2015).
143 Abrahams, B. S. *et al.* SFARI Gene 2.0: a community-driven knowledgebase for the autism spectrum disorders (ASDs). *Mol. Autism* **4**, 36, doi:10.1186/2040-2392-4-36 (2013).
144 Ushijima, T. *et al.* Light Controls Protein Localization through Phytochrome-Mediated Alternative Promoter Selection. *Cell* **171**, 1316-1325.e1312, doi:*https://doi.org/10.1016/j.cell.2017.10.018* (2017).
145 Kirkconnell, K. S. *et al.* Gene length as a biological timer to establish temporal transcriptional regulation. *Cell cycle (Georgetown, Tex.)* **16**, 259-270, doi:10.1080/15384101.2016.1234550 (2017).
146 Hayashi, T. *et al.* Single-cell full-length total RNA sequencing uncovers dynamics of recursive splicing and enhancer RNAs. *Nature Communications* **9**, 619, doi:10.1038/s41467-018-02866-0 (2018).
147 Fiszbein, A., Krick, K. S., Begg, B. E. & Burge, C. B. Exon-Mediated Activation of Transcription Starts. *Cell* **179**, 1551-1565.e1517, doi:10.1016/j.cell.2019.11.002 (2019).
148 Sibley, C. R. *et al.* Recursive splicing in long vertebrate genes. *Nature* **521**, 371-375, doi:10.1038/nature14466 (2015).
149 Nielsen, M. *et al.* Transcription-driven chromatin repression of Intragenic transcription start sites. *PLoS Genet.* **15**, e1007969, doi:10.1371/journal.pgen.1007969 (2019).
150 Bina, R. *et al.* De novo variants in SUPT16H cause neurodevelopmental disorders associated with corpus callosum abnormalities. *J. Med. Genet.* **57**, 461-465, doi:10.1136/jmedgenet-2019-106193 (2020).
151 Parra-Damas, A., Rubió-Ferrarons, L., Shen, J. & Saura, C. A. CRTC1 mediates preferential transcription at neuronal activity-regulated CRE/TATA promoters. *Sci. Rep.* **7**, 18004, doi:10.1038/s41598-017-18215-y (2017).
152 Doshi, J., Willis, K., Madurga, A., Stelzer, C. & Benenson, Y. Multiple Alternative Promoters and Alternative Splicing Enable Universal Transcription-Based Logic Computation in Mammalian Cells. *Cell Reports* **33**, 108437, doi:*https://doi.org/10.1016/j.celrep.2020.108437* (2020).
153 Vallianatos, C. N. *et al.* Altered Gene-Regulatory Function of KDM5C by a Novel Mutation Associated With Autism and Intellectual Disability. *Front. Mol. Neurosci.* **11**, doi:10.3389/fnmol.2018.00104 (2018).
154 Langmead, B. & Salzberg, S. L. Fast gapped-read alignment with Bowtie 2. *Nat. Methods* **9**, 357, doi:10.1038/nmeth.1923

https://www.nature.com/articles/nmeth.1923#supplementary-information (2012).
155 Kim, D. *et al.* TopHat2: accurate alignment of transcriptomes in the presence of insertions, deletions and gene fusions. *Genome Biol.* **14**, R36, doi:10.1186/gb-2013-14-4-r36 (2013).

156 Liao, Y., Smyth, G. K. & Shi, W. featureCounts: an efficient general purpose program for assigning sequence reads to genomic features. *Bioinformatics* **30**, 923-930, doi:10.1093/bioinformatics/btt656 (2014).
157 Iwase, S. *et al.* A Mouse Model of X-linked Intellectual Disability Associated with Impaired Removal of Histone Methylation. *Cell reports*, doi:10.1016/j.celrep.2015.12.091 (2016).
158 Langmead, B., Trapnell, C., Pop, M. & Salzberg, S. L. Ultrafast and memory-efficient alignment of short DNA sequences to the human genome. *Genome biology* **10**, R25, doi:10.1186/gb-2009-10-3-r25 (2009).
159 Zhang, Y. *et al.* Model-based analysis of ChIP-Seq (MACS). *Genome Biol.* **9**, R137, doi:10.1186/gb-2008-9-9-r137 (2008).
160 Orlando, D. A. *et al.* Quantitative ChIP-Seq normalization reveals global modulation of the epigenome. *Cell reports* **9**, 1163-1170, doi:10.1016/j.celrep.2014.10.018 (2014).
161 Egan, B. *et al.* An Alternative Approach to ChIP-Seq Normalization Enables Detection of Genome-Wide Changes in Histone H3 Lysine 27 Trimethylation upon EZH2 Inhibition. *PloS one* **11**, e0166438, doi:10.1371/journal.pone.0166438 (2016).
162 Yu, G., Wang, L. G. & He, Q. Y. ChIPseeker: an R/Bioconductor package for ChIP peak annotation, comparison and visualization. *Bioinformatics* **31**, 2382-2383, doi:10.1093/bioinformatics/btv145 (2015).
163 Quinlan, A. R. & Hall, I. M. BEDTools: a flexible suite of utilities for comparing genomic features. *Bioinformatics* **26**, 841-842, doi:10.1093/bioinformatics/btq033 (2010).
164 Liao, Y., Wang, J., Jaehnig, E. J., Shi, Z. & Zhang, B. WebGestalt 2019: gene set analysis toolkit with revamped UIs and APIs. *Nucleic Acids Res.* **47**, W199-w205, doi:10.1093/nar/gkz401 (2019).